ADVANCING THORACIC SPINE BIOMECHANICAL RESEARCH

By

Erin M. Mannen

Submitted to the graduate degree program in Mechanical Engineering and the Graduate Faculty of the University of Kansas in partial fulfillment of the requirements for the degree of Doctor of Philosophy.

_____

Chairperson Elizabeth Friis, Ph.D.

_____

Sara Wilson, Ph.D.

_____

Carl Luchies, Ph.D.

_____

Ronald Dougherty, Ph.D.

_____

Erik Van Vleck, Ph.D.

_____

Paul Arnold, M.D.

Date Defended: September 26, 2014

The Dissertation Committee for Erin M. Mannen

certifies that this is the approved version of the following dissertation:

ADVANCING THORACIC SPINE BIOMECHANICAL RESEARCH

_____

Chairperson Elizabeth Friis, Ph.D.

Date approved: September 26, 2014

ii

Abstract

The long term objective of this research was to elucidate issues with current thoracic spine testing methods and develop more accurate ways to quantify the biomechanical impact of surgical procedures or medical devices. The ability to perform thoracic spine testing with a rib cage is limited by test machine variability and experimental design inconsistency, so surgeons are left with little reliable information on the biomechanical impacts of procedures and implants. This research sought to validate a novel spine test machine, provide biomechanical data to support the inclusion of an intact rib cage when testing the thoracic spine, and quantify the biomechanical impacts of sequential Ponte osteotomies.

Specific Aim 1 validated the accuracy of the spine test machine for rigidity ranges that represent cadaveric specimen rigidities present in the spine. Cervical, thoracic, and lumbar spine specimens were modeled with synthetic rubber that represented the breadth of rigidities, and testing was conducted in bending and axial rotation. The maximum machine displacement error was less than 2° for lumbar and thoracic specimens, so it is suggested that researchers use an external motion-tracking system in conjunction with the test machine when high accuracy measurements are required.

Specific Aim 2 quantified the biomechanical differences of testing full cadaveric thoracic spine specimens with and without an intact rib cage. While it was presumed that the rib cage provides structural stability to the thoracic spine, the extent to which the rib cage contributes to spinal motion had not been fully quantified. Testing quantified the motion and stiffness values of an intact thoracic spine specimen, and results showed that testing without a rib cage changes both motion and stiffness values.

Specific Aim 3 quantified the biomechanical impact of sequential Ponte osteotomies in cadaveric thoracic spine specimens with intact rib cages. Overall and regional changes in motion due to Ponte osteotomies were analyzed, and results showed increased flexibility in the sagittal plane on both overall and regional levels.

The results from this work could provide researchers and surgeons the tools they need to better understand and improve spine procedures and implants, which could ultimately improve the quality of life for patients.

Table of Contents

List of Tables

List of Abbreviations

AIS	Adolescent Idiopathic Scoliosis
AP	anterior-posterior translation
AR	axial rotation
ATS	Applied Test Systems
ATSST	Applied Test Systems spine tester
C1-C7	cervical spine levels 1 through 7
E	extension
EZ	elastic zone
EZS	elastic zone stiffness
F	flexion
FE	flexion-extension
FSU	functional spine unit
KU	University of Kansas
L1-L5	lumbar spine levels 1 through 5
LB	lateral bending
MoB	mode of bending
NZ	neutral zone
NZS	neutral zone stiffness
PO	Ponte osteotomy
RL	right-left translation
ROM	range-of-motion
SI	superior-inferior translation
SK	Scheuermann's Kyphosis
T1-T12	thoracic spine levels 1through 12

CHAPTER 1:

Introduction

The long term objective of this research was to elucidate issues with current thoracic spine testing methods and develop more accurate ways to quantify the biomechanical impact of surgical procedures or medical devices. A novel spine testing machine developed by Applied Test Systems (Butler, PA) has undergone many prototype revisions in the KU Spine Biomechanics Lab. Validation of this machine would allow researchers to analyze the biomechanical changes in cadaveric thoracic spine specimens with an intact rib cage in flexion-extension, lateral bending, and axial rotation. The biomechanical question of quantifying differences in testing a cadaveric thoracic specimen with or without a rib cage, and the clinical question of quantifying the mechanical impacts of systematic Ponte Osteotomies (POs) could then be answered through this research.

Most commercial biomechanical spine testing machines have limits on specimen size, range-of-motion allowed, or continuous loading capability. The limitations inherent in the test machines also restrict the type of testing that can be done. It is nearly if not fully impossible to continuously test a cadaveric thoracic spine specimen with an intact rib cage in existing machines. Thus, research on the thoracic region is currently conducted with a partial thoracic segment with ribs attached or on a full thoracic spine with no rib cage intact. It can be inferred that these current test setups do not provide as physiologically-accurate of models as full thoracic spines with intact rib cages would offer. However, the extent of the differences in testing with versus without an intact rib cage on a full thoracic spine is not yet quantified.

Because of these limitations in cadaveric spine test setups, it has been difficult for researchers to accurately quantify thoracic-specific surgical procedures such as POs. It is

expected that, by using the validated spine test machine and the novel cadaveric test design with the full thoracic region and intact rib cage, accurate and quantifiable results can be obtained for thoracic surgical techniques and implants.

Specific Aim 1 validated the accuracy of the spine test machine for rigidity ranges that represent the variety of cadaveric spine specimens that could be tested in the machine. Cervical, thoracic, and lumbar spine specimens were modeled with synthetic rubber that represented the breadth of rigidities. Data from a motion-capture system and displacement data from the spine test machine was collected and compared in bending and torsion for each specimen to determine the inherent error within the spine test machine at each rigidity range. It was hypothesized that testing within each rigidity range would result in less than 1 degree for a loading range of ±15 Nm for bending and torsion. Chapter 3 addresses Specific Aim 1.

Specific Aim 2 quantified the biomechanical differences of testing full cadaveric thoracic spine specimens with and without an intact rib cage. While it is known that the rib cage provides structural stability to the thoracic spine, the extent to which the rib cage contributes to spinal motion has not been fully quantified. It was hypothesized that range-of-motion and stiffness parameters would also be significantly different in specimens without a rib cage. Chapters 4 and 5 address Specific Aim 2 by quantifying the biomechanics of a human thoracic spine with an intact rib cage, then comparing the overall mechanics of the spine with and without a rib cage for instrumented and uninstrumented conditions. An additional manuscript analyzing the regional and local motion of the thoracic spine with an intact rib cage is planned but not included in this dissertation.

Specific Aim 3 quantified the biomechanical impact of sequential POs in cadaveric thoracic spine specimens with intact rib cages. Using the validated spine test machine, sequential

POs were analyzed in each mode of bending for local vertebral levels, regional segments, and overall specimen behavior. Range-of-motion, stiffness values, and out-of-plane motions were calculated. It was hypothesized that sequential POs would result in statistically significant additive overall range of motion in the sagittal plane, and that the stiffnesses and out-of-plane motions would change after each sequential PO. Chapter 6 addresses the overall and regional range-of-motion analysis. Additional data analysis and manuscripts analyzing the local and out-of-plane motions are planned but are not included of this dissertation.

In summary, the ability to perform thoracic spine testing with a full rib cage is limited, so surgeons are left with little reliable information on the biomechanical impacts of procedures and implants. This research sought to (1) validate a novel spine test machine, (2) provide biomechanical data to support the necessary inclusion of an intact rib cage when testing a full thoracic spine, and (3) quantify the biomechanical impacts of sequential Ponte osteotomies. The results from this study could provide researchers and surgeons the tools they need to better understand and improve spine procedures and implants, which could ultimately improve the quality of life for patients.

CHAPTER 2:

Background and Significance

2.1 Basic spinal anatomy

The three main functions of the spinal column are to (1) protect the spinal cord, nerve roots, and internal organs, (2) enable a broad range of motion, and (3) provide balance and structural support to enable upright posture.[1] There are three distinct sections of the human spine: cervical, thoracic, and lumbar. The *cervical* spine is the top section of the spine and consists of the top 7 vertebrae, abbreviated C1 to C7 (superior to inferior). The *thoracic* spine is the section directly below the cervical region and consists of 12 vertebrae, abbreviated T1 to T12 (superior to inferior). The thoracic vertebrae are larger than the cervical vertebrae, have longer spinous processes, and have rib attachments resulting in the most stable and stiff region of the spinal column. The rib cage protects internal organs and restricts excessive motion. The *lumbar* spine is the section of the spine directly below the thoracic region and consists of 5 large vertebrae, abbreviated L1 to L5 (superior to inferior). The bulky size and broad shape of the lumbar vertebrae are designed to carry most of the load of the body.

The three body planes used to describe the two-dimensional surfaces of the spinal column are the frontal or coronal plane (divides the front and back halves of the body), the median or sagittal plane (divides the right and left sides of the body), and the transverse or axial plane (divides the top and bottom of the body at the waist) [1]. Normal curvature of the spine is described in each of the three body planes. When viewed from the coronal plane, the spine is straight. When viewed from the sagittal plane, the spine has three curves that are kyphotic (convex curve toward the back) or lordotic (concave curve towards the back). The thoracic region exhibits kyphotic curvature while the cervical and lumbar spinal regions exhibit lordotic

curves. Two adjacent vertebrae with the intervertebral disc and associated ligaments are referred to as a functional spine unit (FSU) and consist of the following components: the vertebral body, the intervertebral disc, seven significant ligaments, and two facet joints. Figure 2.1 depicts an FSU with associated body planes labeled.

2.2 Deformity in the Human Spine

2.2.1 Adolescent Idiopathic Scoliosis

Adolescent Idiopathic Scoliosis (AIS) is a three-dimensional spinal curvature deformity condition of unknown origin that affects 2 to 2.5 percent of the population, with 10 percent of those cases being progressive curves requiring treatment [2]. The disorder occurs during adolescence and is diagnosed using the Cobb technique to measure the lateral curvature of the spine (see Figure 2.2B). Progressive curves requiring surgical intervention are defined as having Cobb angles of 30° or greater, with the potential to increase. If left untreated, AIS can cause a myriad of problems including physical deformities such as rib humps, uneven shoulders and hips, and loss of height. These cosmetic abnormalities serve to intensify already sensitive body issues that are common in adolescents. Female teenagers with AIS were found to be over 1.5 times as likely to have suicidal thoughts and 3.5 times as likely to abuse alcohol versus their peers without AIS [3]. Researchers have also found strong correlations between teenagers with AIS and dangerous eating disorders such as anorexia nervosa or bulimia nervosa [4]. Aside from serious mental conditions, AIS patients also have dangerous health concerns that can arise from the physical deformity. The occurrence of back pain is significantly higher for people with moderate AIS compared to those without the disease [5-8]. Perhaps the most life-threatening risk factor of progressive AIS is a decrease in pulmonary function that can sometimes lead to

5

death [2, 9]. For mild and non-progressive AIS curves, treatment methods include monitoring and bracing. Bracing for mild curves has been shown to halt curve progression in 74 percent of cases [10]. Surgical intervention is most often prescribed for immature patients with a progressive Cobb angle of 40° or higher and for older teens with a Cobb angle of 50° or more [2]. The primary goal of surgery is to halt curvature progress while a secondary goal, which is often more important to the patient, is to improve the aesthetics of the spine.

2.2.2 Scheuermann's Kyphosis

Scheuermann's Kyphosis (SK) is defined as a hyperkyphosis in the thoracic spine due to wedged vertebrae. The origin of SK is unknown, and the disorder occurs in approximately 1 to 8 percent of the population [11]. Patients display a rigid hyperkyphotic curve in the mid to lower thoracic regions, with compensatory hyperlordosis of the cervical and lumbar spine (see Figure 2.2A). SK is diagnosed if there is wedging of at least 5° of three consecutive vertebrae, endplate irregularities, loss of disc space, and Schmorl nodes [12]. If left untreated, researchers have found that the incidence of pain in patients with SK versus patients without SK is higher [11, 13]. While SK appears to be a benign condition in most cases, cardio-respiratory problems can occur in patients with severe deformities [14]. Just as in patients with AIS, body image issues are also a problem in patients with SK, though it has not been as thoroughly studied.

Likewise, surgical treatments for patients with SK are not as well-defined as those with AIS. While non-pathogenic *lateral* curvature of the spine is the same from birth to maturity (zero degrees), non-pathogenic *sagittal* spine curvature changes with growth. Non-pathogenic kyphotic curvature develops during adolescents and increases from 20° in childhood to 40° at skeletal maturity [15]. Because of the large amount of variation between non-pathogenic

6

curvatures, it is often difficult to determine the risk for a young patient's curve to increase. For patients with growth remaining and flexible kyphotic deformity, bracing and casting are used to halt the curve progression in the sagittal plane. Compliant patients who wore a brace for a minimum of 18 months were able to avoid surgical intervention in 70 percent of cases. However, curves greater than 75° have a higher failure rate of brace treatment [16]. Indications for surgery for patients with SK include a failure of non-surgical treatments, T2-T12 deformity greater than 75°or thoracolumbar deformity of greater than 40°, and wedging of the vertebrae [17].

2.3 Spinal Fusion and Ponte Osteotomies

The most common surgical treatment method for both AIS and SK is spinal fusion, a procedure that utilizes metal rods and screws or hooks to force the spine into a more upright, derotated orientation (see Figures 2.3 and 2.4). A successful AIS or SK spinal fusion is one that stops the progression of the curvature and aesthetically appeals to the patient. Avoidance of adjacent level problems and follow-up surgeries is also desirable. Anterior releases were once considered necessary in stiff curves, increasing risk to the patient and operating room time as both the anterior and posterior approaches were required to complete the fusion. Current surgical techniques utilize instrumentation and tools that help surgeons physically derotate and translate the spine, sometimes exclusively posteriorly, before placing the rods. Ponte first described a posterior shortening procedure to help reduce sagittal curvature without an anterior approach [18]. This procedure and other advances in posterior approach technology decrease the physical deformities caused by AIS and SK and provide a more aesthetically appealing outcome for the patient while decreasing the risks associated with an anterior approach. For these

reasons, surgeons have begun to frequently utilize the Ponte osteotomy as a way to obtain the desired curvature without anterior releases. The Ponte osteotomy (PO) is a removal of the posterior spinous process, the ligamentum flavum, and the facets at the apex of the sagittal curve (see Figure 2.5) [18]. While the technique avoids the morbidity risks associated with an anterior approach, added neurological risks are presented as the spinal cord is exposed during surgery. Surgeons generally agree that a one-level Ponte Osteotomy results in an additional 5° of extension to correct hyperkyphosis. However, there is little research to support this rule-of-thumb. The problem is that surgeons are utilizing POs at many levels to correct hyperkyphosis in AIS and SK patients without truly understanding the biomechanical impact of the procedure.

Some hypothesize that forcing a large curve correction to obtain an aesthetic ideal can lead to increased forces and thus a high risk for adjacent level issues in the future. However, as society continues to desire the aesthetic ideal as a necessary outcome of a spinal fusion, surgeons are being forced to perform additional releases such as POs to obtain enough flexibility, resulting in longer operating room time which introduces a higher risk of infection and complications to the patient. One gap in understanding is the increase in range of motion for which Ponte Osteotomies provide to the surgeons. The rule-of-thumb is that 5° can be gained for one PO, yet is it unknown if this target is accurate, if sequential POs are additive, and if the loading curve is altered due to the releases.

2.4 Biomechanical Spine Testing

Biomechanical effects of spine-related medical devices and surgical procedures are often understood through testing of cadaveric spines. Currently accepted methods for conducting mechanical testing of non-pathologic cadaveric spines in a way that is physiologically relevant,

as first discussed by Panjabi and later by Wilke, include unconstrained superior motion and application of pure moments in bending and axial rotation [19, 20]. In recent years, the abilities to test in continuous motion and to accommodate larger specimens which may include whole spinal regions or thoracic segments with attached ribs have been shown to be beneficial [21, 22]. Researchers currently utilize a range of test systems to conduct cadaveric spine testing [20, 23-26], but there currently exists no single commercially-available automated mechanical test machine that provides for all of the spinal testing recommendations.

Current test machines can be classified into two categories: manual and automated. Manual testing systems utilize pulley-and-weight systems to discretely load a proximally unconstrained specimen. The systems are typically designed and constructed by the user, so error and repeatability issues within these systems are rarely accounted for or documented. Automated test machines utilize adapted or novel robotic machines to continuously load specimens, but errors within these machines and loading constraints are not often measured.

Testing is performed in lateral bending (LB), flexion-extension (FE), and axial rotation (AR). Figure 2.1 depicts an FSU with the three modes of bending. The main parameters that are considered in spine testing as first described by Panjabi et al. and further explained by Wilke et al. [19, 20] are:

- *Range-of-motion (ROM):* the sum of the neutral zone and the elastic zone in one direction of motion, measured in degrees.
- *Neutral zone (NZ):* "the region of intervertebral motion around the neutral posture where little resistance is offered by the passive spinal column," measured in degrees.
- *Elastic zone (EZ):* "the deformation measured from the end of the neutral zone to the point of maximal loading," measured in degrees.

- *Neutral zone stiffness (NZS):* the slope of the load-displacement curve within the NZ, measured in Nm/degree or degrees/Nm.

- *Elastic zone stiffness (EZS):* the slope of the load-displacement curve within the EZ, measured in Nm/degree or degrees/Nm.

Figure 2.6 shows a diagram of a typical loading curve to better explain the relationship between the five measured parameters. The NZ and NZS have been shown to be clinically relevant as they greatly affect stability and will change with injury or muscle weakening [27]. The EZ and EZS correspond to the behavior of the spinal segment at the limits of the ROM. These five parameters are typically reported for lumbar and cervical spine testing, but due to limitations in data collection hardware, software, and methodology, thoracic spine researchers typically focus only on the overall ROM, creating a gap of knowledge in the field of thoracic spine biomechanics.

Analysis methods for determining LB, FE, and AR vary widely, but the most common techniques include the projection method and the Euler method [28]. The Euler method has been shown to closely predict both in-plane (primary) and out-of-plane (secondary) motions, though there is a need to standardize the analysis method in the field so that results from different studies can be more easily compared. Researchers develop local coordinate systems based on anatomical points on the vertebrae to find both out-of-plane and in-plane rotations of a specific vertebrae [29]. Because of the nature of thoracic spine testing with an intact rib cage, modifications to these techniques were developed to define local coordinate systems on thoracic vertebrae. Appendix A explains in detail the data analysis techniques utilized in this study.

2.5 Current Ponte Osteotomy Studies

The popularity of utilizing POs in surgery has increased in the past few years, so biomechanical evaluation of the procedure is limited. Sangiogorio et al. recently analyzed the quantitative correction potential for Ponte osteotomies in the treatment of rigid AIS by testing five human cadaveric thoracic specimens (T1-T6 or T7-T12) with rib segments (not full ribs). In this limited study, it was found that one PO resulted in increases up to 1.6° in flexion and 2.8° in AR ROM per PO, and overall flexibility increasing by 69 $\pm$ 39 percent [21]. However, the cadaveric models utilized in this study were not full, intact thoraxes, and ROM was the only parameter analyzed. Weimann et al. found in a four specimen cadaveric study, that a single PO decreased the torque required for a 25° axial deflection by 18 percent, though the torque was applied by hand rather than in a standard test machine [30]. The study, however, only reports ROM in AR and excludes FE and LB.

2.6 Current Thoracic Spine Testing Methods

The main problems with current PO studies and in thoracic spine testing in general are that the cadaveric specimens are not full thoracic sections with intact ribs and thoracic spine researchers tend to ignore the shape of the load-displacement curve and focus only on the ROM parameter. To address the first point, it is known that the rib cage provides significant stability for the thoracic region [31-33], yet researchers are often not using those intact ribs in cadaveric models to answer biomechanical questions. In one of the most thorough studies published on the subject, Watkins et al. found that the rib cage provides 31.4 percent of thoracic stiffness in AR, 35.4 percent of stiffness in LB, and 39.8 percent of stiffness in FE [33]. While these parameters show the stiffness contribution based on ROM and provide a *basic* understanding of rib cage

contribution, they do not tell the whole story of the changes in loading due to the rib cage. NZ, EZ, NZS, and EZS are not reported, and the testing was conducted to a low load of 2 Nm. It is necessary that the thoracic spine biomechanical testing community better understands (1) the implications associated with utilizing cadaveric models that do or do not include a full torso with intact rib cage and (2) the entire story of the biomechanical contribution of the rib cage in thoracic spine testing by analyzing changes in not only ROM, but also in NZ, EZ, NZS, and EZS.

2.7 Current Test Machine Limitations

While it is agreed that the rib cage significantly impacts the biomechanics of the thoracic spine, one reason that most researchers do not test with the entire intact thorax is due to limitations in test machines. The parameters required to conduct full thoracic spine and rib cage cadaveric testing include: unconstrained superior motion, application of pure moments, clearance for large specimens, nearly 360^0 of access to the specimen, and continuous loading capabilities. There are no commercially available test machines that provide all of these benefits, so the few researchers who have conducted full thoracic and rib cage testing have modified or developed one-of-a-kind test machines. One problem with these custom-built machines is that they are not validated with any standard procedures to ensure that the results are correct, so there is a need in the field for a validated spine test system that is commercially available.

Applied Test Systems (ATS) is a mechanical test system company that was founded in 1965 by The University of Kansas (KU) alumnus, Norm Carroll. This company provides commercial test equipment for mechanical applications ranging from asphalt testing to pipe pressure testing. After understanding the need for a spine test machine that can accommodate

12

testing for a diverse range of cadaveric specimens, ATS has been collaborating with Dr. Lisa Friis and the Spine Biomechanics Lab at KU since 2009 to develop such a system. Through five design iterations and associated testing, a final design has been implemented and <u>validation of the Applied Test Systems Spine Tester (ATSST) must be completed to ensure accurate testing results.</u> The ATSST should be designed to allow for testing of the three spine regions: cervical, thoracic, and lumbar. Each of these regions has different bending and torsional stiffness ranges, and the ATSST machine must accommodate all of these specimen types.

2.8 Background Summary

The biomechanical impact of sequential POs have not been fully quantified in a cadaveric model with a full thoracic spine with intact rib cage, yet the procedures are being used clinically; chapter 6 will address this problem [38]. Current biomechanical test methods in the thoracic spine may be inadequate because they do not include a full thoracic spine and intact rib cage, and researchers are focusing exclusively on ROM, ignoring NZ, EZ, NZS, and EZS; chapters 4 and 5 will address these issues [36, 37]. Current commercial mechanical test machines do not allow for full thoracic spine testing with an intact rib cage without significant and invalidated modifications. The ATSST provides a solution to the problem, but should be validated to ensure reliable displacement results; chapter 3 will address this need [35].

2.9 References

[1] Kurtz, S. M., and Edidin, A., 2006, Spine Technology Handbook, Academic Press, Burlington, MA, USA.

[2] Asher, M. A., and Burton, D. C., 2006, "Adolescent idiopathic scoliosis: natural history and long term treatment effects," Scoliosis, 1(1), p. 2.

[3] Payne, W. K., 3rd, Ogilvie, J. W., Resnick, M. D., Kane, R. L., Transfeldt, E. E., and Blum, R. W., 1997, "Does scoliosis have a psychological impact and does gender make a difference?," Spine, 22(12), pp. 1380-1384.

[4] Alborghetti, A., Scimeca, G., Costanzo, G., and Boca, S., 2008, "The prevalence of eating disorders in adolescents with idiopathic scoliosis," Eating disorders, 16(1), pp. 85-93.

[5] Pratt, R. K., Burwell, R. G., Cole, A. A., and Webb, J. K., 2002, "Patient and parental perception of adolescent idiopathic scoliosis before and after surgery in comparison with surface and radiographic measurements," Spine, 27(14), pp. 1543-1550; discussion 1551-1542.

[6] Weinstein, S. L., Dolan, L. A., Spratt, K. F., Peterson, K. K., Spoonamore, M. J., and Ponseti, I. V., 2003, "Health and function of patients with untreated idiopathic scoliosis: a 50-year natural history study," JAMA : The Journal of the American Medical Association, 289(5), pp. 559-567.

[7] Mayo, N. E., Goldberg, M. S., Poitras, B., Scott, S., and Hanley, J., 1994, "The Ste-Justine Adolescent Idiopathic Scoliosis Cohort Study. Part III: Back pain," Spine, 19(14), pp. 1573-1581.

[8] Danielsson, A. J., Cederlund, C. G., Ekholm, S., and Nachemson, A. L., 2001, "The prevalence of disc aging and back pain after fusion extending into the lower lumbar spine. A matched MR study twenty-five years after surgery for adolescent idiopathic scoliosis," Acta radiologica (Stockholm, Sweden : 1987), 42(2), pp. 187-197.

[9] Weinstein, S. L., Zavala, D. C., and Ponseti, I. V., 1981, "Idiopathic scoliosis: long-term follow-up and prognosis in untreated patients," The Journal of bone and joint surgery. American volume, 63(5), pp. 702-712.

[10] Nachemson, A. L., and Peterson, L. E., 1995, "Effectiveness of treatment with a brace in girls who have adolescent idiopathic scoliosis. A prospective, controlled study based on data from the Brace Study of the Scoliosis Research Society," The Journal of bone and joint surgery. American volume, 77(6), pp. 815-822.

[11] Arlet, V., and Schlenzka, D., 2005, "Scheuermann's kyphosis: surgical management," European spine journal : official publication of the European Spine Society, the European Spinal Deformity Society, and the European Section of the Cervical Spine Research Society, 14(9), pp. 817-827.

[12] KH, S., 1964, "Scheuermann's Juvenile Kyphosis: Clinical Appearances," Radiography, Aetiology, and Prognosis.

[13] Lonner, B. S., Newton, P., Betz, R., Scharf, C., O'Brien, M., Sponseller, P., Lenke, L., Crawford, A., Lowe, T., Letko, L., Harms, J., and Shufflebarger, H., 2007, "Operative management of Scheuermann's kyphosis in 78 patients: radiographic outcomes, complications, and technique," Spine, 32(24), pp. 2644-2652.

[14] Murray, P. M., Weinstein, S. L., and Spratt, K. F., 1993, "The natural history and long-term follow-up of Scheuermann kyphosis," The Journal of bone and joint surgery. American volume, 75(2), pp. 236-248.

[15] Fon, G. T., Pitt, M. J., and Thies, A. C., Jr., 1980, "Thoracic kyphosis: range in normal subjects," AJR. American journal of roentgenology, 134(5), pp. 979-983.

[16] Sachs, B., Bradford, D., Winter, R., Lonstein, J., Moe, J., and Willson, S., 1987, "Scheuermann kyphosis. Follow-up of Milwaukee-brace treatment," The Journal of bone and joint surgery. American volume, 69(1), pp. 50-57.

[17] Geck, M. J., Macagno, A., Ponte, A., and Shufflebarger, H. L., 2007, "The Ponte procedure: posterior only treatment of Scheuermann's kyphosis using segmental posterior shortening and pedicle screw instrumentation," J Spinal Disord Tech, 20(8), pp. 586-593.

[18] Ponte, A., Siccardi, G., and Ligure, P., 1995, "Posterior shortening procedure by segmental closing wedge resections," Journal of pediatric orthopedics, 15, p. 404.

[19] Wilke, H. J., Wenger, K., and Claes, L., 1998, "Testing criteria for spinal implants: recommendations for the standardization of in vitro stability testing of spinal implants," European spine journal : official publication of the European Spine Society, the European Spinal Deformity Society, and the European Section of the Cervical Spine Research Society, 7(2), pp. 148-154.

[20] Panjabi, M. M., Krag, M. H., and Goel, V. K., 1981, "A technique for measurement and description of three-dimensional six degree-of-freedom motion of a body joint with an application to the human spine," J Biomech, 14(7), pp. 447-460.

[21] Sangiorgio, S. N., Borkowski, S. L., Bowen, R. E., Scaduto, A. A., Frost, N. L., and Ebramzadeh, E., 2013, "Quantification of Increase in Three-dimensional Spine Flexibility Following Sequential Ponte Osteotomies in a Cadaveric Model," Spine Deformity, 1(3), pp. 171-178.

[22] Goertzen, D. J., Lane, C., and Oxland, T. R., 2004, "Neutral zone and range of motion in the spine are greater with stepwise loading than with a continuous loading protocol. An in vitro porcine investigation," J Biomech, 37(2), pp. 257-261.

[23] Kelly, B. P., and Bennett, C. R., 2013, "Design and validation of a novel Cartesian biomechanical testing system with coordinated 6DOF real-time load control: application to the lumbar spine (L1-S, L4-L5)," J Biomech, 46(11), pp. 1948-1954.

[24] Goel, V. K., Clark, C. R., McGowan, D., and Goyal, S., 1984, "An in-vitro study of the kinematics of the normal, injured and stabilized cervical spine," J Biomech, 17(5), pp. 363-376.

[25] Wilke, H. J., Drumm, J., Haussler, K., Mack, C., Steudel, W. I., and Kettler, A., 2008, "Biomechanical effect of different lumbar interspinous implants on flexibility and intradiscal pressure," European spine journal : official publication of the European Spine Society, the European Spinal Deformity Society, and the European Section of the Cervical Spine Research Society, 17(8), pp. 1049-1056.

[26] Ilharreborde, B., Zhao, K., Boumediene, E., Gay, R., Berglund, L., and An, K. N., 2010, "A dynamic method for in vitro multisegment spine testing," Orthopaedics & traumatology, surgery & research : OTSR, 96(4), pp. 456-461.

[27] Panjabi, M. M., 1992, "The stabilizing system of the spine. Part II. Neutral zone and instability hypothesis," Journal of spinal disorders, 5(4), pp. 390-396; discussion 397.

[28] Crawford, N. R., Yamaguchi, G. T., and Dickman, C. A., 1996, "Methods for determining spinal flexion/extension, lateral bending, and axial rotation from marker coordinate data: Analysis and refinement," Human Movement Science, 15(1), pp. 55-78.

[29] Wilke, H. J., Jungkunz, B., Wenger, K., and Claes, L. E., 1998, "Spinal segment range of motion as a function of in vitro test conditions: effects of exposure period, accumulated cycles, angular-deformation rate, and moisture condition," The Anatomical record, 251(1), pp. 15-19.

[30] Wiemann, J., Durrani, S., and Bosch, P., 2011, "The effect of posterior spinal releases on axial correction torque: a cadaver study," Journal of children's orthopaedics, 5(2), pp. 109-113.

[31] Oda, I., Abumi, K., Cunningham, B. W., Kaneda, K., and McAfee, P. C., 2002, "An in vitro human cadaveric study investigating the biomechanical properties of the thoracic spine," Spine, 27(3), pp. E64-70.

[32] Brasiliense, L. B., Lazaro, B. C., Reyes, P. M., Dogan, S., Theodore, N., and Crawford, N. R., 2011, "Biomechanical contribution of the rib cage to thoracic stability," Spine, 36(26), pp. E1686-1693.

[33] Watkins, R. t., Watkins, R., 3rd, Williams, L., Ahlbrand, S., Garcia, R., Karamanian, A., Sharp, L., Vo, C., and Hedman, T., 2005, "Stability provided by the sternum and rib cage in the thoracic spine," Spine, 30(11), pp. 1283-1286.

[34] Weinstein, S. L., Dolan, L. A., Cheng, J. C., Danielsson, A., and Morcuende, J. A., 2008, "Adolescent idiopathic scoliosis," Lancet, 371(9623), pp. 1527-1537.

[35] Mannen, E. M., Ranu, S. S., Villanueva, A. M., and Friis, E. A., 2015, "Validation of a Novel Spine Test Machine," J Med Dev, 9(1).

[36] Mannen, E. M., Anderson, J. T., Arnold, P. M., and Friis, E. A., 2014, "Mechanical Analysis of a Human Cadaveric Thoracic Spine with Intact Rib Cage," J Biomech (Under Review).

[37] Mannen, E. M., Anderson, J. T., Arnold, P. M., and Friis, E. A., 2014, "Mechanical Contribution of the Rib Cage in the Cadaveric Thoracic Spine," Spine (Under Review).

[38] Mannen, E. M., Anderson, J. T., Arnold, P. M., and Friis, E. A., 2014 (Under Revision), "Overall and Regional Range-of-Motion Analysis of Sequential Ponte Osteotomies on a Human Thoracic Cadaver with an Intact Rib Cage."

2.10 Figures
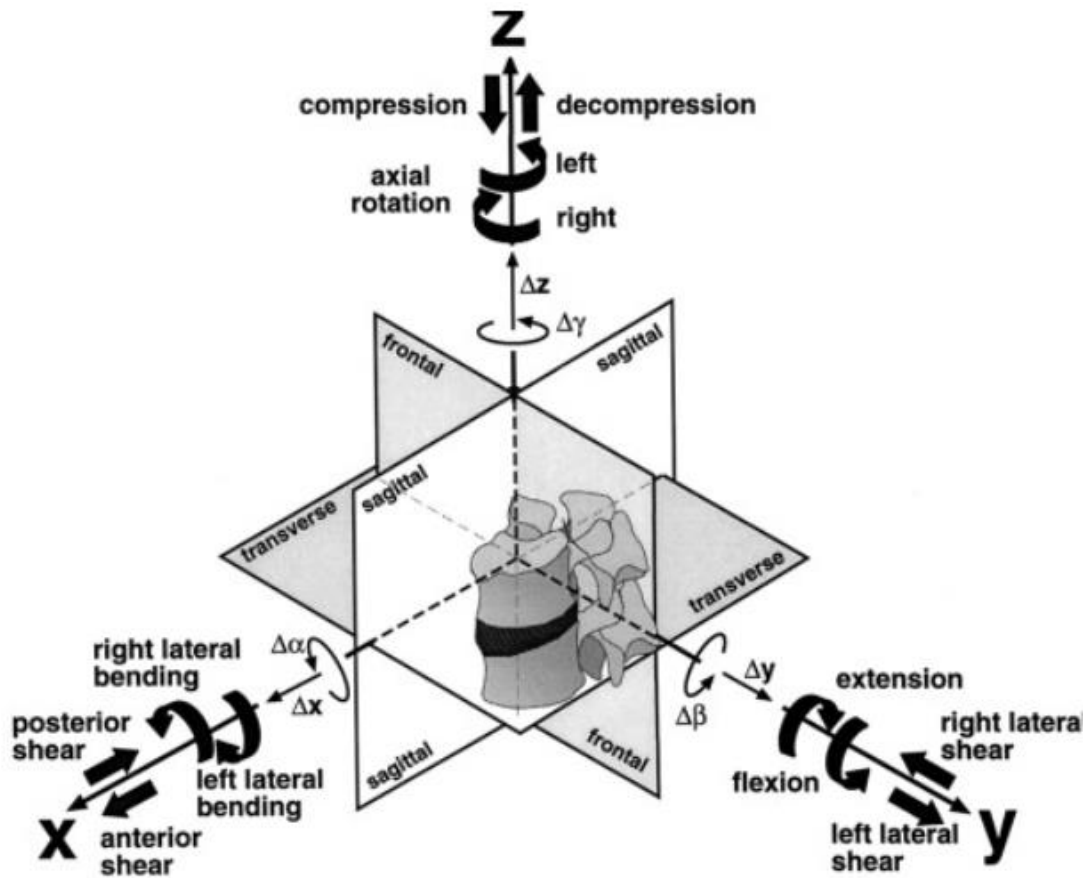
Figure 2.1: Schematic of two vertebral levels with associated rotations (right and left lateral bending, flexion and extension, and right and left axial rotation) and body planes (frontal or coronal, sagittal, and transverse) [19]. Image reprinted with permission of Springer©.
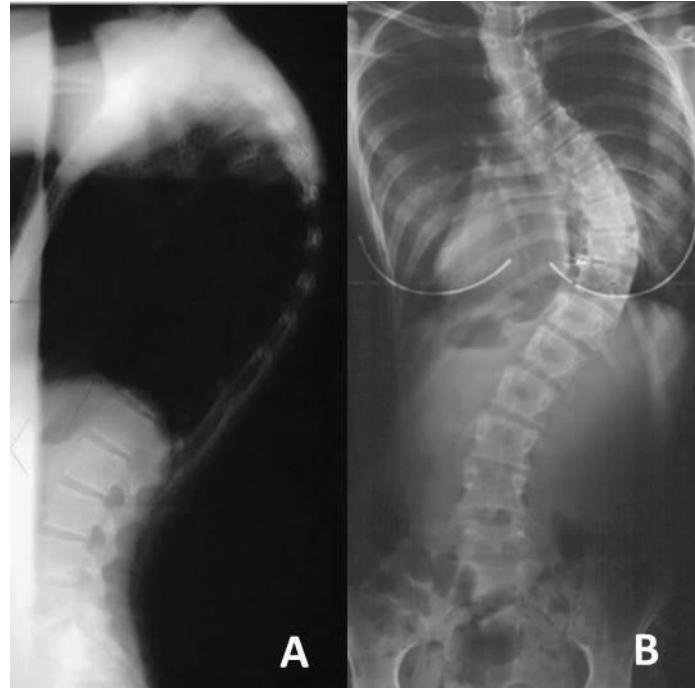
Figure 2.2: Radiographs of a person with Scheuermann's Kyphosis (A) and a person with adolescent idiopathic scoliosis (B) [17, 34]. Reprinted with the permissions of Lippincot, Williams, and Wilkins© and Lancet Publishing Group©.
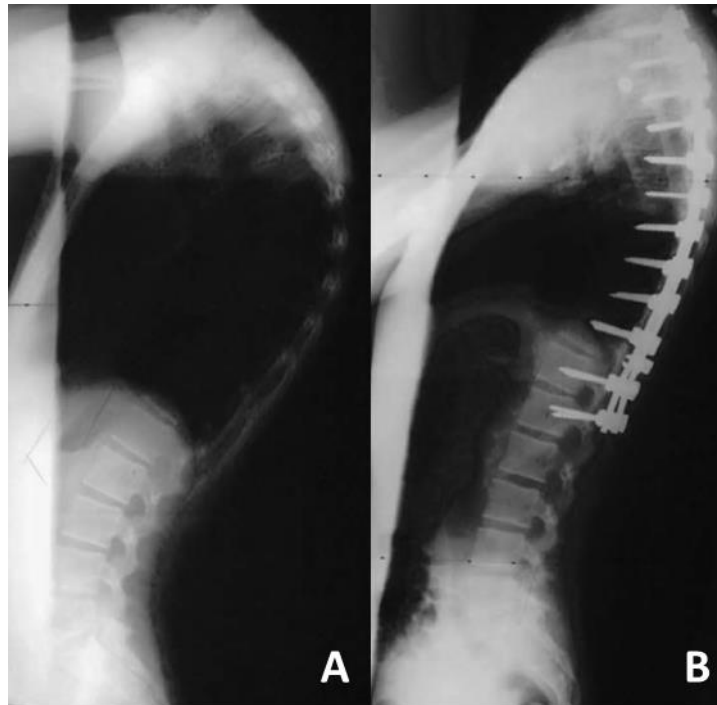
Figure 2.3: Radiographs of a person with Scheuermann's Kyphosis before (A) and after (B) spinal fusion corrective surgery [34]. Reprinted with the permission of Lancet Publishing Group©.

Figure 2.4: Sagittal and frontal radiographs of a person with adolescent idiopathic scoliosis before (A and B) and after spinal fusion surgery (C and D) [34]. Reprinted with the permission of Lancet Publishing Group©.

Figure 2.5: Depiction of a four-level Ponte osteotomy from the posterior (A) and left lateral (B) views showing the removal of the posterior spinous process, the ligamentum flavum, and the facets [17]. Reprinted with the permission of Lippincot, Williams, and Wilkins©.
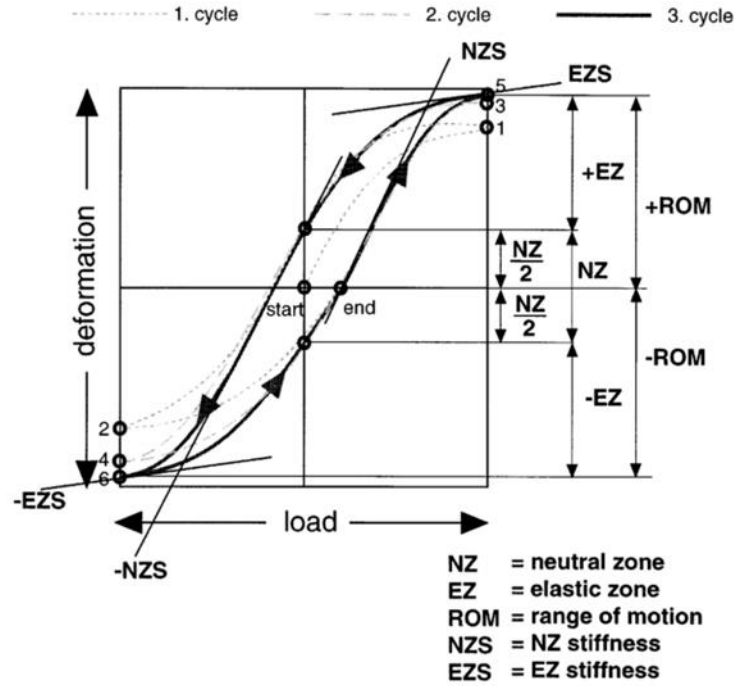
Figure 2.6: Schematic of an angular deformation v. load curve with associated measures including range of motion (ROM), neutral zone (NZ) elastic zone (EZ), NZ stiffness, and EZ stiffness [19]. Image reprinted with permission of Springer©.

CHAPTER 3:

Validation of a Novel Spine Test Machine

Manuscript accepted into the Journal of Medical Devices.

This study presents the design and usage of a novel method of evaluating a spine test machine. Erin Mannen had primary responsibility for the experimental design, data collection, data analysis, writing of the first draft, and editing as recommended by the peer-review process of the Journal of Medical Devices.

Validation of a Novel Spine Test Machine

Erin M. Mannen[1], Sahibjit S. Ranu[2], Ana M. Villanueva[1], Elizabeth A. Friis[1]*

[1] *The University of Kansas, Mechanical Engineering, 1530 W 15th St., Learned Hall Room 3138,*

Lawrence, KS 66045

[2] *The University of Kansas, Bioengineering Graduate Program, 1530 W 15th St., Learned Hall*

Lawrence, KS 66045

* Corresponding author, lfriis@ku.edu

Abstract

A novel spine test machine was developed for physiological loading of spinal segments. It can be used in conjunction with external motion-capture systems (EMCS) to measure angular displacement, but can also measure in-plane rotations directly, though the inherent error is unknown. This study quantified error inherent in the displacement measurement of the machine. Synthetic specimens representative of cadaveric spinal specimens were tested.   Machine displacement was compared to EMCS displacement. The maximum machine displacement error was <2° for lumbar and thoracic specimens. The authors suggest that researchers use EMCS in conjunction with the test machine when high accuracy measurements are required.

3.1 Introduction

A novel test machine was designed and developed to accomplish pure-moment loading of spinal segments in a single plane. Because a calibrated torque transducer applies the load directly to the specimen, the test machine can confidently be used in conjunction with an external motion-capture system to load and measure the displacement of spinal specimens. The spine test machine can also independently measure angular displacement in the loading plane in real-time without the need for an external motion-capture system. The goal of this study was to understand and quantify the error in the angular displacement output of the spine test machine. Quantification of the error would allow researchers to confidently use the product to gather meaningful real-time overall angular displacement data on the biomechanical impact of spine-related medical devices or surgical procedures in all regions of the spine. A secondary goal of this study was to identify a new method of analyzing overall displacement error in new spine test machines for the purpose of suggesting a standard procedure that could be applied in the analysis of other machines. This would provide the spine testing community with a standard and repeatable method with which to compare the error of test systems.

Biomechanical effects of spine-related medical devices and surgical procedures are often understood through testing of cadaveric spines. Currently accepted methods for conducting mechanical testing of non-pathologic cadaveric spines in a way that is physiologically relevant, as first discussed by Panjabi and later by Wilke, include unconstrained superior motion and application of pure moments in bending and axial rotation [1-3]. In recent years, the abilities to test in continuous motion and to accommodate larger specimens which include whole spinal regions or thoracic segments with attached ribs have been shown to be beneficial [4, 5]. Researchers currently utilize a range of test systems to conduct cadaveric spine testing [1, 6-9],

but there currently exists no single commercially-available automated mechanical test machine that provides for all of the spinal testing recommendations.

Current test machines can be classified in two categories: manual and automated. Manual testing systems utilize pulley-and-weight systems to discretely load a proximally unconstrained specimen. The systems are typically designed and constructed by the user, so error and repeatability issues within these systems are rarely accounted for or documented. Automated test machines utilize adapted or novel robotic machines to continuously load specimens, but error within these machines and loading constraints are not often measured. The test machine examined in this study seeks to provide a simple solution for the spine testing field. Since the test machine incorporates a calibrated torque transducer that directly loads the specimen in a single plane, the machine can currently be used with confidence in conjunction with an external motion-capture system. However, because the machine can be used independently to measure in-plane rotations, understanding the displacement error inherent in the machine will enhance overall user ability and confidence in testing spine segments and other cadaveric specimens appropriately.

3.2 Methods

3.2.1. The System

The authors worked with Applied Test Systems (Butler, PA, USA) to develop an automated test machine that continuously applied a pure moment on a spinal specimen through a range-of-motion consistent with current spinal testing practices. The design requirements of the system included: (1) application of a continuous pure moment in bending and axial rotation with real-time in-plane angular displacement feedback, (2) control over rate of load or displacement

27

so as to respect the viscoelastic nature of cadaveric specimens, (3) ability to test under load or displacement control to a specific load or displacement, (4) synched continuous data acquisition capability from a motion-capture system, and (5) ability to easily change between bending and axial rotational loading without altering the specimen experimental setup.

The machine included separate drive assemblies (one for bending, one for axial rotation) to transmit pure moments in one plane to a test specimen via a calibrated torque transducer (Interface Mfg, Scottsdale, AZ, USA). A three-dimensional, low-friction sliding mechanism and a universal joint allowed the moment to be applied at a range of angles at the superior end of a free-standing specimen, avoiding an artificially-constrained experimental setup. The mounting systems allowed the drive assemblies to follow the natural movement of the specimen as it was bent or rotated in response to the applied load [10]. Although not included in the current test system, a 6 degree-of-freedom (DOF) load cell was rigidly attached to the loading platform to gain a basic understanding of out-of-plane moments on a rigid steel post to confirm pure moment loading. Figure 3.1A is a photo of the entire spine test machine. The upper arm applies axial rotation load and the lower arm attached to the specimen applies a bending load. Figure 3.1B and Figure 3.1C are close-up photos of the axial rotation and the bending drive assemblies attached to specimens, respectively. Either drive assembly can be applied separately and can be changed between loading modes without disrupting or moving the specimen by utilizing quick-release mechanisms to detach the assembly from the specimen and rotate the bending or axial rotation arm. The software package collects and records time, load, and in-plane angular displacement as measured by the spine test machine. Users have the option of utilizing an external motion tracking system which can by synched with the spine test machine software to provide additional motion output.

3.2.2. Study Overview

In-plane displacement accuracy of the spine test machine was measured for specimen rigidities that represented the range of typical cadaveric spine specimens. Cervical, thoracic, and lumbar spine specimens exhibit different axial rotation and bending stiffness ranges. Segments from each spinal region were modeled with solid polyurethane rods that represented the range of cadaveric physiological rigidities reported in the literature [6, 11-20]. A repeatability study was conducted to ensure consistency in testing. Data from an external motion-capture system and displacement data from the spine test machine were collected and compared in bending and axial rotation for each rigidity range to determine the inherent error within the spine test machine at each rigidity range.

3.2.2.1. Synthetic Specimen Manufacturing

To measure the accuracy of the machine, synthetic specimens representative of the cadaveric rigidity ranges were constructed. Bending and axial rotation stiffness ranges of spinal cadaveric specimens that could be tested in the machine were gathered from published literature. Bending and axial rotation stiffness ranges that have been reported in literature for cervical, thoracic, and lumbar spinal segments are shown in **Table 3.1** [6, 11-20]. These ranges served as the target bending and axial rotation stiffness ranges for the synthetic specimens. By creating synthetic specimens that fell into each of these ranges [stiff (lumbar), moderate (thoracic), and flexible (cervical)], the machine could be validated on representative synthetic specimens to ensure data accuracy and repeatability for the range of cadaveric spinal specimens.

In order to reduce variability in synthetic specimens, each was the same material, length, and cross-sectional shape. The material chosen for the synthetic specimens was polyurethane

due to the range of geometries, stability over time, and availability of the material in various durometers. A 15.2 cm (6.00") length was determined to be an acceptable length for the specimens based on average heights of cadaveric specimens that are currently tested. A 15.2 cm (6.00") synthetic specimen length represented a compromise between a much shorter functional spinal unit length and a much longer full lumbar spinal segment. Rod lengths were measured with digital calipers to ensure that the lengths were within ±0.635 cm (0.250") of the 15.2 cm (6.00") length. A solid cylinder was chosen as the cross-sectional shape of the synthetic specimens to avoid buckling issues, so it was necessary to change the diameter of the synthetic specimens to accurately replicate each rigidity range.

Polyurethane rods of a 90 Shore A durometer (McMaster-Carr Supply Co., Elmhurst, IL, USA) with diameters of 3.18 cm (1.25"), 4.45 cm (1.75"), and 6.35 cm (2.50") were chosen to best represent flexible (cervical), moderate (thoracic), and stiff (lumbar) spinal specimens based on target bending rigidity ranges. Diameters of 4.45 cm (1.75"), 6.35 cm (2.50") and 7.62 cm (3.00") were chosen to best represent flexible (cervical), moderate (thoracic), and stiff (lumbar) spinal specimens based on target axial rotation stiffness ranges. Error inherent in the specimens was up to ±5 Shore A durometer, ±0.127 cm (0.0500") diameter, and ±0.635 cm (0.250") length. Rod diameters were measured with digital calipers at five locations and two rotations along the length of the rod to ensure that the diameters were consistent and within 0.127 cm (0.0500") of the acceptable diameter range. Theoretical error calculations were performed to determine how tolerance error within the specimens would contribute to overall theoretical stiffness.

Each rod surface was roughened for 1.91 cm (0.750") on each end and screws were inserted in each end to aid in bonding of the rod with auto-body filler potting (3M, St. Paul, MN, USA) as is commonly done in cadaveric spine testing. Five specimens were manufactured for

each of the targeted rigidity range. Figure 3.2 depicts a completed stiff (lumbar) synthetic specimen loaded in the spine test machine bending mode with an optical motion-capture research pin inserted into the top potting.

3.2.2.2. Repeatability Study

The purpose of this study was to determine if the specimen behavior was repeatable. One bending specimen [stiff (lumbar)] and one axial rotation [moderate (thoracic)] specimen were loaded independently for five trials to ± 15 Nm at a displacement rate of 0.5 degrees per second for five cycles per trial with at least five minutes between trials. It was assumed that the repeatability of the specimen behavior would be consistent among different specimen diameters, so only one specimen was tested in each bending and axial rotation. As reported in the literature, cadaveric spinal specimens are typically loaded to a maximum of 15 Nm at a displacement rate between 0.5 and 5 degrees per second; test parameters in this study were selected to mimic cadaveric testing conditions [21]. An optical motion tracking research pin (Northern Digital Inc., Waterloo, ON, Canada) was used to track the motion of the superior end of each specimen. Error in the motion tracking diodes is ± 0.1 mm (0.004") which results in up to ± 0.06 degrees for the research pin. It was therefore assumed that the data collected from the pin represented the actual displacement of the specimen. Figure 3.2 shows the test setup for the stiff (lumbar) bending repeatability test. Torque was recorded from the spine test machine, and displacement data was recorded from the optical motion-capture research pin and the spine test machine. In accordance with standard spine testing practice, the third cycle of the data was analyzed at 10 target load ranges between -15 Nm and 15 Nm on the load-displacement graph [3]. Load ranges were chosen based on typical ranges used in a variety of cadaveric test configurations. The

stiffness of a synthetic specimen was defined as the maximum load in Newton-meters divided by the maximum displacement in degrees. Stiffness values were found for each specimen during each trial. The mean and standard deviation of the measured rigidity of the specimens were calculated using the optical motion-capture research pin displacement data. Error was defined as the average maximum absolute difference between the spine test machine displacement data and the optical motion tracking research pin displacement data at each of the 10 target load ranges. One-way ANOVA was performed to determine if the results between individual trials were significantly different at $p<0.05$.

3.2.2.3. Stiffness and Error Study

Stiffness values and displacement error in the spine test machine were determined at each rigidity range in both bending and axial rotation. Five specimens of all rigidities [stiff (lumbar), moderate (thoracic), and flexible (cervical)] were tested in both bending and axial rotation for five cycles at a displacement rate of 0.5 degrees per second to a load limit of ±15 Nm. An optical motion tracking research pin was used to track the motion of the superior end of each specimen. Data collected from the pins represented the actual displacement of the specimen. The third cycle of the optical motion-capture data was used in the stiffness calculations. The stiffness of a synthetic specimen was defined as the maximum applied load (15 Nm) divided by the maximum displacement in degrees. Stiffness values were found for all rigidity ranges in both bending and torsion, and compared to cadaveric stiffness values reported in the literature.

The third cycle of the spine test machine displacement data was compared with optical motion-capture research pin displacement data at 10 target load ranges between -15 Nm and 15 Nm on the load-displacement graph to determine the displacement error inherent in the spine test

machine. The mean and standard deviation of the measured rigidities of the specimens were calculated using pin displacement data, and a post hoc power analysis was performed. Error was defined as the average maximum absolute difference between the spine test machine displacement data and the pin displacement data at each of the 10 target load ranges. Data was compared using load v. displacement graphs to show the difference between the pin displacement data and spine test machine data in a typical cycle.

3.3. Results

Six DOF load cell results confirmed that pure moment loading was achieved with up to 4.5 percent out-of-plane moments. A parametric analysis revealed that this error could have been generated by only 2.5 degrees of misalignment between the loading axis of the specimen and the axis of the loading mechanism.

3.3.1 Repeatability Study Results

The lengths of all rods were found to be within ± 0.635 cm (0.250") of 15.2 cm (6.00"), and the diameters of all rods were found to be within 0.127 cm (0.0500") of the acceptable diameter range. The theoretical error analysis revealed that error in the diameter would cause the greatest error. Since the diameters of all specimens fell within the tolerance range, all rods were therefore considered acceptable for use in the manufacturing of the synthetic samples.

Stiffnesses of the synthetic bending stiff (lumbar) specimens and the axial rotation moderate (thoracic) specimens were 2.90 ± 0.0035 and 5.52 ± 0.030 Nm/degree, respectively, resulting in standard deviations of 0.12 and 0.54 percent of the means, respectively. One-way

ANOVA testing showed no significant difference between the errors found in the trials either in bending [$F(4,45) = 0.0875$, $p = 0.986$], or axial rotation [$F(4,45) = 0.0393$, $p = 0.997$].

3.3.2 Stiffness and Error Study Results

The bending stiffnesses for the stiff (lumbar), moderate (thoracic), and flexible (cervical) synthetic specimens were found to be 4.71 ± 0.50, 1.28 ± 0.020, and 0.262 ± 0.022 Nm/degree, respectively. The axial rotation stiffnesses for the stiff (lumbar), moderate (thoracic), and flexible (cervical) synthetic specimens were found to be 6.41 ± 0.35, 3.02 ± 0.32, and 0.737 ± 0.041 Nm/degree, respectively. Figure 3.3 shows where each of these values fall within the stiffness ranges of cadaveric spine specimens reported in literature. A power greater than 0.9 was achieved for all tests.

Typical load-displacement graphs are depicted in Figure 3.4 for bending (Figure 3.4A) and axial rotation (Figure 3.4B). The solid lines represent the actual displacements of the synthetic specimens as measured by the optical motion-capture research pins, while the dashed lines represent the displacements measured directly by the spine test machine. The absolute difference between the two lines represents the displacement error inherent in the spine test machine.

The error, defined as the average maximum absolute difference between the spine test machine displacement data and the pin displacement data at 10 target load ranges, is depicted in Figure 3.5 for bending (Figure 3.5A) and axial rotation (Figure 3.5B). The greatest errors in bending and axial rotation occurred in the flexible (cervical) trials. The maximum errors found in bending for stiff (lumbar), moderate (thoracic), and flexible (cervical) were 1.22, 1.29, and 6.42 degrees, respectively. The maximum errors found in axial rotation for stiff (lumbar),

moderate (thoracic), and flexible (cervical) were 1.76, 2.14, and 3.56 degrees, respectively. The average maximum error found in bending and axial rotation for the stiff (lumbar) and moderate (thoracic) specimens was 1.60 ± 0.43 degrees.

3.4 Discussion

The novel spine test machine allowed for a range of test capabilities on cadaveric spine specimens. The machine applied pure moments on superiorly unconstrained specimens, which allowed for continuous loading and acquisition of the specimen displacement using both machine data and an external optical motion-capture system data. Because the load is applied directly via a calibrated torque transducer, when used with the external optical motion-capture system, the spine test machine allows for accurate testing of all types of spinal cadaveric specimens. All measured stiffness values of the synthetic specimens were within the desired rigidity ranges, thus validating the assumption that the synthetic specimens accurately represented the rigidities of cadaveric specimens in bending and axial rotation for stiff (lumbar), moderate (thoracic), and flexible (cervical) regions.

Without the use of an external motion-capture system, users would depend on the real-time in-plane displacements measured by the spine test machine. The error that occurred around 0 Nm in both bending and axial rotation was expected and can be attributed to the mechanical play in the system, particularly at the universal joint which transfers the load to the specimen. When a universal joint disengages, there is a small amount of motion in the joint before it re-engages, causing the most of the error in angular displacement. Though the majority of the error in this spine test machine can be attributed to the universal joint, this type of error around the transition from positive to negative loads is inherent in all mechanical test systems. Care should

be taken in the interpretation of data during the transition between negative and positive loading, regardless of the test system used.

It is clear that the maximum errors in both bending and axial rotation occur when testing flexible (cervical) specimens (Figure 3.5). This can be attributed to the large angular displacements in bending (60.2 degrees) and axial rotation (21.2 degrees) in this experiment. These large displacements put increased strain on the mechanical components of the spine test system, resulting in larger displacement errors. It is not unreasonable to assume that the spine test machine may be more accurate when testing cervical specimens shorter than 15.2 cm (6.00") with a lower overall angular displacement, and less accurate when testing specimens longer than 15.2 cm (6.00") with a higher overall angular displacement. Additional studies should be done to understand the limits in length and angular displacement of flexible specimens that result in large error.

One limitation of the study was the use of the synthetic specimens with linear elastic properties. Spinal cadaveric specimens exhibit both nonlinear and viscoelastic behavior, with lower stiffness values occurring near the neutral zone, and higher stiffness values occurring near the limits of motion in the extension zone [3]. While cadaveric specimens are not linear elastic, utilizing linear elastic synthetic specimens in these experiments did reduce the variability in both specimen manufacturing and in test setups as confirmed by the results of the repeatability study. Utilizing controlled and reproducible specimens with known mechanical behavior allowed for the evaluation of the machine that was not influenced by the large variability in mechanical properties between cadaveric specimens. A future study could examine the error within the machine on nonlinear models of spinal specimens. Use of a recently developed synthetic analogue spine model with more physiological nonlinear mechanical behavior would give

researchers an even better understanding of the performance of the test machine on lumbar spinal specimens, and would still have the benefit of specimen repeatability that cadaveric specimens lack [22, 23].

It is known that mechanical stiffness between cadaveric specimens can vary up to 100 percent [24, 25]. With this in mind, one could speculate that two degrees or less of error is more than acceptable to obtain reasonable and valid results in some experiments. The error in the real-time displacement data is low enough for users to gain confidence that the experimental setup and specimen behavior is reasonable in most experimental designs. However, utilizing an external motion-capture system in conjunction with the spine test machine will result in accurate angular displacement measurements for all ranges of mechanical spine testing.

The displacement and loading rates of the machine depend on the in-plane rotation displacement data as read from the spine test machine. Because there is error in the angular displacement measurement of the system, there will also be error in the angular displacement and loading rates. However, it has been shown that cadaveric spinal behavior shows no difference in loading patterns across the range of typical displacement rates of 0.5 to 5.0 degrees/second [21]. In addition to the error caused by the motion in the universal joint, it should be noted that loading universal joints at large angles may alter the displacement and loading rates. Mechanical changes that would eliminate the need for a universal joint are being investigated by the manufacturers; evaluation of the performance of the new joint will be necessary. In cases where very precise angular displacement or loading rates are required, this machine should not be used. However, in the majority of cadaveric spinal experiments where small variations in the displacement or loading rates are insignificant, this machine could be used to obtain quality results.

In this study, the spine test machine was used in angular displacement rate control (0.5 degrees/ second) to a load limit ($\pm$15 Nm). This mode of testing simulates the conditions applied by manual systems, but does so with control over the rate of displacement and in continuous loading through the range of motion. Unlike manual systems, this machine also has the capability of loading a specimen to a specific displacement while continuously measuring the load. The machine can also be used in loading rate control while measuring in-plane angular displacement. While there is still debate in the field as to which method best replicates in vivo motion, this study was conducted in angular displacement rate control limited by load because many researchers with automated test machines utilize this test method [26]. A future study could examine the characteristics of the machine in loading rate control to a targeted angle with various rigidity specimens so as to measure the error on the moment applied to the specimens.

Current spine test machines fall into two categories: manual and automated. Manual spine test machines such as that developed by Goel, utilize a pulley-and-weight system to apply unconstrained discrete loads to a spinal specimen [1, 7]. It has been shown that discrete loading and continuous loading of the porcine spinal segments give significantly different results, and it can be argued that continuous loading may be more physiologically appropriate [4].

Automated spine test machines offer continuous testing capabilities, and include those that have been adapted from commercial loading systems with x-y tables or bending jigs (MTS Systems Corporation, Eden Prairie, MN, USA) and those that have been custom built for spine testing [6-9]. Adapted machines offer the benefit of accommodating other mechanical test needs within the initial system, but often have drawbacks when adapted for spine testing. The x-y table adaptation along with the initial system is too bulky to allow for testing of specimens with a large footprint, and again, error in the machine is not always well-understood or documented.

Custom-built spine test machines offer users specific benefits, but may not accommodate the large range of cadaveric spine testing stiffness ranges and sizes.

Additionally, a standard validation procedure for custom machines does not currently exist. The novel 6 degree-of-freedom robotic test machine designed by Kelly and Bennett provides many benefits to the user interested in lumbar testing, but a basic mechanical analysis of the displacement error inherent in the system has not been published to the authors' knowledge. Instead, like many other researchers, cadaveric lumbar segments were tested in the machine, and the results were compared to those reported in literature [6]. While this information is important to ensure the machine gives reasonable results when testing viscoelastic cadaveric specimens, perhaps more important would be the understanding of the machine behavior on specimens of known flexibility. It would be beneficial for the spine testing community to develop a standard protocol utilizing two specimens of each stiffness range (as suggested by an *a priori* power analysis) by which results of various types of spine testing systems could be compared on synthetic specimens.

While a 6 DOF load cell is not a part of the current test machine, users can easily modify the current loading platform to incorporate the load cell if so desired. Previous testing of the complete machine load train incorporating a 6 DOF load cell revealed that up to 4.5 percent error in out-of-plane moments could be generated, possibly from misalignment of the loading axis relative to the loading mechanism. A parametric analysis demonstrated that these moments could be accounted for by misalignment between the loading axis of the specimen and the axis of the loading mechanism of only 2.5 degrees, which is not unreasonable in cadaveric testing. Further work in analysis of the loading capabilities of the system utilizing a 6 DOF load cell to measure resultant loads is recommended for this and all spinal test systems.

Follower loads or compressive preloads are often used in cervical and lumbar spine testing to mimic physiological loading [27-32]. While this spine test machine does not include automated follower load technology, there is adequate space below the loading platform for users to manually apply follower loads using hung weights. Researchers who are considering utilizing the spine test machine displacement data rather than external motion-capture system data would need to consider the additional mechanical losses (e.g., friction) due to those follower loads.

Another parameter that is favorable in some spinal testing configurations is the ability to test in more than one mode concurrently. Some commercial test machines allow for this type of loading, but the spine testing community has yet to define the most appropriate techniques for applying such loads. Although the mechanics to accommodate combined loading of axial rotation and either flexion-extension or lateral bending are in place, the software of the novel spine test machine does not currently allow for combined loading. Once this technology has been developed, an additional study should look at the displacement errors caused by combined loading.

The overall design specifications for the spine test machine were as follows: unconstrained superior motion, application of pure moments in bending and axial rotation, clearance for large specimens, and continuous loading capabilities. To determine if these specifications were met, the spine test machine was used to test a full thoracic cadaveric specimen with an intact ribcage. Figure 3.6 shows a typical bending test setup with optical motion-capture pins at the top potting (T1) and at T6-T11. The spine test machine software syncs the external motion-capture data with the loading data to most accurately track displacement. The test machine continuously loaded the large, superiorly unconstrained cadaveric specimen in both bending and axial rotation. Transition between the flexion-

extension, lateral bending, and axial rotation loading modes was easily done without disturbing the specimen position.

The results of this study show that researchers can be confident using the spine test machine displacement data to gain a reasonable, real-time understanding of in-plane rotations with less than two degrees of error in both bending and axial rotation for moderate (thoracic) and stiff (lumbar) spine specimens for the range of typical physiological spinal loads. If a spinal testing protocol demands increased precision or the measurement of out-of-plane rotations is necessary, an external motion-capture system should be implemented in conjunction with the spine testing machine.

The benefits of the test machine should not be limited to spine testing only. Researchers in other areas of biomechanics that require unconstrained and continuous motion of cadaveric specimens could utilize the test machine. Wrist, ankle, shoulder, and hip testing present similarly complicated cadaveric testing needs when compared to the spine. With adaptations to accommodate the specific needs of these fields, the spine test machine could be used to enhance many areas of biomechanical research.

3.5 Conclusions

The novel spine test machine evaluated in this study offers solutions to physiological cadaveric spine testing for lumbar and thoracic spines with real-time in-plane displacement errors of less than two degrees in both bending and axial rotation. When used in conjunction with an external motion-capture system, accurate angular displacement results limited by the external motion-capture system itself can be obtained for cervical, thoracic and lumbar mechanical spine testing up to ± 15 Nm. The machine allows for application of unconstrained

non-pathologic physiologically-accurate pure-moment loading [1-3] on the superior end of a specimen in bending and axial rotation with real-time in-plane displacement feedback, continuous loading through the range-of-motion, load or displacement control, and flexibility to accommodate small and large specimens from all regions of the spinal column. Quantified error gives researchers more confidence in understanding and interpreting the results of cadaveric biomechanical testing. Spine researchers should consider developing a standard protocol for evaluation of error on adapted or custom-built spine testing machines to ensure results are reasonable. Further revisions of the spine test machine should be considered to improve accuracy of the displacement measurement. The novel spine test machine offers the benefit of physiological testing of spinal specimens, and has the future potential to provide solutions for many other orthopedic testing fields.

3.6 References

[1] Panjabi, M. M., Krag, M. H., and Goel, V. K., 1981, "A technique for measurement and description of three-dimensional six degree-of-freedom motion of a body joint with an application to the human spine," J Biomech, 14(7), pp. 447-460.

[2] Panjabi, M. M., Hausfeld, J. N., and White, A. A., 3rd, 1981, "A biomechanical study of the ligamentous stability of the thoracic spine in man," Acta Orthopaedica Scandinavica, 52(3), pp. 315-326.

[3] Wilke, H. J., Wenger, K., and Claes, L., 1998, "Testing criteria for spinal implants: recommendations for the standardization of in vitro stability testing of spinal implants," European Spine Journal, 7(2), pp. 148-154.

[4] Goertzen, D. J., Lane, C., and Oxland, T. R., 2004, "Neutral zone and range of motion in the spine are greater with stepwise loading than with a continuous loading protocol. An in vitro porcine investigation," J Biomech, 37(2), pp. 257-261.

[5] Sangiorgio, S. N., Borkowski, S. L., Bowen, R. E., Scaduto, A. A., Frost, N. L., and Ebramzadeh, E., 2013, "Quantification of Increase in Three-dimensional Spine Flexibility Following Sequential Ponte Osteotomies in a Cadaveric Model," Spine Deformity, 1(3), pp. 171-178.

[6] Kelly, B. P., and Bennett, C. R., 2013, "Design and validation of a novel Cartesian biomechanical testing system with coordinated 6DOF real-time load control: application to the lumbar spine (L1-S, L4-L5)," J Biomech, 46(11), pp. 1948-1954.

[7] Goel, V. K., Clark, C. R., McGowan, D., and Goyal, S., 1984, "An in-vitro study of the kinematics of the normal, injured and stabilized cervical spine," J Biomech, 17(5), pp. 363-376.

[8] Wilke, H. J., Drumm, J., Haussler, K., Mack, C., Steudel, W. I., and Kettler, A., 2008, "Biomechanical effect of different lumbar interspinous implants on flexibility and intradiscal pressure," European Spine Journal, 17(8), pp. 1049-1056.

[9] Ilharreborde, B., Zhao, K., Boumediene, E., Gay, R., Berglund, L., and An, K. N., 2010, "A dynamic method for in vitro multisegment spine testing," Orthopaedics & Traumatology, Surgery & Research : OTSR, 96(4), pp. 456-461.

[10] Carroll, N. L., Cartwright, E. C., Gephardt, R. J., Dixon, C. L., Goel, V. K., and Friis, E. A., 2013, "Simplified spine testing device," U.S. Patent Publication No. WO2013020125 A1. Washington, DC: U.S. Patent and Trademark Office.

[11] Myers, B. S., McElhaney, J. H., and Doherty, B. J., 1991, "The viscoelastic responses of the human cervical spine in torsion: experimental limitations of quasi-linear theory, and a method for reducing these effects," J Biomech, 24(9), pp. 811-817.

[12] Brodke, D. S., Gollogly, S., Alexander Mohr, R., Nguyen, B. K., Dailey, A. T., and Bachus a, K., 2001, "Dynamic cervical plates: biomechanical evaluation of load sharing and stiffness," Spine, 26(12), pp. 1324-1329.

[13] Panjabi, M. M., Goel, V. K., and Takata, K., 1982, "Physiologic strains in the lumbar spinal ligaments. An in vitro biomechanical study 1981 Volvo Award in Biomechanics," Spine, 7(3), pp. 192-203.

[14] Panjabi, M. M., Brand, R. A., Jr., and White, A. A., 3rd, 1976, "Three-dimensional flexibility and stiffness properties of the human thoracic spine," J Biomech, 9(4), pp. 185-192.

[15] Panjabi, M. M., Brand, R. A., Jr., and White, A. A., 3rd, 1976, "Mechanical properties of the human thoracic spine as shown by three-dimensional load-displacement curves," The Journal of Bone and Joint Surgery. American Volume, 58(5), pp. 642-652.

[16] Nibu, K., Panjabi, M. M., Oxland, T., and Cholewicki, J., 1997, "Multidirectional stabilizing potential of BAK interbody spinal fusion system for anterior surgery," Journal of Spinal Disorders, 10(4), pp. 357-362.

[17] Guan, Y., Yoganandan, N., Moore, J., Pintar, F. A., Zhang, J., Maiman, D. J., and Laud, P., 2007, "Moment–rotation responses of the human lumbosacral spinal column," J Biomech, 40(9), pp. 1975-1980.

[18] Crawford, N. R., Peles, J. D., and Dickman, C. A., 1998, "The spinal lax zone and neutral zone: measurement techniques and parameter comparisons," Journal of Spinal Disorders, 11(5), pp. 416-429.

[19] Hitchon, P. W., Brenton, M. D., Serhan, H., Goel, V. K., and Torner, J. C., 2002, "In vitro biomechanical studies of an anterior thoracolumbar implant," J Spinal Disord Tech, 15(5), pp. 350-354.

[20] Ogon, M., Bender, B. R., Hooper, D. M., Spratt, K. F., Goel, V. K., Wilder, D. G., and Pope, M. H., 1997, "A dynamic approach to spinal instability. Part I: Sensitization of intersegmental motion profiles to motion direction and load condition by instability," Spine, 22(24), pp. 2841-2858.

[21] Wilke, H. J., Jungkunz, B., Wenger, K., and Claes, L. E., 1998, "Spinal segment range of motion as a function of in vitro test conditions: effects of exposure period, accumulated cycles, angular-deformation rate, and moisture condition," The Anatomical Record, 251(1), pp. 15-19.

[22] Friis EA, P. C., Graber CD, Montoya JA, 2002, "Mechanical Analogue Model of the Human Lumbar Spine: Development and Initial Evaluation," Spinal Implants: Are We Evaluating Them Appropriately?, ASTM STP 1431, M. N. Melkerson, S. L. Griffith, and J. S. Kirkpatrick, Eds., ASTM International, West Conshohocken, PA.

[23] Domann JP, F. E., Mar D, Johnson A, James J, "The Analogue Spine Model: The First Anatomically and Mechanically Correct Synthetic Physical Model of the Lumbar Spine," Proc. North American Spine Society Annual meeting.

[24] McLain, R. F., Yerby, S. A., and Moseley, T. A., 2002, "Comparative morphometry of L4 vertebrae: comparison of large animal models for the human lumbar spine," Spine, 27(8), pp. E200-206.

[25] Shea, M., Edwards, W. T., White, A. A., and Hayes, W. C., 1991, "Variations of stiffness and strength along the human cervical spine," J Biomech, 24(2), pp. 95-107.

[26] Goel, V. K., Wilder, D. G., Pope, M. H., and Edwards, W. T., 1995, "Biomechanical testing of the spine. Load-controlled versus displacement-controlled analysis," Spine, 20(21), pp. 2354-2357.

[27] Patwardhan, A. G., Havey, R. M., Carandang, G., Simonds, J., Voronov, L. I., Ghanayem, A. J., Meade, K. P., Gavin, T. M., and Paxinos, O., 2003, "Effect of compressive follower preload on the flexion-extension response of the human lumbar spine," Journal of Orthopaedic Research, 21(3), pp. 540-546.

[28] Fielding, L. C., Alamin, T. F., Voronov, L. I., Carandang, G., Havey, R. M., and Patwardhan, A. G., 2013, "Parametric and cadaveric models of lumbar flexion instability and flexion restricting dynamic stabilization system," European Spine Journal, 22(12), pp. 2710-2718.

[29] Patwardhan, A. G., Havey, R. M., Ghanayem, A. J., Diener, H., Meade, K. P., Dunlap, B., and Hodges, S. D., 2000, "Load-carrying capacity of the human cervical spine in compression is increased under a follower load," Spine, 25(12), pp. 1548-1554.

[30] Fry, R. W., Alamin, T. F., Voronov, L. I., Fielding, L. C., Ghanayem, A. J., Parikh, A., Carandang, G., McIntosh, B. W., Havey, R. M., and Patwardhan, A. G., 2014, "Compressive preload reduces segmental flexion instability after progressive destabilization of the lumbar spine," Spine, 39(2), pp. E74-81.

[31] Patwardhan, A. G., Havey, R. M., Meade, K. P., Lee, B., and Dunlap, B., 1999, "A follower load increases the load-carrying capacity of the lumbar spine in compression," Spine, 24(10), pp. 1003-1009.

[32] Goel, V. K., Panjabi, M. M., Patwardhan, A. G., Dooris, A. P., and Serhan, H., 2006, "Test protocols for evaluation of spinal implants," The Journal of Bone and Joint Surgery. American Volume, 88 Suppl 2, pp. 103-109.

3.7 Acknowledgements

3.8 Funding

3.9 Tables

Table 3.1: Range of bending and axial rotation stiffness values found in cadaveric spine studies in the literature [6, 11-20]. The data ranges include studies of functional spine units and larger spinal segments both with and without instrumentation in order to best represent the scope of cadaveric spine testing.

Spinal Region	Bending (Nm/degree)	Axial Rotation (Nm/degree)
Cervical	0.33 to 2.0	0.19 to 1.76
Thoracic	0.75 to 6.7	0.75 to 1.8
Lumbar	3.1 to 16	1.8 to 5.54

3.10 Figures
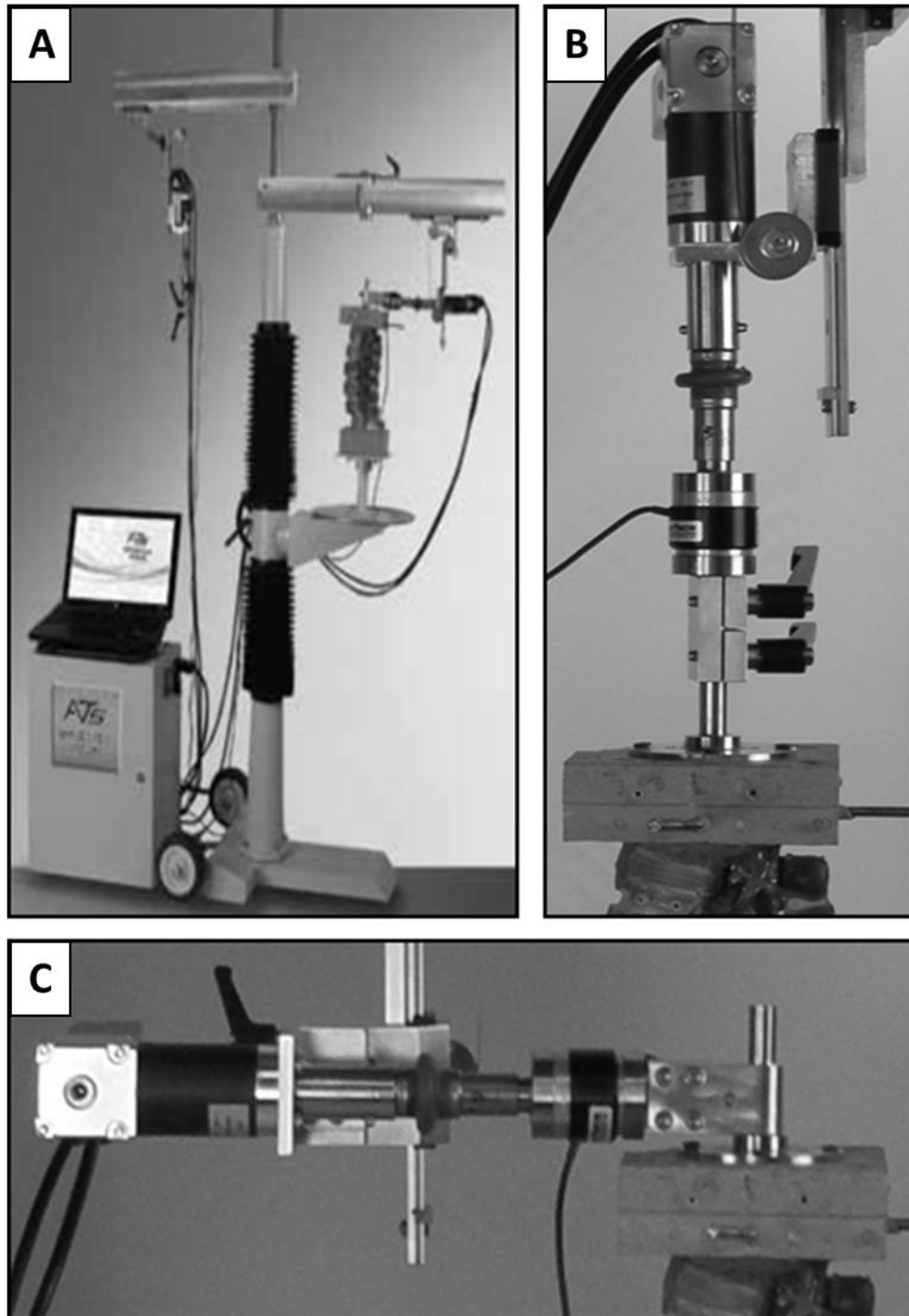
Figure 3.1: The spine test machine includes the frame with two drive assemblies, a control box, and a computer with software (A). It is depicted here with a synthetic spine. The upper arm is the axial rotation drive (B), and the lower arm is the bending drive (C).

Figure 3.2: Stiff (lumbar) synthetic specimen in bending mode with an optical motion tracking pin inserted to measure actual displacement of the specimen.
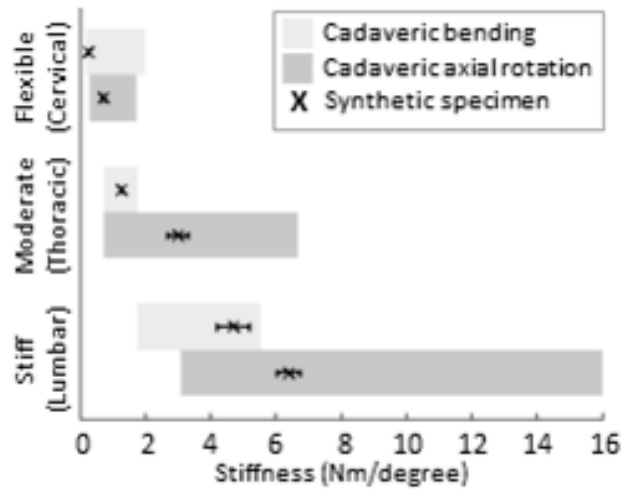
Figure 3.3: Ranges of both bending and axial rotation stiffness values found in cadaveric studies in the literature [6, 11-20]. The means $\pm$ standard deviation of the bending and axial rotation stiffness values measured in the synthetic specimens fall within these ranges for each specimen type.
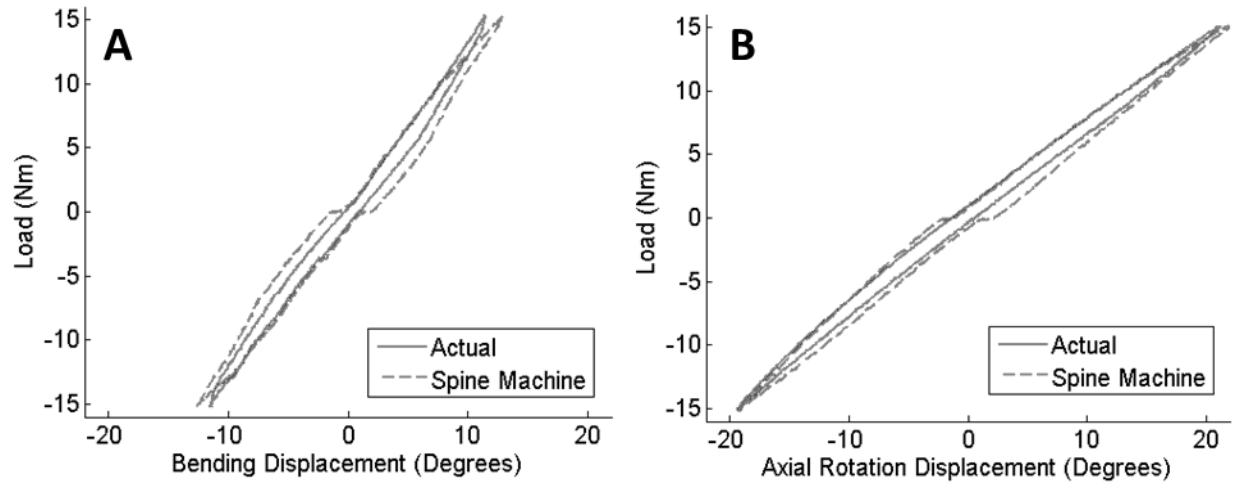
Figure 3.4: Typical one-cycle load v. displacement graphs are shown for a moderate (thoracic) synthetic specimen in bending (A) and a flexible (cervical) synthetic specimen in axial rotation (B). The solid lines represent the actual displacements as measured by the optical motion tracking pin, and the dashed lines represent the displacements as measured by the spine test machine.
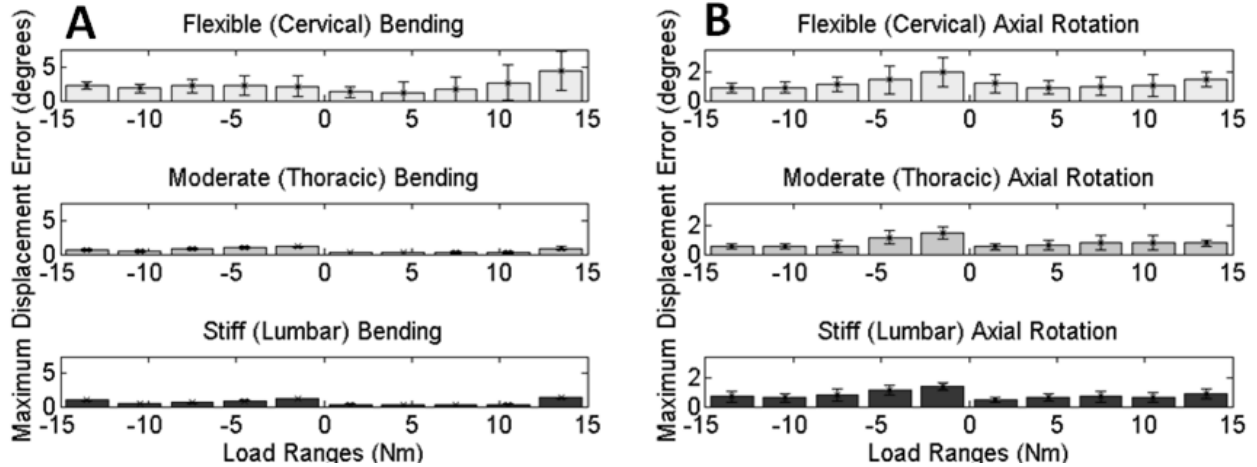
Figure 3.5: Mean ± standard deviation of the maximum displacement errors at each target loading range between -15 and 15 Nm in the spine test machine for each stiffness range: flexible (cervical), moderate (thoracic), and stiff (lumbar) in both bending (A) and axial rotation (B). The error is defined as the difference between the actual displacement measured by the optical motion tracking pin and the displacement measured by the spine test machine. Note the different y-axis scales for bending and axial rotation.

Figure 3.6: Bending test setup of a full thoracic cadaveric specimen with attached ribcage test loaded in the spine test machine

CHAPTER 4:

Mechanical Analysis of the Human Cadaveric Thoracic Spine with Intact Rib Cage

Manuscript currently under review with the Journal of Biomechanics, Submitted August 2014

This study analyzed the overall motion of a human cadaveric thoracic spine with intact rib cage. Erin Mannen had primary responsibility for the experimental design, data collection, data analysis, and writing of first draft. Details on the experimental design and data analysis can be found in Appendix A.

Additional data analysis and a manuscript regarding the motion of the human cadaveric thoracic spine with an intact rib cage on regional (T6-T10) and local (T6, T7, T8, T9, and T10) levels will be done in the future. More in-depth analyses of out-of-plane and coupled motions are also of interest, and continuation of this work in the Spine Biomechanics Lab will give further insight into the mechanics of the human thoracic spine. These planned manuscripts are not included in this dissertation.

Mechanical Analysis of the Human Cadaveric Thoracic Spine with Intact Rib Cage

Erin M. Mannen[1], John T. Anderson[2], Paul M. Arnold[3], Elizabeth A. Friis[1*]

[1]University of Kansas, Mechanical Engineering, 1530 W 15th St., Learned Hall Room 3138, Lawrence, KS 66045

[2]Children's Mercy Hospital and Clinics of Kansas City, Orthopaedic Surgery, 2401 Gillham Rd., Kansas City, MO 64108

[3]University of Kansas Medical Center, Department of Neurosurgery, 3901 Rainbow Blvd. MS 3021, Kansas City, KS 66160

*Corresponding author, lfriis@ku.edu

Abstract

The goal of this study was to characterize the overall in-plane and basic coupled motion of a cadaveric human thoracic spine with intact true ribs. Researchers are becoming increasingly interested in the thoracic spine due to both the high prevalence of injury and pain in the region and also innovative surgical techniques that utilize the rib cage. Computational models can be useful tools to predict loading patterns and understand effects of surgical procedures or medical devices, but they are often limited by insufficient cadaveric input data. In this study, pure moments to ± 5 Nm were applied in flexion-extension, lateral bending, and axial rotation to seven human cadaveric thoracic spine specimens (T1-T12) with intact true ribs to determine symmetry of in-plane motion, differences in neutral and elastic zone motion and stiffness, and significance of out-of-plane rotations and translations. Results showed that lateral bending and axial rotation exhibited symmetric motion, neutral and elastic zone motion and stiffness values were significantly different for all modes of bending ($p < 0.05$), and out-of-plane rotations and translations were greater than zero for most rotations and translations. Overall in-plane rotations were $7.7° \pm 3.4°$ in flexion, $9.6° \pm 3.7°$ in extension, $23.3° \pm 8.4°$ in lateral bending, and $26.3° \pm 12.2°$ in axial rotation. Results of this study could provide inputs or validation comparisons for computational models. Future studies should characterize coupled motion

patterns and local and regional level biomechanics of cadaveric human thoracic spines with intact true ribs.

4.1 Introduction

Research of the thoracic spine and the thoracolumbar regions is attracting interest due to both the potential to utilize the rib cage to explore fusion alternatives and also to study causes and treatment options of problems occurring in these areas. Medical device developers are designing systems such as the VEPTR (Synthes Inc., West Chester, PA, USA), which attaches directly to the rib cage as a way to treat patients with thoracic insufficiency syndrome or scoliosis (Campbell, 2013). While these surgical methods are innovative, there is currently a lack of data regarding the optimal method to test the biomechanical impact of these devices on a computational or cadaveric model. In addition, pain and vertebral fractures are common occurrences in the thoracic spine (Andersen et al., 2007; Delmas et al., 2005; Melton et al., 1993), but little information currently exists to understand the loading mechanics that may lead to these conditions. The goal of this study was to characterize the overall in-plane and basic coupled motion patterns of a human cadaveric thoracic spine with intact true ribs.

Computational modeling may help inform medical device design or surgical procedure planning, but the few thoracic models that exist may not be appropriately informed by mechanical cadaveric testing because research on a full thoracic spine is sparse (Andriacchi et al., 1974; Bruno et al., 2012; Closkey et al., 1992; Iyer et al., 2010). Vertebral fracturing, scoliosis, and back pain in the thoracic spine could be better understood if the computational models to predict loading patterns were more robust. Understanding the basic mechanics of the thoracic spine with an intact rib cage is the first step to improving upon current thoracic computational models. *This study sought to provide a thorough understanding of the overall biomechanical motion of the human thoracic spine with intact rib cage for the purpose of*

providing reliable inputs and validation comparison values for computational models that could
be used to understand and advance thoracic spine treatments.

The thoracic spine, due to the rib cage, presents added challenges in mechanical testing when compared to the lumbar or cervical spine. While methods for mechanical testing in the lumbar and cervical regions are well-developed and frequently conducted, testing of the thoracic spine is much less common and standardized. One reason for the rarity of testing is the complicated nature of the rib cage and the size limitations of commercially available test machines. Some researchers have analyzed functional spine units or short segments of the thoracic spine (Oda et al., 2002; Panjabi et al., 1976; Sangiorgio et al., 2013). Others have analyzed segments of the thoracic spine without the rib cage intact, dissecting the ribs a few centimeters lateral to the costovertebral joints (Ilharreborde et al., 2010; Sangiorgio et al., 2013). However, one study suggests that the rib cage provides 30 to 40 percent of the stability in the thoracic region (Watkins et al., 2005); it is therefore critical to understand the overall biomechanics of the full thoracic region with an intact rib cage. There are only three studies that have examined full thoracic spine biomechanics (T1-T12) of a human cadaveric spine with an intact rib cage (Healy et al., 2014; Horton et al., 2005; Watkins et al., 2005); one study looked at T2-T10 (Feiertag et al., 1995). None of this work has provided biomechanical information of the intact specimen other than in-plane range-of-motion (ROM) data. *There remains a significant gap in the understanding of the overall in-plane and basic coupled motion of a human cadaveric thoracic specimen an intact rib cage.*

This research effort aimed to understand the motion of a human cadaveric thoracic spine with an intact rib cage. The following hypotheses were tested for overall motion: (i) in-plane motion will be symmetric for right and left lateral bending, and right and left axial rotation, (ii)

neutral and elastic zones, and neutral and elastic zone stiffness values will be significantly different in all modes of bending, and (iii) significant out-of-plane rotations and translations in all planes will occur in all modes of bending.

4.2 Methods

4.2.1 Experimental Design

Seven human fresh-frozen cadaver thoracic specimens (T1-T12) were dissected to include only vertebrae, true ribs (T1-T10), sternum, intervertebral discs, and stabilizing ligaments. Age at time of death was 71 ± 7 years. All specimens were x-rayed to determine existence of fractures, severe abnormalities or osteophytes, or previous surgeries that would cause exclusion. All specimens were considered acceptable to be included in the study (n=7). Table 4.1 provides a detailed description of the specimen group.

Specimens were kept hydrated and thawed to room temperature before testing. Screws were inserted into the T1 and T12 vertebrae, and each end was potted parallel to the vertebral end plate using auto-body filler potting (Bondo, 3M, St. Paul, MN, USA). Each specimen was aligned and mounted in a novel spine testing machine (Applied Test Systems, Butler, PA, USA) which allowed for the continuous application of a pure moment to a specified load limit with control over the rate of displacement (Mannen et al., 2014). The inferior end (T12) was rigidly mounted to the machine, and the superior end (T1) was unconstrained and free to move in all directions.

An optical motion-capture research pin with three non-collinear markers (Optotrak, Northern Digital Inc., Waterloo, ON, Canada) was inserted into the posterior edge of the superior potting (considered T1). Motion-capture pins were also inserted into the right pedicles of T6,

T7, T8, T9, T10, and T11; the pins did not change the mechanics of the specimen or disrupt surrounding ligaments. Data from these pins was not used in the overall analysis. Error in the motion-capture diodes was ±0.1mm which resulted in ±0.06° for the research pin. It was assumed that the data measured from the pin represented the actual displacement of T1 with respect to T12. Anatomical points were probed in accordance with recommendations from Wilke et al., with adaptations to account for the intact rib cage to determine the local coordinate system at T1 (Wilke et al., 1998). Figure 4.1 is a photo of the experimental setup.

Pure moments were applied to a load limit of ±5Nm at a displacement rate of 1 degree/second in three modes of bending [flexion-extension (FE), lateral bending (LB), and axial rotation (AR)] applied in a random order. Each specimen was tested for five cycles; the third cycle was used for data analysis. Saline solution was sprayed on the specimen throughout testing to preserve mechanical integrity. Load was recorded from the test machine, and angular and translational displacements were calculated from the displacement data from the optical motion-capture pin at T1.

4.2.2 Data and Statistical Analysis

Matlab (MathWorks, Natick, MA, USA) was used to analyze the data and perform statistics. Euler decomposition techniques in which the first Euler rotation corresponded with the mode of bending were used to determine both in-plane and out-of-plane rotations (Crawford et al., 1996). The following in-plane rotation and stiffness parameters were found for each mode of bending (flexion, extension, right LB, left LB, right AR, and left AR) and were reported in degrees or degrees/Nm (Wilke et al., 1998):

- Neutral Zone (NZ): Angulation difference at zero load (for complete FE, LB, and AR cycles),

- Neutral Zone Stiffness (NZS): Slope of the load v. angular displacement curve at 0 Nm,

- Elastic Zone (EZ): Angular displacement from the end of NZ to the point of maximum loading ($\pm$5Nm),

- Elastic Zone Stiffness (EZS): Slope of the load v. angular displacement curve at the point of maximum loading ($\pm$5Nm),

- Range-of-Motion (ROM): Angular displacement from 0Nm to maximum load ($\pm$5Nm).

Mean overall in-plane ROM, EZ, NZS, and EZS were calculated for flexion, extension, right and left LB, and right and left AR, individually. Mean NZ was calculated for the entire cycles of FE, LB, and AR.

Mean out-of-plane rotation ROMs were reported as percentages of the in-plane rotation ROM for each mode of testing (FE, LB, and AR), normalized for each specimen. Mean FE ratios, LB ratios, and AR ratios were found for every mode of bending. Each ratio was defined as the ROM in any given direction (FE, LB, or AR) divided by the in-plane ROM specific to that mode of bending. For example, the FE ratio for the LB mode of bending was defined as the out-of-plane ROM in FE divided by the in-plane ROM in LB, reported as a percentage.

Mean translational displacements of T1 were defined as deviations from the neutral position at $\pm$5Nm for right-left lateral (RL), anterior-posterior (AP), and superior-inferior (SI) translations. The mean deviations in every direction (AP, RL, and SI) for each mode of testing (FE, LB, and AR) were reported for overall motion.

To test the stated hypotheses, student t-tests at a $p < 0.05$ significance level were used to compare: (i) in-plane ROM, EZ, NZS, and EZS to determine symmetry between right and left

LB and right and left AR, (ii) NZ to EZ, and NZS to EZS in all modes of bending, and (iii) all out-of-plane rotations and translations to zero motion in all modes of bending.

4.3 Results

4.3.1 In-Plane Analysis

Typical in-plane angular displacement v. load cycles for FE, LB, and AR are depicted in Figure 4.2. No significant difference was found between right and left LB or right and left AR for ROM, EZ, NZS, or EZS, so all LB and AR values were reported for the total of the LB or AR cycle.

Overall in-plane ROM values for all modes of bending are depicted in Figure 4.3. Mean in-plane ROM for F, E, FE, LB, and AR were $7.7°\pm3.4°$, $9.6°\pm3.7°$, $17.3°\pm7.0°$, $23.3°\pm8.4°$, and $26.3°\pm12.2°$, respectively. ROM values were significantly different for F and E, FE and LB, and FE and AR.

NZ and EZ values are depicted in Figure 4.4. Mean NZ values for FE, LB, and AR were $2.3°\pm1.0°$, $4.5°\pm3.2°$, and $3.0°\pm1.6°$, respectively. Mean EZ values for F, E, LB, and AR were $6.6°\pm3.1°$, $8.4°\pm3.3°$, $9.4°\pm3.2°$, and $11.6°\pm5.5°$, respectively. NZ values were significantly different for FE and LB. EZ values were significantly different for F and E, F and LB, and F and AR. NZ and EZ values were significantly different for LB and AR.

Mean NZS and EZS values are depicted in Figure 4.5. Mean NZS values for F, E, LB, and AR were $0.40Nm/°\pm0.22$ $Nm/°$, 0.44 $Nm/°\pm0.30Nm/°$, $0.23Nm/°\pm0.13Nm/°$, and 0.26 $Nm/°\pm0.16Nm/°$, respectively. NZS values were significantly different for F and LB, E and LB, and E and AR. Mean EZS values for F, E, LB, and AR were $2.12Nm/°\pm1.22Nm/°$, $1.22Nm/°\pm0.82Nm/°$, $1.48Nm/°\pm0.95Nm/°$, and $1.47Nm/°\pm1.43Nm/°$, respectively. No ESZ

values were significantly different. NZS and EZS were significantly different in E and LB, and not significantly different in F (p=0.08) or AR (p=0.06).

4.3.2 Out-of-Plane Analysis

Out-of-plane rotation data are depicted in Figure 4.6. In FE, LB and AR ratios were 24.0%$\pm$15.3% and 25.5%$\pm$17.7%, respectively. In LB, FE and AR ratios were 14.0%$\pm$9.2% and 12.1%$\pm$10.5%, respectively. In AR, FE and LB ratios were 18.2%$\pm$26.0%, 12.4%$\pm$8.6%, respectively. In-plane primary ROM compared to both out-of-plane rotations for each mode of bending were significantly different. All out-of-plane rotations in all modes of bending were significantly different when compared to zero motion except FE motion in AR (p=0.19).

4.3.3 Translations

Translational data are depicted in Figure 4.7. In FE, mean translations of T1 in AP, RL, and SI were 12.6mm$\pm$11.1mm, 2.9mm$\pm$1.9mm, and 3.4mm$\pm$4.3mm, respectively; AP and RL, and AP and SI were significantly different. In LB, mean translations in AP, RL, and SI were 3.9mm$\pm$2.6mm, 30.4mm$\pm$23.5mm, and 4.2mm$\pm$3.6mm, respectively; RL and AP, and RL and SI were significantly different. In AR, mean translations in AP, RL, and SI were 6.7mm$\pm$5.1mm, 8.6mm$\pm$9.1mm, and 1.6mm$\pm$1.4mm, respectively; none were found to be significantly different compared to one another. All translations in all modes of bending were significantly different when compared to zero motion except SI motion in FE (p=0.08).

4.4 Discussion

4.4.1 In-Plane Analysis: Overall Range-of-Motion (ROM)

As seen in Figure 4.3, the mean in-plane ROM was largest in AR followed by LB, though no significant difference was found between the two. The lowest ROM occurred in FE, with extension exhibiting a significantly larger ROM than flexion. The standard deviations ranged from 36%-46% of the mean ROM values. Null hypothesis (i) that overall in-plane motion will be symmetric for right and left LB and right and left AR failed to be rejected for ROM values, indicating symmetry in ROM.

These results were comparable to previously published literature. Table 4.2 is a summary of the in-plane ROM data from the present study alongside the results of four previous studies known to the authors that analyzed intact human cadaveric full (T1-T12) or nearly-full (T2-T10) thoracic segments with intact rib cages (Feiertag et al., 1995; Healy et al., 2014; Horton et al., 2005; Watkins et al., 2005)

Healy et al. sought to understand the changes in ROM of the thoracic region after a series of decompression surgical techniques utilizing a custom-made automated robotic test system. As a part of the study, the in-plane ROM values were reported for FE, LB, and AR. When compared to the present study, results agree that FE ROM was the stiffest of all modes of bending, while LB and AR showed larger and comparable ROM values. However, the study reported larger ROM values for all modes of bending. This could be contributed to the much lower average age of the specimens used in Healy et al. study when compared to the present research.

Watkins et al. used an adapted automated test machine for the purpose of understanding the contribution of the rib cage and sternum to thoracic stability in FE, LB, and AR. Specimens

were tested in three conditions: intact, fractured sternum, and rib cage removed. Intact LB and AR results were difficult to compare to the present study because maximum loads were $\pm$2Nm compared to $\pm$5Nm used in the present study. Intact results in AR are comparable and similar to the present study, as the load limit was $\pm$5Nm in AR.

The two other studies used manual loading techniques to examine the role of various anatomical elements or the effect of the sequence of surgical releases in FE and LB ROM of the thoracic region. Because these studies were conducted on manual machines, it is more difficult to directly compare ROM results with present study. Feiertag et al. included only T2-T10, so lower ROM values are to be expected when compared with studies conducted on the full thoracic segment of T1-T12. Assuming that the T2-T10 segment (9 vertebrae) constitutes 75% of the T1-T12 segment (12 vertebrae), it is interesting to note that FE ROM reported is 72% of FE ROM in the present study, and LB ROM reported is 57% of LB ROM in the present study. While several considerations (e.g., vertebral level, true v. floating rib levels, load limits, and vertebral height) were not taken into account when making these basic observations, they highlight the need to understand motion at local and regional levels as well as overall motion in the thoracic spine.

4.4.2 In-Plane Analysis: Neutral Zone (NZ) and Elastic Zone (EZ)

To the authors' knowledge, no NZ or EZ data for intact human cadaveric thoracic spines with attached rib cages have been reported in previously published literature. EZ values were symmetric for right and left LB, and right and left AR, thus failing to reject null hypothesis (i). As expected, sigmoidal behavior which has been previously reported in the lumbar and cervical regions of the spine was also found in the full thoracic region (see Figure 4.2). NZ values were

significantly lower than EZ values for all modes of bending (see Figure 4.4), thus failing to reject null hypothesis (ii).

Researchers have reported that NZ values of cadaveric canine thoracic sections range from 0.6°-5.9° for all modes of bending (Oda et al., 1996; Takeuchi et al., 1999), while NZ results from the present study range from 2.3°-4.5°, within the range reported for the canine studies. Further testing should be done to better understand NZ and EZ regions of the human thoracic spine.

4.4.3 In-Plane Analysis: Neutral Zone Stiffness (NZS) and Elastic Zone Stiffness (EZS)

Stiffness data has been reported for the cervical and lumbar regions (Panjabi, 1992), but to the authors' knowledge, no NZS or EZS data for intact human cadaveric thoracic spines with attached rib cages is available in previously published literature. NZS and EZS values were symmetric for right and left LB, and right and left AR, thus failing to reject null hypothesis (i). As shown in Figure 4.5, NZS values in the full thoracic spine were found to be significantly lower than EZS values in extension and LB; trends for this same behavior were also observed for flexion and AR (p=0.08 and p=0.06). This initial stiffness data along with ROM, NZ, and EZ data can provide researchers with a baseline understanding of the shape of the in-plane displacement v. loading curve of the thoracic spine with intact rib cage.

4.4.4 Out-of-Plane Motion

To the authors' knowledge, no out-of-plane motion data for human cadaveric thoracic spines with intact rib cages have been reported in previously published literature. As presented in Figure 4.6, out-of-plane rotations were seen in all modes of bending except FE motion in AR.

66

In AR, the standard deviation of the FE ratio was over 100% of the mean value which may be attributed to a large out-of-plane rotation of 65% for the FE ratio in specimen two. As seen in Table 4.1, specimen two was the youngest of all cadaveric specimens and exhibited the largest ROM in AR. While conclusions cannot be drawn based on one specimen, the large out-of-plane rotation brings into question the significance that age plays in thoracic motion and coupling mechanics. Future work should study the effect of age on thoracic motion and coupling patterns.

Coupled motion has been studied in the thoracic spine on animal models, living humans, and human functional spine units (Fujimori et al., 2012; Fujimori et al., 2013; Panjabi et al., 1976; Sizer et al., 2007; Takeuchi et al., 1999; Willems et al., 1996). Results of these studies generally agree that (1) LB and AR tend to exhibit coupling, (2) coupling patterns may not be consistent throughout the entire thoracic spine, (3) a large variation in coupling mechanics between specimens is present even within the same study, and (4) there is a poor correlation between computational modelling and experimental results. The limitations of these studies make comparison of data difficult.

In the present study, it was observed that the coupling patterns may not remain constant throughout the loading and unloading cycles; this data will reported in subsequent manuscripts. While the results of the present study give researchers a basic understanding of coupled motion in the full human thoracic spine, there is much work to be done to understand the shape of the coupled motion patterns. A thorough understanding of the patterns of coupled motion in the cadaveric thoracic spine, both on a complete specimen and on local and regional levels, is necessary to fully characterize the biomechanics in the human thoracic spine with an intact rib cage.

4.4.5 Translations

To the authors' knowledge, no translational motion data for human cadaveric thoracic spines with intact rib cages have been reported in previously published literature. As expected, in FE and LB, the largest translations of T1 were exhibited in AP and RL planes, respectively (see Figure 4.7). Likewise, in AR, the largest and most comparable translations were seen in AP and RL, though no significant difference was found between any planes.

The importance of allowing unconstrained motion on the superior end was supported by measured translations compared to zero motion that occurred in all directions in all modes of bending (statistically significant except for trend of SI motion in FE at p=0.08). More in depth analysis including local and regional vertebral translations will be reported in subsequent manuscripts.

4.4.6 Study Limitations:

A major limitation of working with cadaveric tissue is the comparison and application of the results to living humans. It would be interesting to better understand the relationship between in vitro human motion and in vivo cadaveric human motion analysis in the thoracic spine so that cadaveric work could be more reliable when applied to living people. In addition, the average age of the specimens in this study was 71 years, so results should be used with caution when applying to a younger demographic.

While the test machine used in this study allowed for the analyzing of the thoracic spine in continuous motion, the displacement rate applied around zero load for this and many test machines is not well understood (Mannen et al., 2014). However, the displacement and load data collected in the study is valid.

This study did not model specific musculature or intra-abdominal pressure, though some researchers are representing these elements in computational models (Bruno et al., 2012; Iyer et al., 2010). Both factors may contribute to increased stability in the thoracic spine and decreased compressive forces (Hodges et al., 2001; Stokes et al., 2010), but more research should be done to better understand the effects of these parameters.

No follower or compressive loads were used in this study. Geometric limitations would have prevented the application of a follower load if the methods utilized in the cervical or lumbar regions were used (Patwardhan et al., 2000), as the anterior portions of the vertebral column were obstructed by the rib cage. To the authors' knowledge, only one study with an intact rib cage has used compressive loads, and only in AR (Watkins et al., 2005). One study suggests that a follower preload in the thoracic spine without a rib cage may mimic physiological loading (Stanley et al., 2004), though more work needs to be done to determine both a method of application and the significance of follower or compressive loads in a thoracic specimen with an intact rib cage.

4.4.7 Future Work

There is much work to be done in mechanical characterization of the thoracic spine. Although some researchers have analyzed overall ROM, the lack of a standardized testing method in the thoracic spine renders it difficult to compare results of different studies. The spine testing community would benefit from defining the preferred testing method for human cadaveric thoracic spine specimens with an intact rib cage.

In addition, while overall behavior is a critical first step in characterizing thoracic spinal motion, local and regional level analyses are necessary to better understand the biomechanics of

the spine and rib cage. This information will give researchers more accurate inputs to improve upon computational models. Finally, by fully understanding the biomechanics of the thoracic spine, researchers could study the overall and local level effects of thoracic instrumentation and surgical procedures in the thoracic region on both cadaveric and computational models.

The results of this study add to the understanding of human thoracic biomechanics. Further work should be done to more fully understand the coupling motion patterns and local and regional level biomechanics of human cadaveric spines with intact rib cages.

4.5 Conflict of Interest

The authors have no financial or personal relationships that would inappropriately influence the results of this study.

4.6 Acknowledgements

4.7 References

Andersen, J.H., Haahr, J.P., Frost, P., 2007. Risk factors for more severe regional musculoskeletal symptoms: a two-year prospective study of a general working population. Arthritis and rheumatism 56, 1355-1364.

Andriacchi, T., Schultz, A., Belytschko, T., Galante, J., 1974. A model for studies of mechanical interactions between the human spine and rib cage. J Biomech 7, 497-507.

Bruno, A.G., Anderson, D.E., D'Agostino, J., Bouxsein, M.L., 2012. The effect of thoracic kyphosis and sagittal plane alignment on vertebral compressive loading. Journal of bone and mineral research : the official journal of the American Society for Bone and Mineral Research 27, 2144-2151.

Campbell, R.M., Jr., 2013. VEPTR: past experience and the future of VEPTR principles. European spine journal : official publication of the European Spine Society, the European Spinal Deformity Society, and the European Section of the Cervical Spine Research Society 22 Suppl 2, S106-117.

Closkey, R.F., Schultz, A.B., Luchies, C.W., 1992. A model for studies of the deformable rib cage. J Biomech 25, 529-539.

Crawford, N.R., Yamaguchi, G.T., Dickman, C.A., 1996. Methods for determining spinal flexion/extension, lateral bending, and axial rotation from marker coordinate data: Analysis and refinement. Human Movement Science 15, 55-78.

Delmas, P.D., van de Langerijt, L., Watts, N.B., Eastell, R., Genant, H., Grauer, A., Cahall, D.L., 2005. Underdiagnosis of vertebral fractures is a worldwide problem: the IMPACT study. Journal of bone and mineral research : the official journal of the American Society for Bone and Mineral Research 20, 557-563.

Feiertag, M.A., Horton, W.C., Norman, J.T., Proctor, F.C., Hutton, W.C., 1995. The effect of different surgical releases on thoracic spinal motion. A cadaveric study. Spine 20, 1604-1611.

Fujimori, T., Iwasaki, M., Nagamoto, Y., Ishii, T., Kashii, M., Murase, T., Sugiura, T., Matsuo, Y., Sugamoto, K., Yoshikawa, H., 2012. Kinematics of the thoracic spine in trunk rotation: in vivo 3-dimensional analysis. Spine 37, E1318-1328.

Fujimori, T., Iwasaki, M., Nagamoto, Y., Matsuo, Y., Ishii, T., Sugiura, T., Kashii, M., Murase, T., Sugamoto, K., Yoshikawa, H., 2013. Kinematics of the thoracic spine in trunk lateral bending: in vivo three-dimensional analysis. The spine journal : official journal of the North American Spine Society.

Healy, A.T., Lubelski, D., Mageswaran, P., Bhowmick, D.A., Bartsch, A.J., Benzel, E.C., Mroz, T.E., 2014. Biomechanical analysis of the upper thoracic spine after decompressive procedures. The spine journal : official journal of the North American Spine Society 14, 1010-1016.

Hodges, P.W., Cresswell, A.G., Daggfeldt, K., Thorstensson, A., 2001. In vivo measurement of the effect of intra-abdominal pressure on the human spine. J Biomech 34, 347-353.

Horton, W.C., Kraiwattanapong, C., Akamaru, T., Minamide, A., Park, J.S., Park, M.S., Hutton, W.C., 2005. The role of the sternum, costosternal articulations, intervertebral disc, and facets in thoracic sagittal plane biomechanics: a comparison of three different sequences of surgical release. Spine 30, 2014-2023.

Ilharreborde, B., Zhao, K., Boumediene, E., Gay, R., Berglund, L., An, K.N., 2010. A dynamic method for in vitro multisegment spine testing. Orthopaedics & traumatology, surgery & research : OTSR 96, 456-461.

Iyer, S., Christiansen, B.A., Roberts, B.J., Valentine, M.J., Manoharan, R.K., Bouxsein, M.L., 2010. A biomechanical model for estimating loads on thoracic and lumbar vertebrae. Clinical biomechanics (Bristol, Avon) 25, 853-858.

Mannen, E.M., Ranu, S.S., Villanueva, A.M., Friis, E.A., 2014. Validation of a Novel Spine Test Machine. J Med Dev (In Press).

Melton, L.J., 3rd, Lane, A.W., Cooper, C., Eastell, R., O'Fallon, W.M., Riggs, B.L., 1993. Prevalence and incidence of vertebral deformities. Osteoporosis international : a journal established as result of cooperation between the European Foundation for Osteoporosis and the National Osteoporosis Foundation of the USA 3, 113-119.

Oda, I., Abumi, K., Cunningham, B.W., Kaneda, K., McAfee, P.C., 2002. An in vitro human cadaveric study investigating the biomechanical properties of the thoracic spine. Spine 27, E64-70.

Oda, I., Abumi, K., Lu, D., Shono, Y., Kaneda, K., 1996. Biomechanical role of the posterior elements, costovertebral joints, and rib cage in the stability of the thoracic spine. Spine 21, 1423-1429.

Panjabi, M.M., 1992. The stabilizing system of the spine. Part II. Neutral zone and instability hypothesis. Journal of spinal disorders 5, 390-396; discussion 397.

Panjabi, M.M., Brand, R.A., Jr., White, A.A., 3rd, 1976. Mechanical properties of the human thoracic spine as shown by three-dimensional load-displacement curves. The Journal of bone and joint surgery. American volume 58, 642-652.

Patwardhan, A.G., Havey, R.M., Ghanayem, A.J., Diener, H., Meade, K.P., Dunlap, B., Hodges, S.D., 2000. Load-carrying capacity of the human cervical spine in compression is increased under a follower load. Spine 25, 1548-1554.

Sangiorgio, S.N., Borkowski, S.L., Bowen, R.E., Scaduto, A.A., Frost, N.L., Ebramzadeh, E., 2013. Quantification of Increase in Three-dimensional Spine Flexibility Following Sequential Ponte Osteotomies in a Cadaveric Model. Spine Deformity 1, 171-178.

Sizer, P.S., Jr., Brismee, J.M., Cook, C., 2007. Coupling behavior of the thoracic spine: a systematic review of the literature. Journal of manipulative and physiological therapeutics 30, 390-399.

Stanley, S.K., Ghanayem, A.J., Voronov, L.I., Havey, R.M., Paxinos, O., Carandang, G., Zindrick, M.R., Patwardhan, A.G., 2004. Flexion-extension response of the thoracolumbar spine under compressive follower preload. Spine 29, E510-514.

Stokes, I.A., Gardner-Morse, M.G., Henry, S.M., 2010. Intra-abdominal pressure and abdominal wall muscular function: Spinal unloading mechanism. Clinical biomechanics (Bristol, Avon) 25, 859-866.

Takeuchi, T., Abumi, K., Shono, Y., Oda, I., Kaneda, K., 1999. Biomechanical role of the intervertebral disc and costovertebral joint in stability of the thoracic spine. A canine model study. Spine 24, 1414-1420.

Watkins, R.t., Watkins, R., 3rd, Williams, L., Ahlbrand, S., Garcia, R., Karamanian, A., Sharp, L., Vo, C., Hedman, T., 2005. Stability provided by the sternum and rib cage in the thoracic spine. Spine 30, 1283-1286.

Wilke, H.J., Wenger, K., Claes, L., 1998. Testing criteria for spinal implants: recommendations for the standardization of in vitro stability testing of spinal implants. European spine journal : official publication of the European Spine Society, the European Spinal Deformity Society, and the European Section of the Cervical Spine Research Society 7, 148-154.

Willems, J.M., Jull, G.A., J, K.F., 1996. An in vivo study of the primary and coupled rotations of the thoracic spine. Clinical biomechanics (Bristol, Avon) 11, 311-316.

4.8 Tables

Table 4.1: Details on cadaveric specimens used in the study. All specimens were white males. Abbreviations: Cause of Death (CoD); End State Debility (ESD); Atherosclerotic Cardiovascular Disease (ACD); Urinary Bladder Cancer (UBC); hypertension (HT); undetermined (U).

Specimen Number	Age (years)	Height (in)	Weight (lbs)	CoD
1	82	71	200	ESD
2	59	70	198	ACD
3	76	72	220	U
4	69	70	160	U
5	66	70	300	ESD
6	70	73	220	UBC
7	73	70	170	HT
Mean ($\pm$ St Dev)	71 (7)	70 (1)	209 (46)	
Range	59 to 82	70 to 73	160 to 300	

Table 4.2: Summary of overall (T1-T12) mean (+ standard deviation) in-plane range-of-motion (ROM) data from published literature from tests done on human cadaveric specimens with intact ribs. Note that Feiertag et al. performed tests on T2-T10 segments, and Horton et al. and Feiertag et al. used manual loading systems while all others used automated test machines. Abbreviations: flexion-extension (FE), lateral bending (LB), axial rotation (AR). --Value not reported; †50N axial preload applied; ‡Standard deviation not reported.

Author (Year)	Age (Years)	Purpose of Study	Load Limits			Overall Range-of-Motion (°)		
			FE	LB	AR	FE	LB	AR
Present Study (2014)	71 (7) 59 to 82	Overall thoracic biomechanical analysis	5 Nm	5 Nm	5 Nm	17.3 (7.0) 8.0 to 25.8	23.3 (8.4) 11.2 to 35.7	26.3 (12.2) 13.3 to 44.6
Healy (2014)	59 (9.5) --	Stability after decompression	5 Nm	5 Nm	5 Nm	26.9 (10.0) --	42.1 (19.0) --	43.7 (16.9) --
Watkins (2005)	72‡ 55 to 91	Stability from ribcage & sternum	2 Nm	2 Nm	5 Nm†	7.93‡ 2.64 to 15.64	10.36‡ 1.92 to 26.81	23.03‡ 6.17 to 51.44
Horton (2005)	73.6‡ 65 to 82	Role of elements in sagittal flexibility	25 N	--	--	30.2 (9.0) --	-- --	-- --
Feiertag (1995)	-- --	Effect of surgical release sequence	89 N	89 N	--	12.6 (5.6) --	14.5 (5.5) --	-- --

4.9 Figures
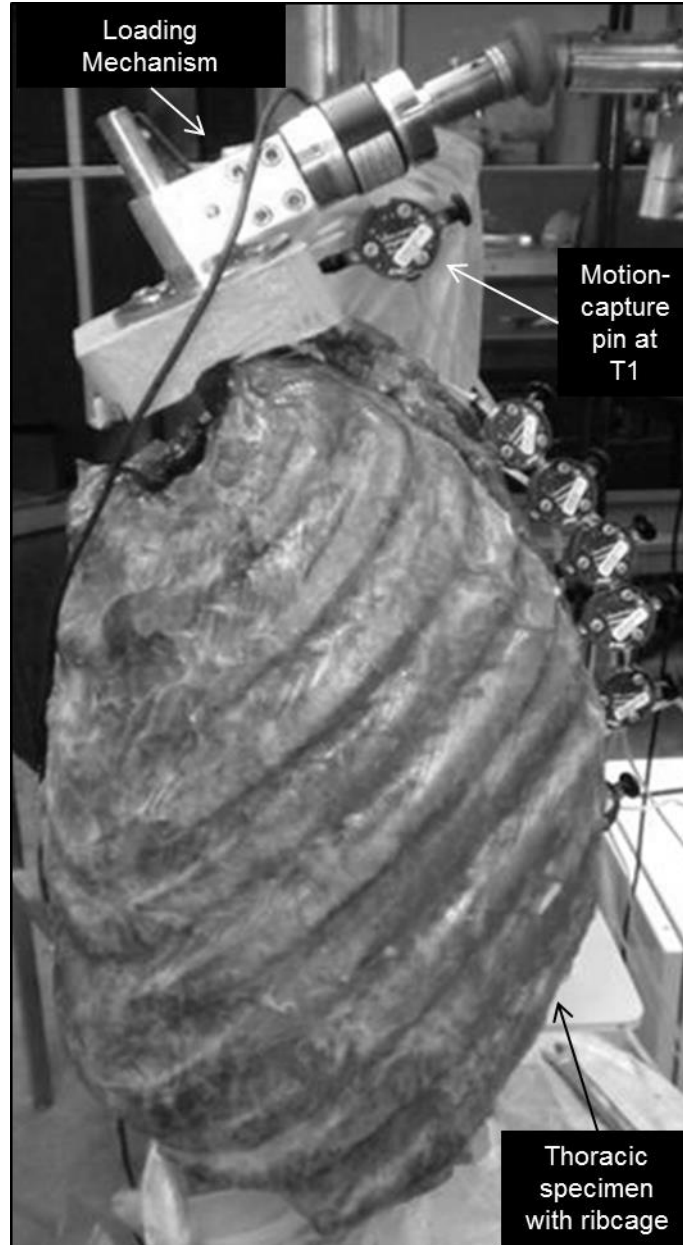
Figure 4.1: Photo of a T1-T12 human cadaveric specimen with intact true ribs, depicted here from the left in the lateral bending testing mode. T1 and T12 were potted, and T12 was fixed rigidly to the base of the spine test machine. Optical motion-capture pins were inserted into the superior potting (T1) and into the right pedicles of T6 through T11. Specimens were loaded to +5 Nm in flexion-extension (FE), lateral bending (LB), and axial rotation (AR).
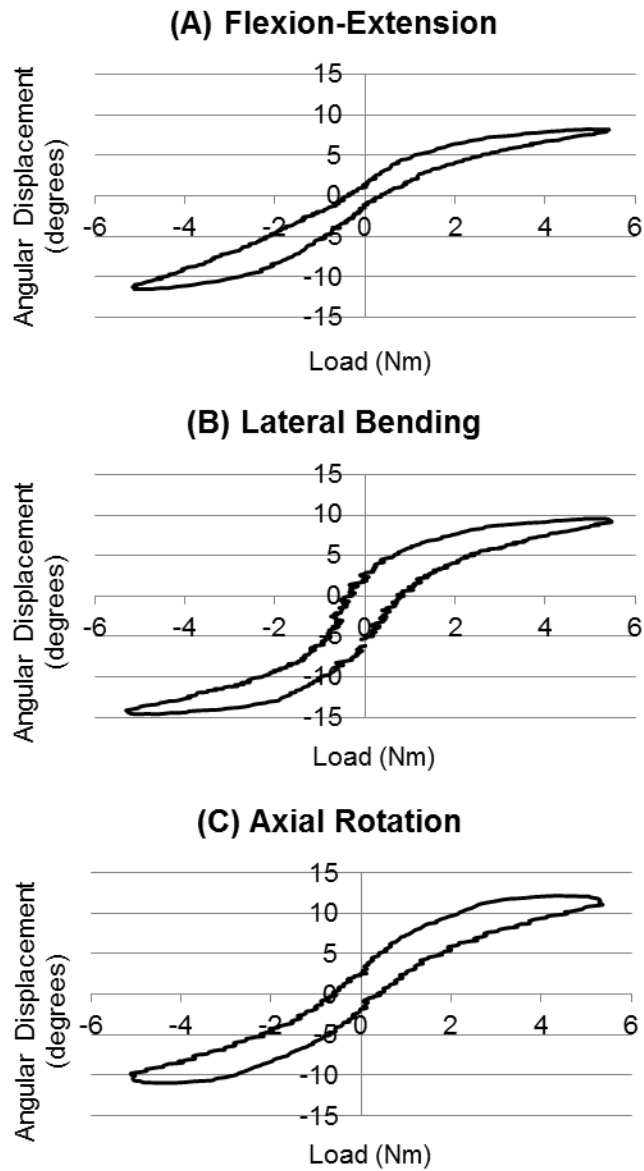
Figure 4.2: Typical overall in-plane angular displacement v. load cycle in (A) flexion(+)/extension(-), (B) right(+)/left(-) lateral bending, and (C) right(+)/left(-) axial rotation for T1. Specimens were loaded to +5 Nm for 5 cycles.
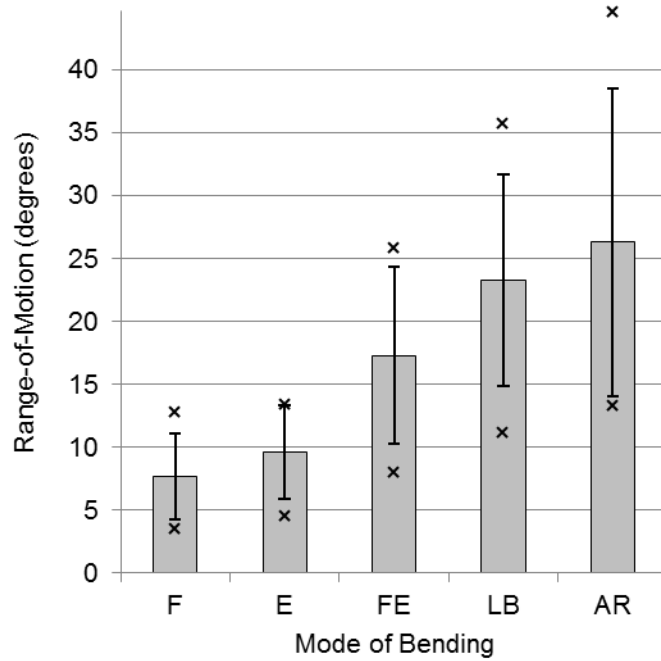
Figure 4.3: Mean overall in-plane range-of-motion values of T1 with respect to T12 for flexion (F), extension (E), flexion-extension (FE), lateral bending (LB), and axial rotation (AR). Standard deviation bars and maximum and minimum values (x) are depicted. Values were significantly different for F and E, FE and LB, and FE and AR ($p < 0.05$).
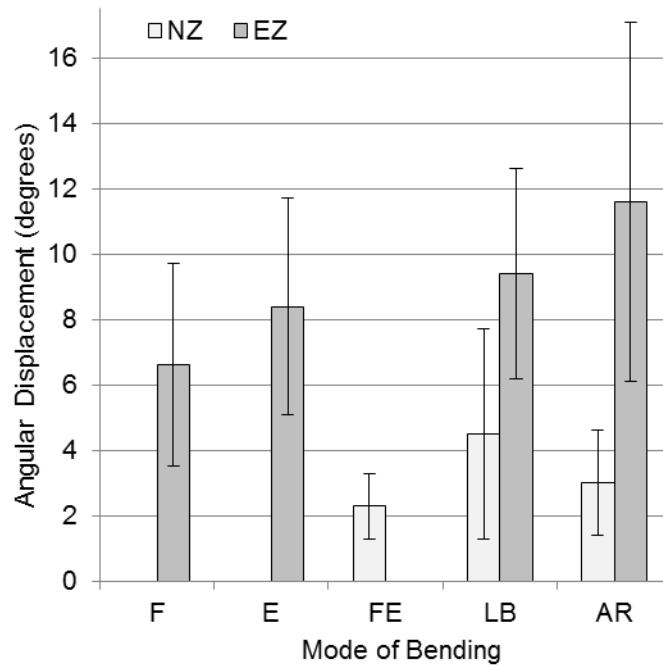
Figure 4.4: Mean and standard deviations of the overall neutral zone (NZ) and elastic zone (EZ) angular displacements for each mode of bending: flexion (F), extension (E), flexion-extension (FE), lateral bending (LB), and axial rotation (AR). NZ values were significantly different in FE and LB ($p < 0.05$). EZ values were significantly different in F and E, F and LB, and F and AR ($p < 0.05$). NZ and EZ values were significantly different in LB and AR ($p < 0.05$).
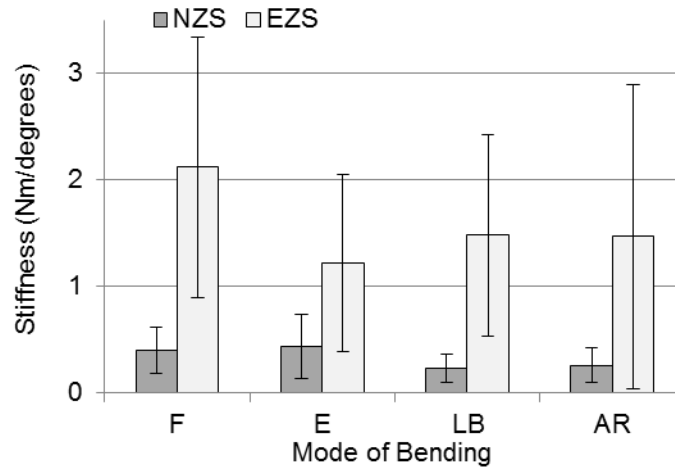
Figure 4.5: Mean and standard deviations of the overall neutral zone stiffness (NZS) and elastic zone stiffness (EZS) for each mode of bending: flexion (F), extension (E), lateral bending (LB), and axial rotation (AR). NZS and EZS were significantly different for E and LB ($p<0.05$). NZS values were significantly different for F and LB, E and LB, and E and AR ($p<0.05$).
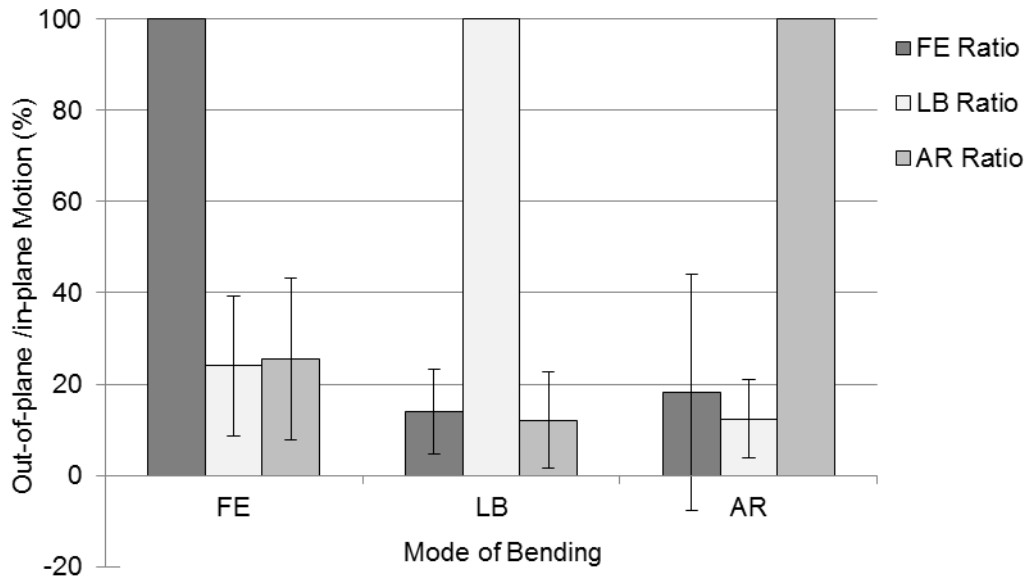
Figure 4.6: Mean and standard deviations of the ratios of angular motions of T1 with respect to T12 in all rotations for all modes of bending [flexion-extension (FE), lateral bending (LB), and axial rotation (AR)]. For example, the FE Ratio represents the motion in the FE plane divided by the in-plane motion of the applied mode of bending. Thus, the FE Ratio is 100% in the FE mode of bending. For each mode of bending, no significant difference was found between the two out-of-plane ROMs. Significance was found between the in-plane ROM and both corresponding out-of-plane ROMs for each mode of bending (p<0.05). All out-of-plane rotations in all modes of bending were found to be significantly different than zero motion (p<0.05) except FE motion in the AR mode of bending (p=0.19).
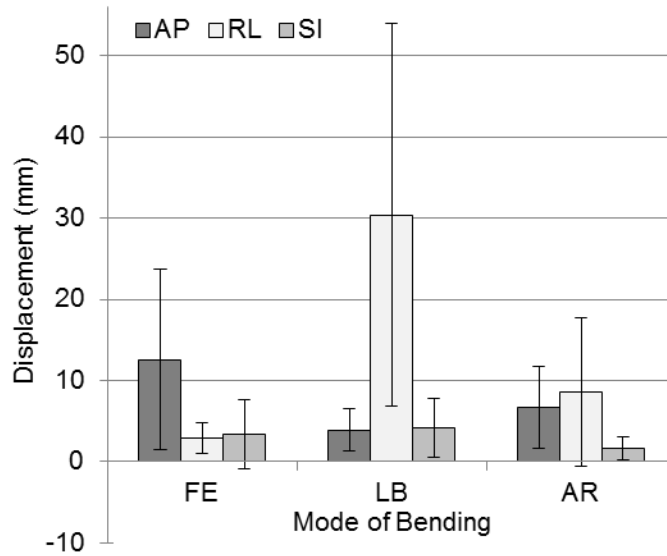
Figure 4.7: Mean and standard deviations of the overall translations in anterior-posterior (AP), right-left (RL), and superior-inferior (SI) of T1 with respect to T12 for each mode of bending: flexion-extension (FE), lateral bending (LB), and axial rotation (AR). In the FE mode of bending, significance was found between AP and RL, and AP and SI ($p < 0.05$). In the LB mode of bending, significance was found between RL and AP, and RL and SI ($p < 0.05$). In the AR mode of bending, no significant difference was found between any translations. All translations in all modes of bending were found to be significantly different when compared to zero motion ($p < 0.05$) except SI motion in the FE mode of bending ($p = 0.08$)

CHAPTER 5:

Mechanical Contribution of the Rib Cage in the Cadaveric Thoracic Spine

Manuscript currently under review with Spine, Submitted September 2014

This study analyzed the overall mechanical contribution of the rib cage in human cadaveric thoracic spine testing for both uninstrumented and instrumented specimens. Erin Mannen had primary responsibility for the experimental design, data collection, data analysis, and writing of the first draft. Details on the experimental design and data analysis can be found in Appendix A.

Mechanical Contribution of the Rib Cage in the Human Cadaveric Thoracic Spine

Erin M. Mannen[1], John T. Anderson[2], Paul M. Arnold[3], Elizabeth A. Friis[1*]

[1]*University of Kansas, Mechanical Engineering, 1530 W 15th St., Learned Hall Room 3138, Lawrence, KS 66045*

[2]*Children's Mercy Hospital and Clinics of Kansas City, Orthopaedic Surgery, 2401 Gillham Rd., Kansas City, MO 64108*

[3]*University of Kansas Medical Center, Department of Neurosurgery, 3901 Rainbow Blvd. MS 3021, Kansas City, KS 66160*

Corresponding author, lfriis@ku.edu

Abstract

Study Design. An *in vitro* biomechanical human cadaveric study of T1-T12 thoracic specimens was performed with four conditions (with and without rib cage, instrumented and uninstrumented) in flexion-extension, lateral bending, and axial rotation.

Objectives. The objective was to understand the influence of the rib cage on motion and stiffness parameters of the human cadaveric thoracic spine. Hypotheses tested for overall motion in all modes of bending for both uninstrumented and instrumented specimens were: (i) in-plane range-of-motion and neutral and elastic zones will be greater without the rib cage, (ii) neutral and elastic zone stiffness values will be different for specimens without the rib cage, and (iii) out-of-plane rotations will be different for specimens without the rib cage.

Summary of Background Data. The rib cage is presumed to provide significant stability to the thoracic spine, but no studies have been conducted to determine the influence of the rib cage in both uninstrumented and instrumented conditions in human cadaveric specimens.

Methods. Seven human cadaveric spine specimens (T1-T12) with four conditions (with and without rib cage, instrumented and uninstrumented) were subjected to 5 Nm pure moments in flexion-extension, lateral bending, and axial rotation. Range-of-motion, neutral and elastic

zones, neutral and elastic zone stiffness values, and out-of-plane rotations were calculated for overall specimens.

Results. In-plane range-of-motion was significantly higher without a rib cage for most modes of bending. Out-of-plane motion was also influenced by the rib cage. Neutral zone stiffness was significantly higher with a rib cage present.

Conclusions. Testing without a rib cage yields different motion and stiffness measures, directly impacting the translation of research results to clinical interpretation. Researchers should consider these differences when evaluating the mechanical impact of surgical procedures or instrumentation in cadaveric or computational models.

5.1 Introduction

Mechanical testing of human cadaveric thoracic spine specimens is performed to understand the impact of instrumentation or surgical procedures on the clinically relevant mechanics of the spine. Studies examining the mechanics of the uninstrumented spine have shown that the rib cage reduces thoracic range-of-motion by up to 77% when compared to testing done with no rib cage [1, 2], but most cadaveric thoracic spine testing with implants and surgical procedures is currently performed on shorter spine segments without intact rib cages. The purpose of this study was to understand the mechanical effects of using full thoracic human cadaveric spine specimens with no rib cage versus an intact rib cage for specimens with surgical procedures performed or instrumentation in place.

A few studies have examined the mechanical impact of the rib cage on thoracic stability [1, 3-5], though only Watkins et al. utilized full (T1-T12) intact human thoracic cadaveric specimens to evaluate changes in range-of-motion due to the rib cage. The present study builds upon this work by evaluating the impact of the rib cage on motion parameters including range-of-motion, neutral and elastic zones, stiffness values, and coupled motion for instrumented and uninstrumented human cadaveric thoracic specimens.

The aim of this study was to understand the mechanical contribution of the intact rib cage in the human cadaveric thoracic spine specimen during testing. The following hypotheses were tested for overall motion in all modes of bending for both uninstrumented and instrumented specimens: (i) in-plane range-of-motion and neutral and elastic zones will be significantly larger for specimens with no ribs compared to intact ribs, (ii) neutral and elastic zone stiffness values will be significantly different for specimens with no ribs compared to intact ribs, and (iii) out-of-plane rotations will be significantly different for specimens with no ribs compared to intact ribs.

This work will help researchers design more clinically applicable testing and better translate their findings to the patient by elucidating the mechanical influence of experimental design options (no ribs v. intact ribs), thus giving clinicians more confidence in interpreting results from thoracic spine testing.

5.2 Materials and Methods

5.2.1 Experimental Design

Seven fresh-frozen human cadaveric spine specimens (T1-T12) were dissected to include only true ribs (T1-T10), sternum, vertebrae, intervertebral discs, and stabilizing ligaments. Specimens were x-rayed to screen for severe abnormalities or osteophytes, previous surgeries, or existing fractures that would cause exclusion. All specimens were included in the study (n=7). Average age at death was 71 ± 7 years.

Specimens were thawed to room temperature prior to testing. Screws for potting were inserted into T1 and T12, and auto-body filler (Bondo, 3M, St. Paul, MN, USA) was used to pot both T1 and T12 parallel to their vertebral end plates. The inferior end of each specimen (T12) was mounted in a novel spine testing machine (Applied Test Systems, Butler, PA, USA). The six degree-of-freedom machine allowed for the continuous application of a pure moment on the unconstrained superior end (T1) [6].

A motion-capture research pin (Optotrak, Northern Digital Inc., Waterloo, ON, Canada) was used to track the motion of T1; error was ± 0.1mm or $\pm 0.06°$ for the research pin. Anatomical points were probed based on Wilke et al., with adaptations to account for the rib cage, in order to determine the local coordinate system at T1 (Figure 5.1) [7]. Four conditions were tested sequentially:

- *Condition 1: Intact Ribs, Uninstrumented*: Considered the baseline condition. Four Ponte osteotomies were performed by a practicing spine surgeon between levels T6-T10 [8], and optical motion-capture pins were inserted into the pedicles of T7-T11 (Figure 5.2).

- *Condition 2: Intact Ribs, Instrumented*: Motion-capture pins at T7-T11 were removed. Multi-axial pedicle screws were inserted bilaterally into T6, T8, and T10 using the free-hand technique by a practicing orthopaedic or neurosurgeon, and 5.5 mm titanium rods were inserted [9].

- *Condition 3: No Ribs, Instrumented*: The rib cage was removed 1" lateral to the costovertebral joints with instrumentation still in place.

- *Condition 4: No Ribs, Non- Instrumented:* Instrumentation was removed.

For each condition, pure moments were applied at a displacement rate of 1 degree/second to a load limit of ± 5 Nm in three modes of bending in a random order: flexion-extension (FE), lateral bending (LB), and axial rotation (AR). Each test was run for five cycles, and the third cycle was analyzed. Saline solution was used to keep the specimen hydrated during testing. Displacement data from the optical motion-capture pin at T1 and load data from the test machine were recorded.

5.2.2 Data Analysis & Statistics

Matlab (MathWorks, Natick, MA, USA) was used to analyze the data and perform statistics. Euler decomposition techniques were used to determine both in-plane and out-of-plane rotations [10]. For each mode of bending (flexion, extension, right LB, left LB, right AR, and left AR) for all conditions, the following parameters were found [7]:

- Neutral Zone (NZ): Angulation difference at zero load (for complete FE, LB, and AR cycles),

- Neutral Zone Stiffness (NZS): Slope of load v. angular displacement at 0 Nm,

- Elastic Zone (EZ): Angular displacement from the end of NZ to the point of maximum loading ($\pm$5 Nm),

- Elastic Zone Stiffness (EZS): Slope of load v. angular displacement at 0 Nm at the point of maximum loading ($\pm$5 Nm),

- Range-of-Motion (ROM): Angular displacement from 0 Nm to maximum load ($\pm$5 Nm).

As seen in Figure 5.1, data comparisons of no ribs v. intact ribs for all parameters were done for uninstrumented Comparison A (Conditions 4 v. 1) and instrumented Comparison B (Conditions 3 v. 2). It has been shown for non-pathogenic thoracic spine specimens with intact rib cages that right and left LB and right and left AR are symmetric for ROM, EZ, NZS, and EZS [2], so ROM, EZ, NZS, and EZS were calculated for the complete LB and AR cycles, and for flexion and extension individually. ROM was also calculated for the complete FE cycle for comparison purposes. NZ was calculated for the complete FE, LB, and AR cycles. Values were reported as percent changes of no ribs v. intact ribs for both uninstrumented Comparison A and instrumented Comparison B.

Two out-of-plane rotation ratios were calculated for each mode of bending. Each out-of-plane rotation was divided by the primary in-plane rotation. For example, in AR, the out-of-plane rotation ratios LB/AR and FE/AR were calculated. Values were reported as percentages of no ribs v. ribs intact for both uninstrumented Comparison A and instrumented Comparison B.

To test the stated hypotheses, student t-tests at a significance level of $p < 0.05$ were used to compare with no ribs v. ribs intact in all modes of bending specimens for both uninstrumented

Comparison A and instrumented Comparison B. Parameters compared were: (i) in-plane ROM, EZ, and NZ (ii) NZS and EZS, and (iii) both out-of-plane rotation percentages.

5.3 Results

5.3.1 In-Plane Motion

Figure 5.3 depicts typical in-plane range-of-motion (ROM) v. load cycles for all four conditions. Figure 5.4 depicts the changes in in-plane ROM of specimens with no ribs v. ribs intact. Changes in in-plane ROM for specimens with no ribs v. intact ribs for uninstrumented specimens (Comparison A) in flexion (F), extension (E), flexion-extension (FE), lateral bending (LB), and axial rotation (AR) were 31.8%$\pm$8.5%, 8.7%$\pm$16.8%, 18.7%$\pm$9.0%, 37.4%$\pm$7.7%, and 77.0%$\pm$44.3%, respectively; all sets were significantly different except in E ($p=0.13$). Changes in in-plane ROM for specimens with no ribs v. intact ribs for instrumented specimens (Comparison B) in F, E, FE, LB, and AR were 15.6%$\pm$9.5%, 8.5%$\pm$16.8%, 11.3%$\pm$11.1%, 29.1%$\pm$7.1%, and 61.5%$\pm$23.3%, respectively; all sets were significantly different except in E ($p=0.18$).

Figure 5.5 depicts the changes in elastic zone (EZ) with no ribs v. ribs intact. Changes in EZ for uninstrumented specimens (Comparison A) of no ribs v. ribs intact in F, E, LB, and AR were 30.8%$\pm$12.6%, 4.3%$\pm$10.0%, 38.7%$\pm$14.1%, and 72.6%$\pm$44.6%, respectively; all sets were significantly different except in E ($p=0.18$). Ratios of EZ for instrumented specimens (Comparison B) of no ribs v. ribs intact in F, E, LB, and AR were 13.7%$\pm$13.0%, 6.1%$\pm$17.4%, 30.8%$\pm$9.8%, and 61.8%$\pm$16.5%, respectively; all sets were significantly different except in E ($p=0.31$).

Figure 5.6 depicts the changes in neutral zone stiffness (NZS) with no ribs v. ribs intact. Changes in NZS for uninstrumented specimens (Comparison A) of no ribs v. ribs intact in F, E, LB, and AR were -27.4%±11.7%, -29.3%±6.5%, -45.9%±9.1%, and -58.0%±9.0%, respectively; all sets were significantly different. Changes in NZS for instrumented specimens (Comparison B) of no ribs v. ribs intact in F, E, LB, and AR were -14.3%±19.0%, -22.3%±19.0%, -40.8%±8.1%, and -52.7%±12.8%, respectively; all conditions were significantly different except in F (p=0.31) and E (p=0.07).

No significant differences for Comparison A and B (i.e., specimens with no ribs v. ribs intact) were found in any NZ or EZS measurements.

5.3.2 Out-of-Plane Rotations

Table 5.2 summarizes the change in maximum out-of-plane motion as a percentage of the in-plane ROM for specimens with no ribs v. intact ribs. Significant differences were found only in ARIGHT AND LEFTB and LB/AR (p<0.01). In LB, for uninstrumented (Comparison A) and instrumented (Comparison B) specimens, the ARIGHT AND LEFTB out-of-plane rotation increased over 2.5 and 4 times, respectively. In AR, for uninstrumented (Comparison A) and instrumented (Comparison B) specimens, the LB/AR out-of-plane rotation decreased by over half.

5.4 Discussion

5.4.1 In-plane motion: Range-of-Motion (ROM) and Elastic Zone (EZ)

The results of the present study support the concept that the rib cage plays a significant role in thoracic stability. Table 5.1 shows a comparison of data from the present study to the

only known similar previous study which reported increases in thoracic flexibility of uninstrumented specimens in FE, LB, and AR of 66.0%, 54.8%, and 45.9%, respectively, with the removal of the rib cage [1]. However, the results in FE and LB should not be directly compared to the present study, as the load limits were 2 Nm rather than 5 Nm used in the present study. One reason for the varied results could be attributed to the idea that the sigmoidal nature of the load v. displacement curve may be more fully developed at 5 Nm as compared to that of 2 Nm. While the current work shows the largest increase in flexibility in AR, followed by LB and FE (see Figure 5.4), both studies confirm the significance of the rib cage in thoracic spine flexibility.

To the authors' knowledge, no previous studies have reported changes in EZ due to testing with no rib cage compared to an intact rib cage for human cadaveric spine specimens. As similarly found in the increase of ROM, the EZ increase was greatest in AR for both uninstrumented and instrumented cases (see Figure 5.5). Null hypothesis (i) failed to be rejected for ROM and EZ for both uninstrumented and instrumented specimen comparisons, indicating a significant increase in motion for specimens with no ribs v. intact ribs.

5.4.2 In-plane motion: Neutral Zone Stiffness (NZS)

To the authors' knowledge, no previous studies have reported changes in NZS due to testing with no ribs compared to intact ribs for human cadaveric spine specimens. While all NZS values decreased in specimens with no ribs compared to intact ribs (see Figure 5.6), the largest decrease was over 50% in AR. This significant change in stiffness near 0 Nm can also be seen in the displacement v. load graph in Figure 5.3 where the NZS is the inverse of the slope of the load

v. displacement curve at 0 Nm. Null hypothesis (ii) failed to be rejected for NZS, indicating a change in stiffness for specimens with no ribs v. intact ribs.

In order to provide maximum understanding of the clinical relevance of surgical procedures or implants, mechanical test models must closely represent living humans to offer a translatable understanding of the mechanical effects on the patient. Parameters such as the NZS can play an important role in understanding the impact of surgical interventions on the thoracic spine. If a surgical procedure or implant causes an increase in stiffness in the neutral zone, more stress would be put on the spine post-operation. Testing without an intact rib cage could fail to identify stress-related complications in patients that influence clinical outcomes. The results of this study support the need to include the intact rib cage in testing of surgical implants and procedures in the thoracic spine.

5.4.3 Out-of-Plane Motion

Although most surgical procedures and devices are designed to compensate for imbalance in one body plane, the influence of these interventions have potentially clinically relevant ramifications in multiple body planes. The results of this study support the idea that AR and LB are often coupled motions, whether or not an intact rib cage is used in testing. This correlation has also been reported in in vivo studies, though more work should be done to understand the significance of the correlation [11].

In LB, the significant increase in the ARIGHT AND LEFTB ratios with the removal of the rib cage support the idea that the rib cage plays a significant role in AR stability of the thoracic spine. Likewise, in AR, the significant decrease in the LB/AR ratios with the removal

of the rib cage could be contributed to the increase in AR ROM with the removal of the rib cage (see Figure 5.4), further supporting the importance of the rib cage in AR stiffness.

5.4.4 Study Considerations

The average age of the specimens in this study was 71 years, so caution must be taken when applying these results to a younger specimen population. It is known that older specimens tend to exhibit higher stiffness than younger specimens, but it is unknown if the effect of mechanical testing with no ribs v. intact ribs is significantly different for various specimen ages; this would be an interesting study that could inform future test design.

The inclusion of follower loads or compressive pre-loads in the thoracic spine is a controversial topic in the testing community. While studies have shown that follower and compressive preloads in the cervical and lumbar regions will change the mechanics of the spine [12-15], little work has been done to understand the effects of these loads on the thoracic spine. In a study conducted on the thoracolumbar region, Stanley et al. found that a compressive preload reduced the overall ROM in the thoracolumbar spine by 22%, though tests did not include an intact rib cage [16]. The present study did not include follower or compressive preloads, as the rib cage prohibited the typical mode of application of such loads. More work should be done to better understand the effects of follower or compressive preloads in the thoracic spine with attached rib cage.

Intra-abdominal pressure and effects of active musculature were not simulated in the present study. Hodges et al. showed that intra-abdominal pressure contributes to thoracic stability [17], though the extent to which the flexibility is affected needs to be studied further. In addition, it is known that active musculature in a living human is different than the passive

motion in cadaveric testing. One group is utilizing a computational model of the thoracic spine including maximum muscle stress to estimate loads on the spine, though trunk muscle attachments were not included in the model [18, 19]. Although more work should be done to determine the extent to which active musculature and intra-abdominal pressure plays in thoracic spine mechanics, the results of the present study support the idea that the rib cage construct should be considered in both cadaveric and computational models that are used in studying and designing implants and surgical procedures.

The overall results of this study demonstrate that the rib cage should be included in cadaveric mechanical testing of the thoracic spine to best simulate clinical conditions. However, it is recognized that there are still many differences between cadaveric specimens and living patients. Further work should be done to elucidate these differences and provide even more translation of mechanical test results to the clinical condition.

5.5 Conclusions

Mechanical testing of human cadaveric thoracic spines without rib cages influences the motion and stiffness values when testing both surgical procedures and mechanical implants. These experimental testing differences directly influence translation of research results to clinical interpretation; researchers should consider these differences when evaluating the mechanical impact of surgical procedures or instrumentation in cadaveric or computational models.

5.6 Acknowledgments

5.7 References

[1] Watkins, R. t., Watkins, R., 3rd, Williams, L., Ahlbrand, S., Garcia, R., Karamanian, A., Sharp, L., Vo, C., and Hedman, T., 2005, "Stability provided by the sternum and rib cage in the thoracic spine," Spine, 30(11), pp. 1283-1286.

[2] Mannen, E. M., Anderson, J. T., Arnold, P. M., and Friis, E. A., 2014, "Mechanical Analysis of a Human Cadaveric Thoracic Spine with Intact Rib Cage," J Biomech (Under Review).

[3] Oda, I., Abumi, K., Cunningham, B. W., Kaneda, K., and McAfee, P. C., 2002, "An in vitro human cadaveric study investigating the biomechanical properties of the thoracic spine," Spine, 27(3), pp. E64-70.

[4] Oda, I., Abumi, K., Lu, D., Shono, Y., and Kaneda, K., 1996, "Biomechanical role of the posterior elements, costovertebral joints, and rib cage in the stability of the thoracic spine," Spine, 21(12), pp. 1423-1429.

[5] Andriacchi, T., Schultz, A., Belytschko, T., and Galante, J., 1974, "A model for studies of mechanical interactions between the human spine and rib cage," J Biomech, 7(6), pp. 497-507.

[6] Mannen, E. M., Ranu, S. S., Villanueva, A. M., and Friis, E. A., 2014, "Validation of a Novel Spine Test Machine," J Med Dev (In Press).

[7] Wilke, H. J., Wenger, K., and Claes, L., 1998, "Testing criteria for spinal implants: recommendations for the standardization of in vitro stability testing of spinal implants," European spine journal : official publication of the European Spine Society, the European Spinal Deformity Society, and the European Section of the Cervical Spine Research Society, 7(2), pp. 148-154.

[8] Ponte, A., Siccardi, G., and Ligure, P., 1995, "Posterior shortening procedure by segmental closing wedge resections," Journal of pediatric orthopedics, 15, p. 404.

[9] Kim, Y. J., and Lenke, L. G., 2005, "Thoracic pedicle screw placement: free-hand technique," Neurology India, 53(4), pp. 512-519.

[10] Crawford, N. R., Yamaguchi, G. T., and Dickman, C. A., 1996, "Methods for determining spinal flexion/extension, lateral bending, and axial rotation from marker coordinate data: Analysis and refinement," Human Movement Science, 15(1), pp. 55-78.

[11] Willems, J. M., Jull, G. A., and J, K. F., 1996, "An in vivo study of the primary and coupled rotations of the thoracic spine," Clinical biomechanics (Bristol, Avon), 11(6), pp. 311-316.

[12] Patwardhan, A. G., Havey, R. M., Ghanayem, A. J., Diener, H., Meade, K. P., Dunlap, B., and Hodges, S. D., 2000, "Load-carrying capacity of the human cervical spine in compression is increased under a follower load," Spine, 25(12), pp. 1548-1554.

[13] Patwardhan, A. G., Havey, R. M., Meade, K. P., Lee, B., and Dunlap, B., 1999, "A follower load increases the load-carrying capacity of the lumbar spine in compression," Spine, 24(10), pp. 1003-1009.

[14] Patwardhan, A. G., Havey, R. M., Carandang, G., Simonds, J., Voronov, L. I., Ghanayem, A. J., Meade, K. P., Gavin, T. M., and Paxinos, O., 2003, "Effect of compressive follower preload on the flexion-extension response of the human lumbar spine," Journal of orthopaedic research : official publication of the Orthopaedic Research Society, 21(3), pp. 540-546.

[15] Fry, R. W., Alamin, T. F., Voronov, L. I., Fielding, L. C., Ghanayem, A. J., Parikh, A., Carandang, G., McIntosh, B. W., Havey, R. M., and Patwardhan, A. G., 2014, "Compressive preload reduces segmental flexion instability after progressive destabilization of the lumbar spine," Spine, 39(2), pp. E74-81.

[16] Stanley, S. K., Ghanayem, A. J., Voronov, L. I., Havey, R. M., Paxinos, O., Carandang, G., Zindrick, M. R., and Patwardhan, A. G., 2004, "Flexion-extension response of the thoracolumbar spine under compressive follower preload," Spine, 29(22), pp. E510-514.

[17] Hodges, P. W., Cresswell, A. G., Daggfeldt, K., and Thorstensson, A., 2001, "In vivo measurement of the effect of intra-abdominal pressure on the human spine," J Biomech, 34(3), pp. 347-353.

[18] Iyer, S., Christiansen, B. A., Roberts, B. J., Valentine, M. J., Manoharan, R. K., and Bouxsein, M. L., 2010, "A biomechanical model for estimating loads on thoracic and lumbar vertebrae," Clinical biomechanics (Bristol, Avon), 25(9), pp. 853-858.

[19] Bruno, A. G., Anderson, D. E., D'Agostino, J., and Bouxsein, M. L., 2012, "The effect of thoracic kyphosis and sagittal plane alignment on vertebral compressive loading," Journal of bone and mineral research : the official journal of the American Society for Bone and Mineral Research, 27(10), pp. 2144-2151.

5.8 Tables

Table 5.1: Summary of overall (T1-T12) mean ($\pm$StDev) change in in-plane range-of-motion (ROM) for no ribs v. intact ribs from testing done on human cadaveric specimens. Abbreviations: flexion-extension (FE), lateral bending (LB), axial rotation (AR). --Value not reported; †50N axial preload applied; ‡Standard deviation not reported.

Author (Year)	Age	Load Limits				Change in ROM for No Ribs v. Intact Ribs (%)		
		FE	LB	AR		FE	LB	AR
Present Study (2014)	71 ± 7 (59 to 82)	5 Nm	5 Nm	5 Nm	Not Instrumented Instrumented	18.6 ± 9.0 11.3 ± 11.1	37.4 ± 7.7 29.1 ± 7.1	77.0 ± 44.3 61.5 ± 23.3
Watkins (2005)	72‡ (55 to 91)	2 Nm	2 Nm	5 Nm†	Not Instrumented Instrumented	66‡ --	54.8‡ --	45.9‡ --

Table 5.2: Mean (StDev) change in out-of-plane/in-plane motion of specimens with no ribs v. intact ribs for Comparison A (uninstrumented) and B (instrumented). ARIGHT AND LEFTB and LB/AR are the ratios of out-of-plane/in-plane motion reported as a percentage. All ratios were significantly different (p<0.01) for specimens with no ribs v. intact ribs.

Out-of-Plane/ In-Plane Motion	Mean (St. Dev) Change in Out-of-Plane/In-Plane Motion of No Ribs v. Intact Ribs (%)	
	Uninstrumented (Comparison A)	Instrumented (Comparison B)
AR/LB	345 (441)	153 (89)
LB/AR	-60 (26.3)	-62.1 (23.1)

5.9 Figures
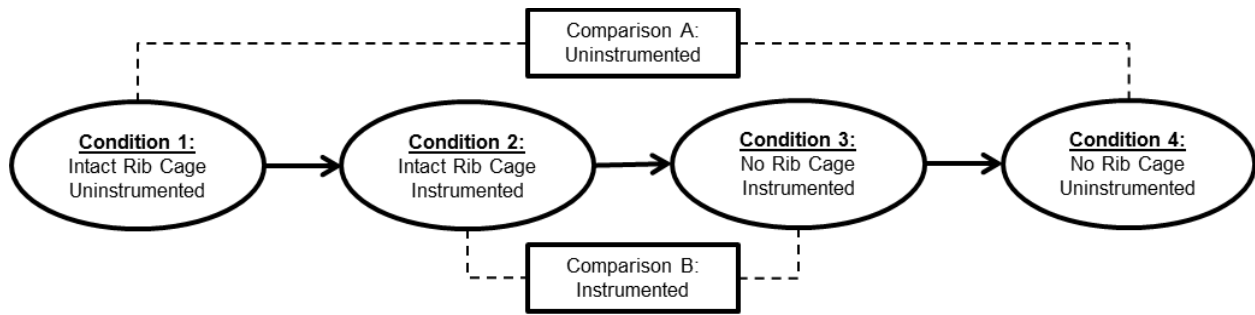
Figure 5.1: Schematic of experimental design including four test conditions (intact rib cage, uninstrumented; intact rib cage, instrumented; no rib cage, instrumented; and no rib cage, uninstrumented) and two data comparisons (A and B).

Figure 5.2: Posterior view of testing of Condition 1 (intact rib cage, uninstrumented). The motion-capture pin at T1 was used to track overall motion of the specimen, and the pins at T6 and T10 were used to calculated regional motion between T6 and T10.
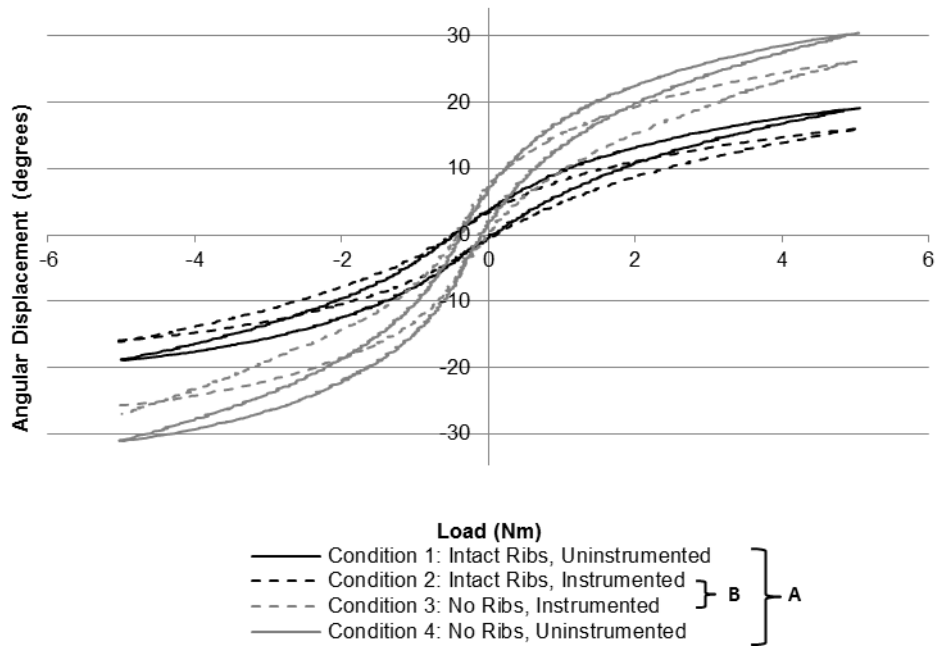
Figure 5.3: Typical in-plane angular displacement v. load cycles for all conditions in axial rotation. Comparisons A (solid) and B (dotted) show motion change of intact ribs (black) v. no ribs (gray) for uninstrumented and instrumented specimens, respectively. A significant increase (p<0.05) in ROM was found for no ribs v. intact ribs.
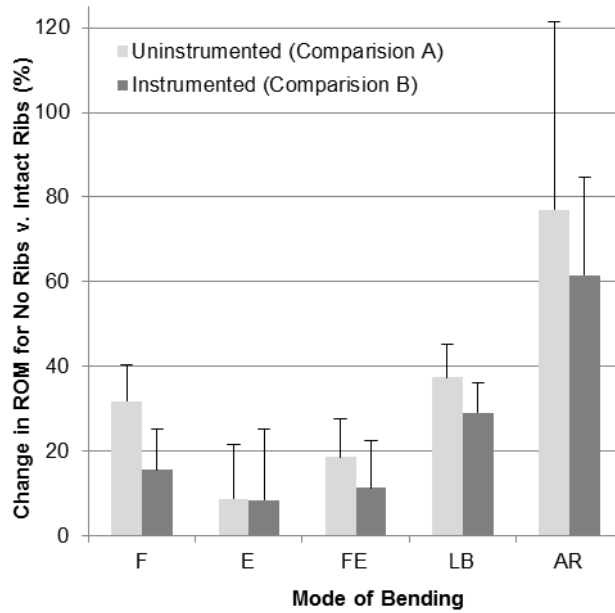
Figure 5.4: Mean (+StDev) change in in-plane range-of-motion (ROM) in specimens with no ribs v. intact ribs for all modes of bending: flexion (F), extension (E), flexion-extension (FE), lateral bending (LB), and axial rotation (AR). Significance ($p<0.05$) between no ribs v. intact ribs was found in all modes of bending except extension.
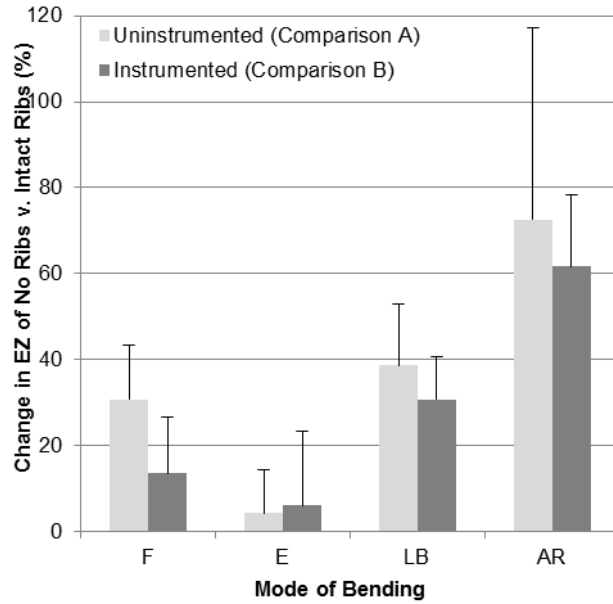
Figure 5.5: Mean (+StDev) change in elastic zone (EZ) in specimens with no ribs v. intact ribs
for all modes of bending: flexion (F), extension (E), lateral bending (LB), and axial rotation
(AR). Significance ($p < 0.05$) between no ribs v. intact ribs was found in all modes of bending
except extension.
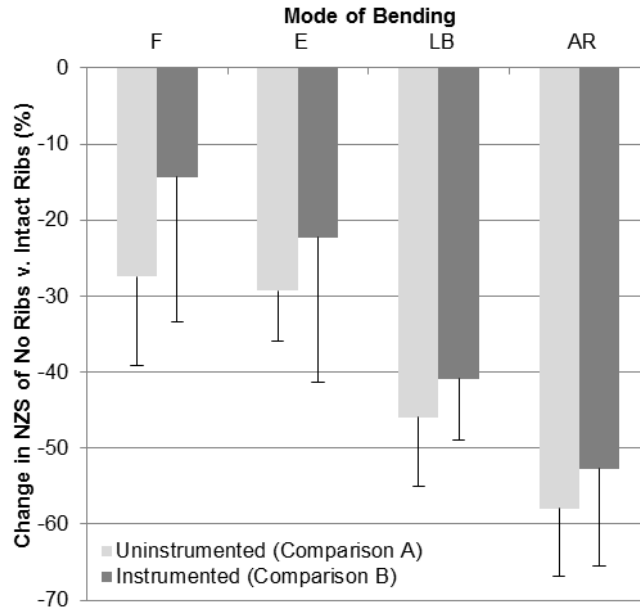
Figure 5.6: Mean (-StDev) change in neutral zone stiffness (NZS) in specimens with no ribs v. intact ribs for all modes of bending: flexion (F), extension (E), lateral bending (LB), and axial rotation (AR). Significance (p<0.05) between no ribs v. intact ribs was found for all cases except instrumented flexion and extension.

CHAPTER 6:

Overall and Regional Range-of-Motion Analysis of Sequential Ponte Osteotomies on a Human Thoracic Cadaver with an Intact Rib Cage

Manuscript currently under revision for eventual submission to Spine Deformity or the Journal of Spinal Disorders, Submission planned for Spring 2014

This study analyzed the overall and regional range-of-motion changes due to sequential Ponte osteotomies. Erin Mannen had primary responsibility for the experimental design, data collection, data analysis, and writing of the first draft. Details on the experimental design and data analysis can be found in Appendix A. Please note that this chapter has not been thoroughly reviewed by the co-authors and does not yet contain all of the data that will be included in the manuscript for submission.

Additional data analysis on the Ponte osteotomy study will focus on local range-of-motion, out-of-plane motion, and stiffness changes on the overall, regional, and local levels. It is necessary to fully quantify the regional and local motions of the intact specimen (Chapter 4) before applying that analysis to this study. The Spine Biomechanics Lab will work together to complete these analyses and submit additional manuscripts by the end of 2014.

Overall and Regional Range-of-Motion Analysis of Sequential Ponte Osteotomies on a Human Thoracic Cadaver with an Intact Rib Cage

Erin M. Mannen[1], Paul M. Arnold[2] John T. Anderson[3], Elizabeth A. Friis[1*]

[1]*University of Kansas, Mechanical Engineering, 1530 W 15th St., Learned Hall Room 3138, Lawrence, KS 66045*

[2]*University of Kansas Medical Center, Department of Neurosurgery, 3901 Rainbow Blvd. MS 3021, Kansas City, KS 66160*

[3]*Children's Mercy Hospital and Clinics of Kansas City, Orthopaedic Surgery, 2401 Gillham Rd., Kansas City, MO 64108*

*Corresponding author, lfriis@ku.edu

Abstract

Patients with adolescent idiopathic scoliosis or Scheuermann's kyphosis often exhibit stiff sagittal curves requiring surgical releases prior to instrumentation. Ponte osteotomies (POs) are posterior procedures that are used to increase flexibility in the sagittal plane, but the mechanical impact of the technique has not been studied on a human thoracic cadaveric model with an intact rib cage. The objective of this study was to determine the change in range-of-motion on overall and regional levels with four sequential POs in the human thoracic spine with an intact ribcage (n=7). Results showed an increase in sagittal flexibility on both the overall and regional levels, but the increase in ROM may not be additive with sequential POs on a regional level. POs provide increased ROM in flexion-extension when studied on a human cadaveric model with an intact rib cage, supporting the usage of the procedure to increase sagittal correction potential before fusion in patients with hyperkyphosis, though more work should be done to determine the effectiveness of sequential POs.

6.1 Introduction

Adolescent Idiopathic Scoliosis (AIS) is a three-dimensional spinal curvature deformity condition that affects 2 to 2.5 percent of the population, with 10 percent of those cases requiring surgical intervention [1]. Scheuermann's Kyphosis (SK) is defined as a hyperkyphosis in the thoracic spine due to wedged vertebrae, and occurs in approximately 1 to 8 percent of the population [2]. AIS and SK can cause both physical pain [3-6] and body image issues that can lead to eating disorders and suicidal thoughts [7, 8]. The primary goal of corrective spinal fusion surgery for AIS or SK is to halt curvature progress, while a secondary goal, which is often more important to the patient, is to improve the aesthetics of the spine.

Although anterior releases were once considered necessary for patients with stiff sagittal curves, some current surgical techniques suggest that a posterior-only approach may provide adequate correction in the sagittal plane [9-11]. The Ponte osteotomy (PO) is one such technique that includes the removal of the posterior spinous process, the ligamentum flavum, and the facets at the apex of the sagittal curve, resulting in a chevron shape removal of tissue between two vertebral levels [10]. While the technique avoids the morbidity risks associated with an anterior approach, added neurological risks are presented as the spinal cord is exposed during surgery. Some studies suggest that one PO will result in 5° to 15° of sagittal correction [9, 12], and surgeons often use sequential POs to produce the desired amount of flexibility. Some researchers have begun to examine the mechanical impact of POs on human cadaveric models[13, 14], but the biomechanical effects of sequential POs in the sagittal as well as the coronal and lateral planes have not been studied in a cadaveric human thoracic model with an intact rib cage. The purpose of this study was to determine the overall (T1-T12) and regional (T6-T10) motion changes due to sequential Ponte osteotomies.

6.2 Methods

Seven fresh-frozen male human cadaveric thoracic specimens (T1-T12) with attached true ribs were dissected to include only stabilizing ligaments, bones, and intervertebral discs. All specimens were x-rayed to ensure no fractures, abnormalities, or previous surgeries would cause exclusion; all specimens were included in the study. Average age was 71 ± 7 years.

Specimens were thawed to room temperature before testing. T1 and T12 were potted with auto-body filler (Bondo, 3M, St. Paul, MN, USA) parallel to the vertebral end plate. Specimens were mounted in a novel six degree-of-freedom spine testing machine (Applied Test Systems, Butler, PA, USA) that allowed for the application of a pure moment with control of displacement rate to a specified load limit [15]. T12 was mounted to the test machine, and T1 was free to move in all directions.

Optical motion-capture research pins (Optotrak, Northern Digital Inc., Waterloo, ON, Canada) were inserted into the T1 potting and into the right pedicles of T6, T7, T8, T9, T10, and T11. Error in the diodes was ±0.1mm, resulting in $\pm0.06°$ for the research pin. Anatomical points were probed, with adaptations to account for the intact rib cage to determine the local coordinate system at T1, T6, and T10 [16]. The experimental setup is depicted in Figure 6.1.

Testing was conducted in all three modes of bending [flexion-extension (FE), lateral bending (LB), and axial rotation (AR)]. Pure moments were applied to T1 at a displacement rate of 1 degree/second to a load limit of ±5 Nm for five cycles, with the third used for analysis for the following five conditions: intact specimen, one-level Ponte osteotomy (P1) at T9-T10, two-level Ponte osteotomy (P2) at T8-T10, three-level Ponte osteotomy (P3) at T7-T10, and four-level Ponte osteotomy (P4) at T6-T10. Ponte osteotomies were performed by practicing surgeons to ensure appropriate techniques. Angular displacements were calculated from the motion-

capture pin data, and loads were recorded by the spine test machine. Saline solution was used to preserve the mechanical integrity of the specimen throughout the duration of testing.

Euler decomposition techniques were utilized to determine angular displacements[17]. Matlab (MathWorks, Natick, MA, USA) was used for data analysis and statistics. For each mode of bending (flexion, extension, right LB, left LB, right AR, and left AR), overall (T1-T12) and regional (T6-T10) range-of-motion (ROM) was found. Studies have shown that non-pathogenic thoracic spine specimens with intact ribs exhibit symmetric behavior in right and left LB and right and left AR [18], so parameters were calculated for the complete LB and AR cycles, for flexion and extension individually, and for the complete FE cycle for comparison purposes. All measures from conditions P1, P2, P3, and P4 were normalized to the intact condition and reported as percentages. Student t-tests at a $p<0.05$ significance level were used to compare ROM parameters from conditions P1, P2, P3 and P4 to parameters from the intact condition.

6.3 Results

Figure 6.2 depicts a typical load v. angular displacement cycle in flexion-extension for all five conditions. Figure 6.3 depicts the overall (T1-T12) change in range-of-motion (ROM) of conditions P1, P2, P3, and P4 compared to the intact condition. Significant changes were found for all conditions P1, P2, P3, and P4 v. intact for flexion only, and were 3.2%±3.3%, 5.5%±4.7%, 10.6%±11.1%, and 12.0%±8.5%, respectively. The maximum increase in the overall ROM in flexion due to one PO was 1.4°. Table 6.1 shows the change in overall ROM for each condition v. intact.

Figure 6.4 depicts the regional (T6-T10) change in ROM of conditions P1, P2, P3, and P4 compared to the intact condition. Significant changes were found for P2 and P3 v. intact in flexion, P1, P3, and P4 v. intact in extension, and for all conditions in FE. In flexion, changes in P1, P2, P3, and P4 v. intact were 29.4%$\pm$29.6%, 29.2%$\pm$19.3%, 42.3%$\pm$21.0%, and 63.9%$\pm$65.0%, respectively. The maximum increase in the regional ROM in flexion due to one PO was 0.7°. In extension, changes in P1, P2, P3, and P4 v. intact were 27.8%$\pm$24.5%, 22.2%$\pm$21.7%, 42.0%$\pm$25.9%, and 71.6%$\pm$59.1%, respectively. The maximum increase in the regional ROM in extension due to one PO was 1.1°. In FE, changes in P1, P2, P3, and P4 v. intact were 27.1%$\pm$19.6%, 25.6%$\pm$18.8%, 43.7%$\pm$20.3%, and 70.4%$\pm$58.4%, respectively. The maximum increase in the regional ROM in FE due to one PO was 1.6°. Table 6.2 shows the change in regional ROM for each condition v. intact.

6.4 Discussion

To the authors' knowledge, no work has been published on the mechanical effect of POs on a superiorly-loaded human thoracic spine with intact rib cage. The results of this study support the clinical practice of utilizing POs to increase sagittal plane flexibility. However, the amount of FE correction potential was found to be much less in both overall and regional analysis than the clinical rule-of-thumb of 5° per PO [9, 12].

The clinical understanding is that each PO provides an equal amount of correction potential in the sagittal plane. Results of the overall ROM changes support this notion, as a four-level PO was found to provide nearly four times the correction potential of a one-level PO (Figure 6.3). However, the regional ROM results of this study suggest that a four-level sequential PO may provide just over 2.5 times the correction potential when compared to a one-

112

level PO (Figure 6.4). The discrepancy in this data could be attributed to the adjacent level effects that the rupturing of ligaments may have on the overall motion. Another consideration is that the levels at which the POs are being performed may not behave in exactly the same way in the intact state. An interesting study would be to evaluate the local motion of an intact specimen, the compare that motion to changes due to subsequent POs.

The present study was limited by the use of cadaveric specimens of advanced age. It is known that younger specimens, both living and cadaveric, exhibit more flexibility and less-brittle bones than the aging population. However, conducting such invasive mechanical testing on living humans is unrealistic, and pediatric cadaveric testing is uncommon. Thus, the authors sought to utilize a cadaveric model that resembled a living patient as closely as possible by including the intact rib cage.

In the most closely related study to the present work, pure moments of ±6 Nm were applied in FE, LB, and AR to partial human thoracic specimens (T2-T5 and T8-T11) with no rib cages for four conditions: intact, one-level PO, two-level PO, and three-level PO [13]. Table 6.3 is a comparison of data of the regional ROM data of the present study to that of Sangiogorio et al. While the results are similar, the present study shows a lower correction potential in the sagittal plane, which would be expected when considering the differences in experimental design. It has been reported that mechanical testing with no rib cage v. an intact rib cage yields up to a 77% higher ROM in all modes of bending [19, 20], so one can assume that the results of the present study would exhibit a lower ROM due to the inclusion of the intact ribcage when compared studies with no rib cage. Similarly, no significant changes were found in AR or LB in the present study compared to a slight increase in AR reported by Sangiogorio et al., likely due to the stiffness provided by the intact ribcage.

In a four-cadaver study of T4-T12 with intact rib cages, Wiemann et al. studied the decrease in force required to manually rotate vertebral levels in the coronal plane after a PO [14]. The results showed that POs decreased the force required to produce a 25° axial rotation by 18%. A novel technique to apply force that may more closely simulate surgical techniques was used in the study, though repeatability of the angle and rate of force application must be considered as the force was not automated but applied by hand. In addition, only axial rotation was considered in this study. For these reasons, it is difficult to directly compare these results to the present study.

While several groups have studied the mechanical impact of various posterior releases on cadaveric models [21-26], to the authors' knowledge, only Healy et al. utilized a full human thoracic spine (T1-T12) with an intact rib cage to evaluate changes in ROM on an overall and regional level. Healy et al. found no significant changes in either overall or regional ROM due to a series of decompressive procedures when compared to an intact specimen, supporting the idea that utilizing the rib cage during mechanical testing may provide substantial stability to the thoracic spine.

Future studies should examine if the level at which the PO is performed affects correction potential. Mechanically, vertebral levels near the apex of the sagittal curve exhibit different behavior and experience altered stresses when compared to other levels. Analyzing motion at a local level may give insight to this question and could inform surgeons of the most appropriate levels for POs.

6.5 Conclusions

Ponte osteotomies provide increased ROM in flexion-extension when studied on a human cadaveric model with an intact rib cage, supporting the usage of the procedure to increase sagittal correction potential before fusion in patients with hyperkyphosis.

6.6 References

[1] Asher, M. A., and Burton, D. C., 2006, "Adolescent idiopathic scoliosis: natural history and long term treatment effects," Scoliosis, 1(1), p. 2.

[2] Arlet, V., and Schlenzka, D., 2005, "Scheuermann's kyphosis: surgical management," European spine journal : official publication of the European Spine Society, the European Spinal Deformity Society, and the European Section of the Cervical Spine Research Society, 14(9), pp. 817-827.

[3] Pratt, R. K., Burwell, R. G., Cole, A. A., and Webb, J. K., 2002, "Patient and parental perception of adolescent idiopathic scoliosis before and after surgery in comparison with surface and radiographic measurements," Spine, 27(14), pp. 1543-1550; discussion 1551-1542.

[4] Weinstein, S. L., Dolan, L. A., Spratt, K. F., Peterson, K. K., Spoonamore, M. J., and Ponseti, I. V., 2003, "Health and function of patients with untreated idiopathic scoliosis: a 50-year natural history study," JAMA : the journal of the American Medical Association, 289(5), pp. 559-567.

[5] Mayo, N. E., Goldberg, M. S., Poitras, B., Scott, S., and Hanley, J., 1994, "The Ste-Justine Adolescent Idiopathic Scoliosis Cohort Study. Part III: Back pain," Spine, 19(14), pp. 1573-1581.

[6] Danielsson, A. J., Cederlund, C. G., Ekholm, S., and Nachemson, A. L., 2001, "The prevalence of disc aging and back pain after fusion extending into the lower lumbar spine. A matched MR study twenty-five years after surgery for adolescent idiopathic scoliosis," Acta radiologica (Stockholm, Sweden : 1987), 42(2), pp. 187-197.

[7] Payne, W. K., 3rd, Ogilvie, J. W., Resnick, M. D., Kane, R. L., Transfeldt, E. E., and Blum, R. W., 1997, "Does scoliosis have a psychological impact and does gender make a difference?," Spine, 22(12), pp. 1380-1384.

[8] Alborghetti, A., Scimeca, G., Costanzo, G., and Boca, S., 2008, "The prevalence of eating disorders in adolescents with idiopathic scoliosis," Eating disorders, 16(1), pp. 85-93.

[9] Geck, M. J., Macagno, A., Ponte, A., and Shufflebarger, H. L., 2007, "The Ponte procedure: posterior only treatment of Scheuermann's kyphosis using segmental posterior shortening and pedicle screw instrumentation," J Spinal Disord Tech, 20(8), pp. 586-593.

[10] Ponte, A., Siccardi, G., and Ligure, P., 1995, "Posterior shortening procedure by segmental closing wedge resections," Journal of pediatric orthopedics, 15, p. 404.

[11] Diab, M. G., Franzone, J. M., and Vitale, M. G., 2011, "The role of posterior spinal osteotomies in pediatric spinal deformity surgery: indications and operative technique," Journal of pediatric orthopedics, 31(1 Suppl), pp. S88-98.

[12] Cho, K.-J., Bridwell, K. H., Lenke, L. G., Berra, A., and Baldus, C., 2005, "Comparison of Smith-Petersen Versus Pedicle Subtraction Osteotomy for the Correction of Fixed Sagittal Imbalance," Spine, 30(18), pp. 2030-2037.

[13] Sangiorgio, S. N., Borkowski, S. L., Bowen, R. E., Scaduto, A. A., Frost, N. L., and Ebramzadeh, E., 2013, "Quantification of Increase in Three-dimensional Spine Flexibility Following Sequential Ponte Osteotomies in a Cadaveric Model," Spine Deformity, 1(3), pp. 171-178.

[14] Wiemann, J., Durrani, S., and Bosch, P., 2011, "The effect of posterior spinal releases on axial correction torque: a cadaver study," Journal of children's orthopaedics, 5(2), pp. 109-113.

[15] Mannen, E. M., Ranu, S. S., Villanueva, A. M., and Friis, E. A., 2014, "Validation of a Novel Spine Test Machine," J Med Dev (In Press).

[16] Wilke, H. J., Wenger, K., and Claes, L., 1998, "Testing criteria for spinal implants: recommendations for the standardization of in vitro stability testing of spinal implants," European spine journal : official publication of the European Spine Society, the European Spinal Deformity Society, and the European Section of the Cervical Spine Research Society, 7(2), pp. 148-154.

[17] Crawford, N. R., Yamaguchi, G. T., and Dickman, C. A., 1996, "Methods for determining spinal flexion/extension, lateral bending, and axial rotation from marker coordinate data: Analysis and refinement," Human Movement Science, 15(1), pp. 55-78.

[18] Mannen, E. M., Anderson, J. T., Arnold, P. M., and Friis, E. A., 2014, "Mechanical Analysis of a Human Cadaveric Thoracic Spine with Intact Rib Cage," J Biomech (Under Review).

[19] Watkins, R. t., Watkins, R., 3rd, Williams, L., Ahlbrand, S., Garcia, R., Karamanian, A., Sharp, L., Vo, C., and Hedman, T., 2005, "Stability provided by the sternum and rib cage in the thoracic spine," Spine, 30(11), pp. 1283-1286.

[20] Mannen, E. M., Anderson, J. T., Arnold, P. M., and Friis, E. A., 2014, "Mechanical Contribution of the Rib Cage in the Cadaveric Thoracic Spine," Spine (Under Review).

[21] Feiertag, M. A., Horton, W. C., Norman, J. T., Proctor, F. C., and Hutton, W. C., 1995, "The effect of different surgical releases on thoracic spinal motion. A cadaveric study," Spine, 20(14), pp. 1604-1611.

[22] Horton, W. C., Kraiwattanapong, C., Akamaru, T., Minamide, A., Park, J. S., Park, M. S., and Hutton, W. C., 2005, "The role of the sternum, costosternal articulations, intervertebral disc, and facets in thoracic sagittal plane biomechanics: a comparison of three different sequences of surgical release," Spine, 30(18), pp. 2014-2023.

[23] Healy, A. T., Lubelski, D., Mageswaran, P., Bhowmick, D. A., Bartsch, A. J., Benzel, E. C., and Mroz, T. E., 2014, "Biomechanical analysis of the upper thoracic spine after decompressive procedures," The spine journal : official journal of the North American Spine Society, 14(6), pp. 1010-1016.

[24] Oda, I., Abumi, K., Lu, D., Shono, Y., and Kaneda, K., 1996, "Biomechanical role of the posterior elements, costovertebral joints, and rib cage in the stability of the thoracic spine," Spine, 21(12), pp. 1423-1429.

[25] Deniz, F. E., Brasiliense, L. B., Lazaro, B. C., Reyes, P. M., Sawa, A. G., Sonntag, V. K., and Crawford, N. R., 2010, "Biomechanical evaluation of posterior thoracic transpedicular discectomy," Journal of neurosurgery. Spine, 13(2), pp. 253-259.

[26] Brasiliense, L. B., Lazaro, B. C., Reyes, P. M., Dogan, S., Theodore, N., and Crawford, N. R., 2011, "Biomechanical contribution of the rib cage to thoracic stability," Spine, 36(26), pp. E1686-1693.

6.7 Tables

Table 6.1: Mean (StDev) of overall (T1-T12) range-of-motion (ROM) changes in degrees in all modes-of-bending (MoB) [flexion (F), extension (E), flexion-extension (FE), lateral bending (LB), and axial rotation (AR)] for one-level (P1), two-level (P2), three-level (P3), and four-level (P4) Ponte osteotomies compared to the intact condition. $*p<0.05$, $\dagger p<0.1$

Mean (StDev) Overall (T1-T12) Change in ROM v. Intact (degrees)			
MoB	P1	P2	P3	P4
F	0.25 (0.26)*	0.47 (0.42)*	1.00 (1.04)*	1.05 (0.95)*
E	0.29 (0.52)	0.31 (1.07)	1.16 (1.73)	1.34 (2.00)
FE	0.54 (0.59)†	0.79 (1.38)	2.16 (2.59)†	2.49 (2.81)†
LB	0.18 (0.87)	0.19 (1.23)	0.24 (1.79)	0.52 (1.38)
AR	-0.06 (0.81)	-1.14 (3.63)	-0.02 (1.46)	-0.73 (2.97)

Table 6.2: Mean (StDev) of regional (T6-T10) range-of-motion (ROM) changes in degrees in all modes-of-bending (MoB) [flexion (F), extension (E), flexion-extension (FE), lateral bending (LB), and axial rotation (AR)] for one-level (P1), two-level (P2), three-level (P3), and four-level (P4) Ponte osteotomies compared to the intact condition. *$p<0.05$, †$p<0.1$

Mean (StDev) Regional (T6-T10) Change in ROM v. Intact (degrees)			
MoB	P1	P2	P3	P4
F	0.19 (0.12)*	0.20 (0.16)*	0.36 (0.31)*	0.47 (0.42)†
E	0.28 (0.19)*	0.20 (0.26)	0.61 (0.67)†	0.87 (0.80)*
FE	0.47 (0.27)*	0.44 (0.37)*	1.00 (0.98)†	1.38 (1.17)*
LB	-0.2 (0.80)	-0.21 (0.54)	-0.43 (1.17)	-0.34 (0.54)
AR	0.37 (0.46)	0.31 (0.80)	0.71 (0.83)†	0.43 (0.99)

Table 6.3: Mean (StDev) regional range-of-motion (ROM) changes in flexion (F), extension (E), and flexion-extenion (FE) modes-of-bending (MoB) of one-level (P1), two-level (P2), three-level (P3), and four-level (P4) Ponte osteotomies compared to intact specimens for the present study and Sangiorgio et al. [13]. Note that in the present study, a full thoracic specimen (T1-T12) with intact rib cage was used with regional motion (T6-T10) reported, while Sangiogorio et al. used short segments (T2-T5 or T8-T11) with no rib cage.

	Regional ROM Change (%) Mean (StDev)					
	Testing Notes	*MoB*	*P1*	*P2*	*P3*	*P4*
Present Study	T1-T12;	F	29 (30)	29 (19)	42 (21)	64 (65)
(2014)	intact rib cage;	E	28 (25)	22 (22)	42 (26)	72 (59)
	T6-T10 motion	FE	27 (20)	26 (19)	44 (20)	70 (58)
Sangiorgio et al	T2-T5 or T8-T11;	F	33 (44)	56 (68)	69 (39)	--
(2013)	no rib cage;	E	12 (32)	34 (38)	56 (95)	--
	segment motion	FE	20 (16)	41 (24)	54 (33)	--

Figure 6.1: Experimental setup depicting a human thoracic spine (T1-T12) with intact rib cage, shown here from the left lateral view. Optical motion-tracking pins are in the top potting of T1 and the pedicles of T6-T10.
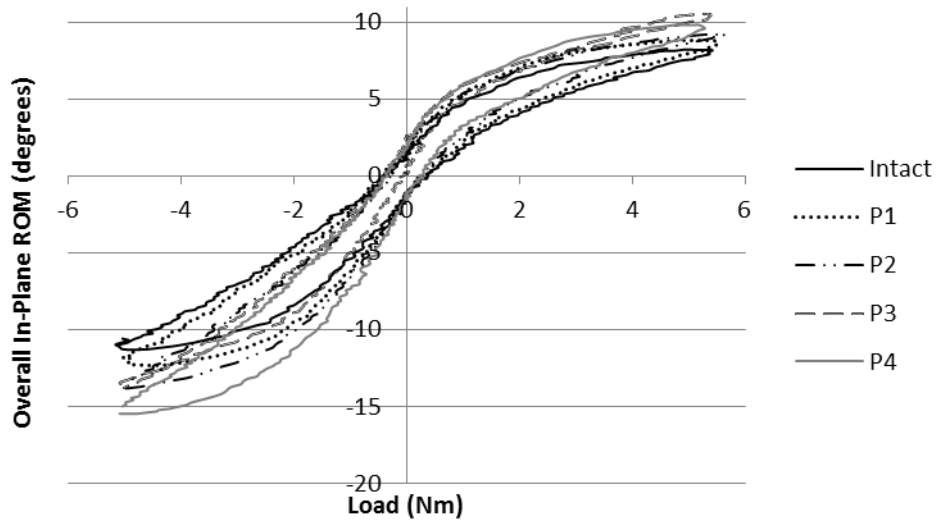
Figure 6.2: Typical overall in-plane angular displacement v. load graph in flexion(+)/ extension (-) for all five conditions: Intact, one-level Ponte osteotomy (PO) between T9-10 (P1), two-level PO between T8-10 (P20, three-level PO between T7-T10 (P3), and four-level PO between T6-T10 (P4). Overall angular displacement tends to increase with increasing POs.
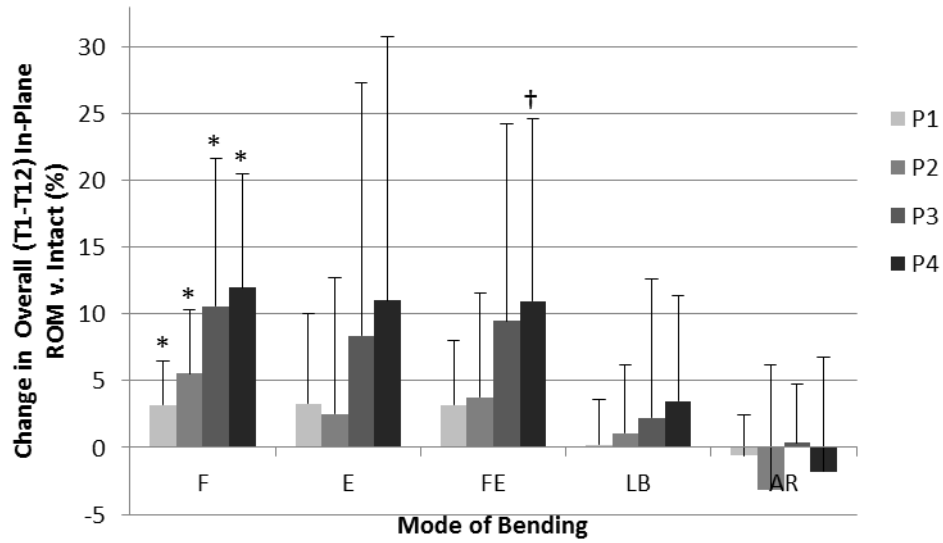
Figure 6.3: Change in overall (T1-T12) in-plane range-of-motion (ROM) v. intact for one-level (P1), two-level (P2), three-level (P3), and four-level (P4) Ponte osteotomies in all modes of bending [flexion(F), extension (E), flexion-extension (FE), lateral bending (LB), and axial rotation (AR). *p<0.05, †p<0.1
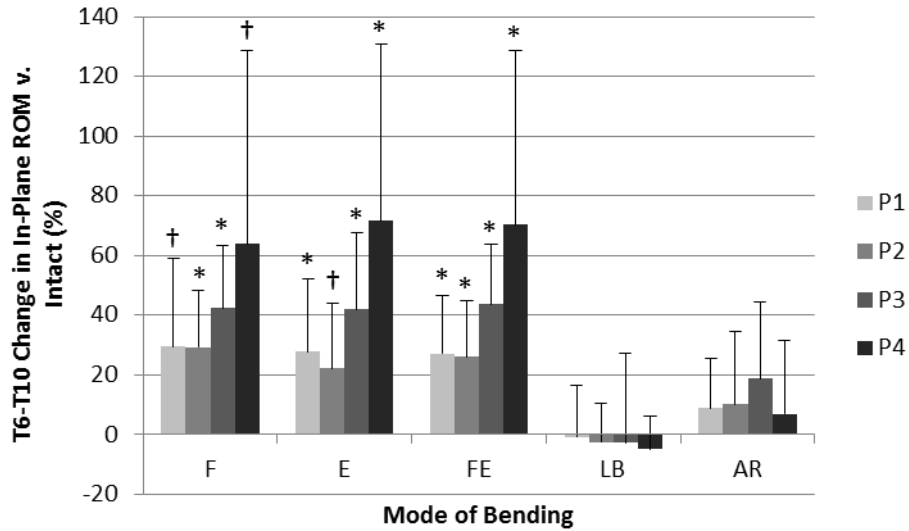
Figure 6.4: Change in regional (T6-T10) in-plane range-of-motion (ROM) v. intact for one-level
(P1), two-level (P2), three-level (P3), and four-level (P4) Ponte osteotomies in all modes of
bending [flexion(F), extension (E), flexion-extension (FE), lateral bending (LB), and axial
rotation (AR). *p<0.05, †p<0.1

CHAPTER 7:

Conclusions and Future Work

The research presented in this dissertation has sought to elucidate issues with current thoracic spine testing methods and develop more accurate ways to quantify the biomechanical impact of surgical procedures or medical devices. A novel spine testing machine developed by Applied Test Systems (Butler, PA), which allows researchers to analyze the biomechanical changes in cadaveric thoracic spine specimens with an intact rib cage in flexion-extension, lateral bending, and axial rotation, was validated in Specific Aim 1 (Chapter 3). The biomechanical questions of (i) quantifying the motion of a full human cadaveric thoracic specimen with an intact rib cage and (ii) understanding the differences in testing specimens with and without a rib cage were addressed in Specific Aim 2 (Chapters 4 and 5). Finally, the clinical question of quantifying the mechanical impacts of sequential Ponte Osteotomies (POs) was studied in Specific Aim 3 (Chapter 6).

Chapter 3 validated the accuracy of the spine test machine for rigidity ranges that represented the variety of cadaveric spine specimens that could be tested in the ATS spine test machine. Results showed that cadaveric spine testing of lumbar and thoracic spines with real-time in-plane displacement errors of less than two degrees in both bending and axial rotation could be achieved by utilizing the spine test machine alone [38]. When used in conjunction with an external motion-capture system, accurate angular displacement results limited by the external motion-capture system itself could be obtained for cervical, thoracic and lumbar mechanical spine testing up to ±15 Nm. Quantified error gives researchers more confidence in understanding and interpreting the results of cadaveric biomechanical testing.

Researchers should consider developing a standard protocol for evaluation of error on adapted or custom-built spine testing machines to ensure that results are reasonable. Further revisions of the spine test machine should be considered in order to improve accuracy of the displacement measurement. The novel spine test machine offers the benefit of physiological testing of spinal specimens and has the future potential to provide solutions for many other orthopedic testing fields.

Chapter 4 quantified the overall in-plane and basic coupled motions of a cadaveric human thoracic spine with intact true ribs. Results showed that lateral bending and axial rotation exhibited symmetric motion, neutral and elastic zone motion and stiffness values were significantly different for all modes of bending, and out-of-plane rotations and translations were greater than zero for most rotations and translations [35]. Future studies should characterize coupled motion patterns and local and regional level biomechanics of cadaveric human thoracic spines with intact true ribs. Attention should also be given to a more in-depth understanding of out-of-plane or coupled motion patterns in the thoracic spine with intact rib cage. This information may be particularly beneficial in the development of thoracic computational models. By fully quantifying the biomechanics of a non-pathologic thoracic specimen, future studies conducted on specific pathologies, procedures, or medical devices can be better understood.

Chapter 5 elucidated the differences of testing cadaveric thoracic spine specimens with and without an intact rib cage. In-plane range-of-motion was significantly higher without a rib cage for most modes of bending, out-of-plane motions were influenced, and neutral zone stiffness was significantly higher with a rib cage present [36]. Testing without a rib cage yielded different motion and stiffness measures, directly impacting the translation of research results to clinical interpretation. Researchers should consider these differences when evaluating the

mechanical impact of surgical procedures or instrumentation in cadaveric or computational models.

Chapter 6 quantified the overall and regional range-of-motion changes due to sequential Ponte osteotomies in cadaveric thoracic spine specimens with intact rib cages. Results showed an increase in sagittal flexibility on both the overall and regional levels, but the increase in range-of-motion may not be additive with sequential Ponte osteotomies on a regional level [37]. Ponte osteotomies were found to provide increased range-of-motion in flexion-extension when studied on a human cadaveric model with an intact rib cage, supporting the usage of the procedure to increase sagittal correction potential before fusion in patients with hyperkyphosis. More work should be done to determine the effectiveness of sequential Ponte osteotomies. In particular, attention should be given to the local changes in range-of-motion as well as coupled motion patterns that may change due to sequential Ponte osteotomies.

In summary, the ability to perform thoracic spine testing with an intact rib cage has been limited by both the lack of test machine availability and also the methodology and understanding of testing with an intact rib cage. This research sought to (1) validate a novel spine test machine, (2) provide biomechanical data to support the necessary inclusion of an intact rib cage when testing a full thoracic spine, and (3) quantify the biomechanical impacts of sequential Ponte osteotomies. The results from this work could provide researchers the tools they need to better understand and test spine procedures or implants, with the ultimate goas of improving surgical planning and patient outcomes.

APPENDIX A: Data Analysis Techniques

A.1 Probed points

Anatomical points were probed before and after testing for each specimen based on recommendations from Wilke and Goel with modifications to account for the intact rib cage [1, 2]. For the top potting, points probed both before and after testing included all points p1, p2, p3, p4, p5, p6, and p7 as seen in Figure A.1. For each vertebral level, points probed before testing included points p8, p9, p10, and p11, while points probed after testing included all points p8, p9, p10, p11, p12, p13, p14, and p15 as seen in Figure A.2. Points p12, p13, p14, and p15 were not probed post-testing for some specimens, and the centroid and local coordinate system analysis for these specimens can be found in section A.3. Points p16 and p17 represent the manubrium and the xiphoid process which probed before testing for all specimens as seen in Figure A.3

A.2 Centroids and Local Coordinate Systems

The first step in understanding spinal motion is to define the centroids and local coordinate systems of the specimen and motion tracking pins at each vertebral level at time = 0 (*t0*). All initial calculations are done with respect to the global reference frame G as seen in Figures A.4 and A.5. It can be assumed that G represents the motion of T12, which is fixed throughout the duration of testing. If no reference frame is noted, it can be assumed that the measure is taken with respect G, though sometimes it will be noted for clarity.

A.2.1 Top Potting (T1) Centroid and Local Coordinate System

Figure A.1 shows the points that were probed on the top potting of each specimen, representing T1. The local coordinate system for T1 was defined as $v_{T1}(x_{T1}, y_{T1}, z_{T1})$ where

$$x_{T1} = \text{p3} - \text{p4} \tag{1}$$

130

$$z_{T1} = (p1 - p2) \times (p4 - p2) \tag{2}$$

$$y_{T1} = z_{T1} \times x_{T1} \tag{3}$$

and $p1, p2, p3,$ and $p4$ are probed points found before testing as seen in Figure A.1 The centroid of the top potting was defined as c_{T1} where

$$c_{T1} = \frac{(p1 + p2 + p3 + p4)}{4} - \frac{1}{2}\left(\frac{(p3 - p4) + (p5 - p6)}{2}\right) \tag{4}$$

and $p1, p2, p3, p4, p5,$ and $p6$ are probed points found before testing as seen in Figure A.1.

A.2.2 Vertebral Level Centroids and Local Coordinate Systems

Figure A.2 shows the anatomical points that were probed at T6. These points were probed in the same way at each level of the vertebral column, so calculations will only be shown for T6. Anatomical points were selected based on recommendations by Wilke et al [2] with modifications to account for thoracic spine anatomy. The local coordinate system for T6 was defined as $v_{T6}(x_{T6}, y_{T6}, z_{T6})$ where

$$x_{T6} = p10 - p9 \tag{5}$$

$$z_{T6} = \frac{(p12-p13)+(p14-p15)}{2} \tag{6}$$

$$y_{T6} = z_{T6} \times x_{T6} \tag{7}$$

and $p9, p10, p11, p12, p13, p14,$ and $p15$ are probed points found after (post) testing as shown in Figure A.2. The centroid of T6 was defined as c_{T6} where

$$c_{T6} = \frac{(p9+p10+p12+p13)}{4} - \frac{z_{T6}}{2|z_{T6}|} \tag{8}$$

and $p9, p10, p12,$ and $p13$ are probed points found after testing as shown in Figure A.2.

A.2.3 Motion Tracking Pins' Centroids and Local Coordinate Systems

The local coordinate systems of the motion tracking pins were defined in the same way for each level as seen in Figures A.4 and A.5, so calculations will only be shown for T6. Each motion tracking pin contained three non-collinear markers on the face of the pin ($m1_{T6}$, $m2_{T6}$, $m3_{T6}$) as shown in Figure A.5. Probed point p11 representing the maker insertion point into the vertebral pedicle as first described in Figure A.2 is also depicted in Figure A.5. The local coordinate system of the motion tracking pin at T6 as shown in Figure A.5 was defined as $v_{T6'}(x_{T6'}, y_{T6'}, z_{T6'})$ where

$$x_{T6'} = m2_{T6} - m1_{T6} \tag{9}$$

$$y_{T6'} = x_{T6'} \times (m3_{T6} - m1_{T6}) \tag{10}$$

$$z_{T6'} = x_{T6'} \times y_{T6'} \tag{11}$$

for all time.

The centroid of the motion tracking pin T6 was defined as $c_{T6'}$ where

$$c_{T6'} = \frac{m1_{T6} + m2_{T6} + m3_{T6}}{3} \tag{12}$$

for all time.

A.2.4 Intermediate Coordinate System

Because the coordinate systems and centroids of the vertebral body T6 and the motion tracking pin T6' were not found at the same time, it was necessary to define an intermediate plane T6'' that was established both before and after testing so that the coordinate systems could be related to one another. Probed points p9, p10, and p11 were probed both before (t0) and after (post) testing, so these three points were used to create the intermediate coordinate system T6'' where

$$x_{T6''} = p9 - p10 \tag{13}$$

$$y_{T6''} = x_{T6''} \times (p11 - p10) \tag{14}$$

$$z_{T6''} = x_{T6''} \times y_{T6''} \tag{15}$$

for both before (t0) and after (post) probing. Figure A.6 depicts the probed points with corresponding coordinate systems both before (t0) and after (post) testing.

A.3 Relationship between Motion Tracking Pins and Vertebral Bodies

The geometric relationship between the motion tracking pin and the vertebral body at each level was assumed to remain constant throughout the duration of testing.

A.3.1 Rotation of Top Potting (T1)

Geometric relationships between the motion tracking pin and the vertebral levels T1 was calculated at *t0* and applied to the entire testing session. The rotation of the T1 vertebral body at *t0* with respect to the global reference frame G was defined as $_G R_{T1}(t0)$ where

$$_G R_{T1}(t0) = \begin{bmatrix} \dfrac{x_{T1}(t0)^T}{|x_{T1}(t0)|} & \dfrac{y_{T1}(t0)^T}{|y_{T1}(t0)|} & \dfrac{z_{T1}(t0)^T}{|z_{T1}(t0)|} \end{bmatrix} \tag{16}$$

for t0.

The rotation of the motion tracking pin attached to the vertebral body T6 with respect to the global reference frame G was defined as $_G R_{T6'}$ where

$$_G R_{T1'} = \begin{bmatrix} \dfrac{x_{T1'}^T}{|x_{T1'}|} & \dfrac{y_{T1'}^T}{|y_{T1'}|} & \dfrac{z_{T1'}^T}{|z_{T1'}|} \end{bmatrix} \tag{17}$$

for all t. The rotation of the vertebral body T1 with respect to the motion tracking pin attached to T1 (which is T1') for *t0* was defined as $_{T1'} R_{T1}$ where

$$_{T1'} R_{T1} = [_G R_{T1'}(t0)]^{-1} [_G R_{T1}(t0)] \tag{18}$$

133

and remained constant throughout the duration of testing. Thus, the rotation of the vertebral body T6 with respect to the global reference frame G was defined as $_GR_{T1}$ where

$$_GR_{T1} = [_GR_{T1'}] [_{T1'}R_{T1}]$$

(19)

for all t.

A.3.2 Translation of Top Potting (T1)

The vector from the centroid of the T1 vertebral body c_{T1} to the centroid of the attached motion tracking pin $c'_{T1}(t0)$ with respect to global reference frame G was defined as $_G\overline{c_{T1}c_{T1'}}(t0)$ where

$$_G\overline{c_{T1}c_{T1'}}(t0) = c_{T1'}(t0) - c_{T1}$$

(20)

and $_G\overline{c_{T1}c_{T1'}}(t0)$ with respect to T1' was defined as $_{T1'}\overline{c_{T1}c_{T1'}}$ where

$$_{T1'}\overline{c_{T1}c_{T1'}} = [_GR_{T1'}(t0)]^{-1} {_G\overline{c_{T1}c_{T1'}}}(t0)$$

(21)

and was assumed to be constant for all t.

Thus, the translation from the centroid of the T1 vertebral body c_{T1} to the centroid of the attached motion tracking pin $c_{T1'}$ with respect to the global reference frame G was defined as $_G\overline{c_{T1}c_{T1'}}$ where

$$_G\overline{c_{T1}c_{T1'}} = [_GR_{T1'}] {_{T1'}\overline{c_{T1}c_{T1'}}}$$

(22)

for all t.

A.3.3 Rotations of Vertebral Levels (T6-T11)

The following analysis technique was done for each vertebral level T6-T11, so calculations will only be shown for T6. The rotation of the motion tracking pin attached to the vertebral body T6 with respect to the global reference frame G was defined as $_GR_{T6'}$ where

134

(23)

$$_G\mathrm{R}_{\mathrm{T}6\prime} = \begin{bmatrix} \dfrac{\boldsymbol{x}_{T6\prime}{}^{\mathbf{T}}}{|\boldsymbol{x}_{T6\prime}|} & \dfrac{\boldsymbol{y}_{T6\prime}{}^{\mathbf{T}}}{|\boldsymbol{y}_{T6\prime}|} & \dfrac{\boldsymbol{z}_{T6\prime}{}^{\mathbf{T}}}{|\boldsymbol{z}_{T6\prime}|} \end{bmatrix}$$

for all t. The rotation of the T6 intermediate coordinate system T6'' at t0 with respect to the global reference frame $\boldsymbol{G}$ was defined as $_G\mathrm{R}_{\mathrm{T}6\prime\prime}(t0)$ where

$$_G\mathrm{R}_{\mathrm{T}6\prime\prime}(t0) = \begin{bmatrix} \dfrac{\boldsymbol{x}_{T6\prime\prime}(t0)^{\mathbf{T}}}{|\boldsymbol{x}_{T6\prime\prime}(t0)|} & \dfrac{\boldsymbol{y}_{T6\prime\prime}(t0)^{\mathbf{T}}}{|\boldsymbol{y}_{T6\prime\prime}(t0)|} & \dfrac{\boldsymbol{z}_{T6\prime\prime}(t0)^{\mathbf{T}}}{|\boldsymbol{z}_{T6\prime\prime}(t0)|} \end{bmatrix} \tag{24}$$

for t0. Thus, the rotation of the motion tracking pin T6' with respect to the intermediate coordinate system T6'' was defined as $_{\mathrm{T}6\prime\prime}\mathrm{R}_{\mathrm{T}6\prime}$ where

$$_{\mathrm{T}6\prime\prime}\mathrm{R}_{\mathrm{T}6\prime} = [_G\mathrm{R}_{\mathrm{T}6\prime\prime}(t0)]^{-1}[_G\mathrm{R}_{\mathrm{T}6\prime}(t0)] \tag{25}$$

and was assumed to remain constant for all t. The rotation of the vertebral body T6 with respect to the global reference frame $\boldsymbol{G}$ was defined as $_G\mathrm{R}_{\mathrm{T}6}(post)$ where

$$_G\mathrm{R}_{\mathrm{T}6}(post) = \begin{bmatrix} \dfrac{\boldsymbol{x}_{T6}{}^{\mathbf{T}}}{|\boldsymbol{x}_{T6}|} & \dfrac{\boldsymbol{y}_{T6}{}^{\mathbf{T}}}{|\boldsymbol{y}_{T6}|} & \dfrac{\boldsymbol{z}_{T6}{}^{\mathbf{T}}}{|\boldsymbol{z}_{T6}|} \end{bmatrix} \tag{26}$$

for after (post) testing. The rotation of the intermediate coordinate system T6'' with respect to the global reference frame $\boldsymbol{G}$ was defined as $_G\mathrm{R}_{\mathrm{T}6\prime\prime}(post)$ where

$$_G\mathrm{R}_{\mathrm{T}6\prime\prime}(post) = \begin{bmatrix} \dfrac{\boldsymbol{x}_{T6\prime\prime}(post)^{\mathbf{T}}}{|\boldsymbol{x}_{T6\prime\prime}(post)|} & \dfrac{\boldsymbol{y}_{T6\prime\prime}(post)^{\mathbf{T}}}{|\boldsymbol{y}_{T6\prime\prime}(post)|} & \dfrac{\boldsymbol{z}_{T6\prime\prime}(post)^{\mathbf{T}}}{|\boldsymbol{z}_{T6\prime\prime}(post)|} \end{bmatrix} \tag{27}$$

for after (post) testing. Thus, the rotation of the vertebral body T6 with respect to the intermediate coordinate system T6'' was defined as $_{\mathrm{T}6\prime\prime}\mathrm{R}_{\mathrm{T}6}$ where

$$_{\mathrm{T}6\prime\prime}\mathrm{R}_{\mathrm{T}6} = [_G\mathrm{R}_{\mathrm{T}6\prime\prime}(post)]^{-1}[_G\mathrm{R}_{\mathrm{T}6}(post)] \tag{28}$$

and was assumed to remain constant for all t. The rotation of the vertebral body T6 with respect to the motion tracking pin T6' was defined as $_{\mathrm{T}6\prime}\mathrm{R}_{\mathrm{T}6}$ where

$$_{\mathrm{T}6\prime}\mathrm{R}_{\mathrm{T}6} = [_G\mathrm{R}_{\mathrm{T}6\prime}]^{-1}[_G\mathrm{R}_{\mathrm{T}6}] \tag{29}$$

and was assumed to remain constant for all t. Finally, the rotation of the vertebral body T6 with

respect to the global reference frame G was defined as $_G R_{T6}$ where

$$_G R_{T6} = [_G R_{T6'}][_{T6'} R_{T6}] \tag{30}$$

for all t.

A.3.4 Translations of Vertebral Levels T6-T11

The distance from the centroid of the motion tracking pin $c_{T6'}$ and probed point p11 found before

(*t0*) testing with respect to the global reference frame G was defined as $_G \overline{c_{T6'}(t0)p11(t0)}$ where

$$_G \overline{c_{T6'}(t0)p11(t0)} = p11(t0) - c_{T6'}(t0) \tag{31}$$

for *t0*. The distance from the centroid of the motion tracking pin c_{T6}' and probed point p11

found before (*t0*) testing with respect to intermediate reference frame T6'' was defined as

$_{T6''} \overline{c_{T6'} p11}$ where

$$_{T6''} \overline{c_{T6'} p11} = [_G R_{T6''}]^{-1} {}_G \overline{c_{T6'}(t0)p11(t0)} \tag{32}$$

and was assumed to remain constant for all t. The distance from the centroid of the vertebral

body c_{T6} to the probed point p11, found after (*post*) testing with respect to the global reference

frame G, was defined as $_G \overline{c_{T6}(post)p11(post)}$ where

$$_G \overline{c_{T6}(post)p11(post)} = p11(post) - c_{T6}(post) \tag{33}$$

for after (*post*) testing. The distance from the centroid of the vertebral body c_{T6} to the probed

point p11 found after (*post*) testing with respect to the intermediate reference frame T6'' was

defined as $_{T6''} \overline{c_{T6} p11}$ where

$$_{T6''} \overline{c_{T6} p11} = [_G R_{T6''}]^{-1} {}_G \overline{c_{T6}(post)p11(post)} \tag{34}$$

and was assumed to remain constant for all t. The distance from the centroid of the motion

tracking pin $c_{T6'}$ to the centroid of the vertebral body c_{T6} with respect to the intermediate

reference frame T6'' was defined as $_{T6''}\overline{c_{T6'}\,c_{T6}}$ where

$$_{T6''}\overline{c_{T6'}\,c_{T6}} = {}_{T6''}\overline{c_{T6'}\,p11} - {}_{T6''}\overline{c_{T6}\,p11} \tag{35}$$

and was assumed to remain constant for all t. The distance from the centroid of the motion

tracking pin $c_{T6'}$ to the centroid of the vertebral body c_{T6} with respect to the global reference

frame G was defined as $_{G}\overline{c_{T6'}\,c_{T6}}$ where

$$_{G}\overline{c_{T6'}\,c_{T6}} = [{}_{G}R_{T6}][{}_{T6''}R_{T6}]^{-1}\,{}_{T6''}\overline{c_{T6'}\,c_{T6}} \tag{36}$$

for all t. Finally, the translations of the vertebral body T6 with respect to the global reference

frame G were defined as $_{G}\begin{bmatrix} \Delta x \\ \Delta y \\ \Delta z \end{bmatrix}_{T6}$ where

$$_{G}\begin{bmatrix} \Delta x \\ \Delta y \\ \Delta z \end{bmatrix}_{T6} = c_{T6'} + {}_{G}\overline{c_{T6'}\,c_{T6}} \tag{37}$$

for all t.

A.3.5 Transformation Matrices

The transformation matrix describing the motion of the vertebral level T6 with respect to the

global reference frame G was defined as $_{G}T_{T6}$ where

$$_{G}T_{T6} = \begin{bmatrix} {}_{G}R_{T6} & {}_{G}\begin{bmatrix} \Delta x \\ \Delta y \\ \Delta z \end{bmatrix}_{T6} \\ 0 \quad 0 \quad 0 & 1 \end{bmatrix} \tag{38}$$

for all t.

A.4 Transformations with respect to Other Vertebral Levels

In many cases, it was desirable to know the rotation and translation of one vertebral body with respect to another vertebral body. The analysis technique described can be used for any vertebral level, but T6 and T7 are shown as an example. The rotation matrix of vertebral body T6 with respect to vertebral body T7 was defined as $_{T7}R_{T6}$ where

$$_{T7}R_{T6} = [_G R_{T7}]^{-1}[_G R_{T6}] \tag{39}$$

and the translation of vertebral body T6 with respect to vertebral body T7 was defined as $_{T7}l_{T6}$ where

$$_{T7}l_{T6} = [_G R_{T7}]^{-1} \begin{bmatrix} \Delta x \\ \Delta y \\ \Delta z \end{bmatrix}_{T7\ T6} \tag{40}$$

for all t. The transformation matrix of vertebral body T6 with respect to vertebral body T7 was then defined as $_{T7}T_{T6}$ where

$$_{T7}T_{T6} = \begin{bmatrix} _{T7}R_{T6} & \begin{bmatrix} \Delta x \\ \Delta y \\ \Delta z \end{bmatrix}_{T7\ T6} \\ 0 \quad 0 \quad 0 & 1 \end{bmatrix} \tag{41}$$

for all t.

A.5 Transformation Decomposition

After transformation matrices have been developed for all t, techniques to manipulate that data into meaningful information were used. Translations and rotations of the centroid of any vertebral body having a motion tracking pin attached with respect to any other vertebral body having a motion tracking pin attached or to the global reference frame G which also represents T12 could be found.

A.5.1 Translations

Any general translation of a vertebral body with respect to the global coordinate system

G was defined as $\begin{bmatrix} \Delta x \\ \Delta y \\ \Delta z \end{bmatrix}$ where Δx represented the lateral translation (positive right and negative

left), Δy represented the sagittal translation (positive anterior and negative posterior), and Δz

represented the vertical translation (positive superior and negative inferior) as seen in Figure A.7.

The translation of the vertebral body from $t0$ was defined as

$$\begin{bmatrix} \Delta x \\ \Delta y \\ \Delta z \end{bmatrix}(t) = \begin{bmatrix} x \\ y \\ z \end{bmatrix}(t) - \begin{bmatrix} x \\ y \\ z \end{bmatrix}(t0) \tag{42}$$

for all t.

A.5.2 Translation Example

This example shows the translation of T6 with respect to G.

Translations were defined as $\begin{bmatrix} \Delta x \\ \Delta y \\ \Delta z \end{bmatrix}_{G \; \text{T6}}$. The translation of the vertebral body from $t0$ was defined

as

$$\begin{bmatrix} \Delta x \\ \Delta y \\ \Delta z \end{bmatrix}_{G \; \text{T6}} = {}_G l_{\text{T6}} - {}_G l_{\text{T6}}(t0) \tag{43}$$

for all t.

A.5.3 Rotations

Rotations were defined as $\begin{bmatrix} \psi \\ \theta \\ \phi \end{bmatrix}$ where ψ represented the sagittal bending angle (positive

flexion and negative extension), θ represented the lateral bending angle (positive right and

negative left), and ϕ represented the axial rotation angle (positive right rotation and negative left

rotation) as seen in Figure A.7. Euler decomposition techniques were used to find angles of

rotation of the vertebral bodies based on the rotation matrices found from the experimental data.

Based on the rotation sequence recommendations of Crawford and the techniques used by Goel

[1, 3-5], the following analyses were done to find rotations.

The matrix describing any general sagittal plane rotation was defined as $R_x(\psi)$ where

$$R_x(\psi) = \begin{bmatrix} 1 & 0 & 0 \\ 0 & \cos\psi & -\sin\psi \\ 0 & \sin\psi & \cos\psi \end{bmatrix} \tag{44}$$

The matrix describing any general lateral plan rotation was defined as $R_y(\theta)$ where

$$R_y(\theta) = \begin{bmatrix} \cos\theta & 0 & -\sin\theta \\ 0 & 1 & 0 \\ \sin\theta & 0 & \cos\theta \end{bmatrix} \tag{45}$$

The matrix describing any general axial plane rotation was defined as $R_z(\phi)$ where

$$R_z(\phi) = \begin{bmatrix} \cos\phi & -\sin\phi & 0 \\ \sin\phi & \cos\phi & 0 \\ 0 & 0 & 1 \end{bmatrix} \tag{46}$$

Any general rotation matrix R can assume the form

$$R = \begin{bmatrix} r_{11} & r_{12} & r_{13} \\ r_{21} & r_{22} & r_{23} \\ r_{31} & r_{32} & r_{33} \end{bmatrix} \tag{47}$$

For axial rotation trials, the rotation sequence of *axial* → *lateral* → *sagittal* was used. In the current coordinate system for any general vertebral body rotation with respect to the global reference frame G, the Euler sequence of $R_z \rightarrow R_y \rightarrow R_x$ denoted as R_z^{zyx} where

$$R_z^{zyx} = R_x(\psi)R_y(\theta)R_z(\phi) \tag{48}$$

and

$$R_z^{zyx} = \begin{bmatrix} \cos\theta\cos\phi & -\cos\theta\sin\phi & -\sin\theta \\ \cos\psi\sin\phi - \sin\psi\sin\theta\cos\phi & \cos\psi\cos\phi + \sin\psi\sin\theta\sin\phi & -\sin\psi\cos\theta \\ \cos\psi\sin\theta\cos\phi + \sin\psi\sin\phi & \sin\psi\cos\phi - \cos\psi\sin\theta\sin\phi & \cos\psi\cos\theta \end{bmatrix} \tag{49}$$

To solve for angles ψ, θ, and ϕ, the following set of equations was used

$$\theta = -\sin^{-1}(r_{13}) \tag{50}$$

$$\phi = -\tan^{-1}\left(\frac{r_{12}}{r_{11}}\right) \tag{51}$$

$$\psi = -\tan^{-1}\left(\frac{r_{23}}{r_{33}}\right) \tag{52}$$

for all t. For lateral bending trials, the rotation sequence of *lateral* → *axial* → *sagittal* was used. This rotation sequence translates to an Euler sequence of $R_y \rightarrow R_z \rightarrow R_x$ denoted as R_y^{yzx} where

$$R_y^{yzx} = R_x(\psi)R_z(\phi)R_y(\theta) \tag{53}$$

and

$$R_y^{yzx} = \begin{bmatrix} \cos\theta\cos\phi & -\sin\phi & -\sin\theta\cos\phi \\ \cos\psi\cos\theta\sin\phi - \sin\psi\sin\theta & \cos\psi\cos\phi & -\cos\psi\sin\theta\sin\phi - \sin\psi\cos\theta \\ \cos\psi\sin\theta + \sin\psi\cos\theta\sin\phi & \sin\psi\cos\phi & \cos\psi\cos\theta - \sin\psi\sin\theta\sin\phi \end{bmatrix} \tag{54}$$

To solve for angles ψ, θ, and ϕ, the following set of equations was used

$$\phi = -\sin^{-1}(r_{12}) \tag{55}$$

$$\theta = -\tan^{-1}\left(\frac{r_{13}}{r_{11}}\right) \tag{56}$$

$$\psi = \tan^{-1}\left(\frac{r_{32}}{r_{22}}\right) \tag{57}$$

for all t. For sagittal plane bending trials, the rotation sequence of *sagittal → axial → lateral* was used. This rotation sequence translates to an Euler sequence of $R_x \to R_z \to R_y$ denoted as $R_x{}^{xzy}$ where

$$R_x{}^{xzy} = R_y(\theta)R_z(\phi)R_x(\psi) \tag{58}$$

and

$$R_x{}^{xzy} = \begin{bmatrix} \cos\theta\cos\phi & -\cos\psi\cos\theta\sin\phi - \sin\psi\sin\theta & \sin\psi\,\cos\theta\,\sin\phi - \cos\psi\sin\theta \\ \sin\phi & \cos\psi\,\cos\phi & -\sin\psi\,\cos\phi \\ \sin\theta\cos\phi & \sin\psi\,\cos\theta - \cos\psi\,\sin\theta\sin\phi & \cos\psi\cos\theta + \sin\psi\,\sin\theta\,\sin\phi \end{bmatrix} \tag{59}$$

To solve for angles $\psi, \theta,$ and ϕ, the following set of equations was used

$$\phi = \sin^{-1}(r_{21}) \tag{60}$$

$$\theta = \tan^{-1}\left(\frac{r_{31}}{r_{11}}\right) \tag{61}$$

$$\psi = -\tan^{-1}\left(\frac{r_{23}}{r_{22}}\right) \tag{62}$$

for all t.

A.5.4 Rotation Example

This example shows the rotation decomposition of T6 with respect to **G** for an axial rotation trial.

In the current coordinate system and using the example of the vertebral body rotation of T6 with respect of the global reference frame **G**, this rotation sequence translates to an Euler sequence of $R_z \to R_y \to R_x$ denoted as $_G[R_z{}^{zyx}]_{T6}$ where

$$_G[R_z{}^{zyx}]_{T6} = {}_G[R_x({}_G\psi_{T6})]_{T6}\, {}_G\left[R_y({}_G\theta_{T6})\right]_{T6}\, {}_G[R_z({}_G\phi_{T6})]_{T6} \tag{63}$$

and

$${}_G[R_z{}^{zyx}]_{T6} \tag{64}$$

$$= \begin{bmatrix} \cos{}_G\theta_{T6}\cos{}_G\phi_{T6} & -\cos{}_G\theta_{T6}\sin{}_G\phi_{T6} & -\sin{}_G\theta_{T6} \\ \cos{}_G\psi_{T6}\sin{}_G\phi_{T6} - \sin{}_G\psi_{T6}\sin{}_G\theta_{T6}\cos{}_G\phi_{T6} & \cos{}_G\psi_{T6}\cos{}_G\phi_{T6} + \sin{}_G\psi_{T6}\sin{}_G\theta_{T6}\sin{}_G\phi_{T6} & -\sin{}_G\psi_{T6}\cos{}_G\theta_{T6} \\ \cos{}_G\psi_{T6}\sin{}_G\theta_{T6}\cos{}_G\phi_{T6} + \sin{}_G\psi_{T6}\sin{}_G\phi_{T6} & \sin{}_G\psi_{T6}\cos{}_G\phi_{T6} - \cos{}_G\psi_{T6}\sin{}_G\theta_{T6}\sin{}_G\phi_{T6} & \cos{}_G\psi_{T6}\cos{}_G\theta_{T6} \end{bmatrix}$$

To solve for angles ${}_G\psi_{T6}$, ${}_G\theta_{T6}$, and ϕ , the following set of equations was used

$${}_G\theta_{T6} = -\sin^{-1}(r_{13}) \tag{65}$$

$${}_G\phi_{T6} = -\tan^{-1}\left(\frac{r_{12}}{r_{11}}\right) \tag{66}$$

$${}_G\psi_{T6} = -\tan^{-1}\left(\frac{r_{23}}{r_{33}}\right) \tag{67}$$

for all t.

A.6 References

[1] Goel, V. K., and Winterbottom, J. M., 1991, "Experimental investigation of three-dimensional spine kinetics. Determination of optimal placement of markers," Spine, 16(8), pp. 1000-1002.

[2] Wilke, H. J., Wenger, K., and Claes, L., 1998, "Testing criteria for spinal implants: recommendations for the standardization of in vitro stability testing of spinal implants," European spine journal : official publication of the European Spine Society, the European Spinal Deformity Society, and the European Section of the Cervical Spine Research Society, 7(2), pp. 148-154.

[3] Crawford, N. R., Yamaguchi, G. T., and Dickman, C. A., 1996, "Methods for determining spinal flexion/extension, lateral bending, and axial rotation from marker coordinate data: Analysis and refinement," Human Movement Science, 15(1), pp. 55-78.

[4] Crawford, N. R., and Dickman, C. A., 1997, "Construction of local vertebral coordinate systems using a digitizing probe. Technical note," Spine, 22(5), pp. 559-563.

[5] Goel, V. K., Wilder, D. G., Pope, M. H., and Edwards, W. T., 1995, "Biomechanical testing of the spine. Load-controlled versus displacement-controlled analysis," Spine, 20(21), pp. 2354-2357.

A.7 Nomenclature

ψ	sagittal bending angle (positive flexion, negative extension)
θ	lateral bending angle (positive right, negative left)
ϕ	axial rotation angle (positive right, negative left)
$_A\overline{BC}\,(t)$	vector from point B to point C in reference frame A at time t
c_{T1}	centroid of T1
$c_{T6'}$	centroid of the Optotrak pin at T6
$_G\begin{bmatrix}\varDelta x\\ \varDelta y\\ \varDelta z\end{bmatrix}_{T6}$	translation of vertebral body T6 with respect to reference frame G
G	global reference frame
$_{T7}l_{T6}$	translation of vertebral body T6 with respect to vertebral body T7
$m1_{T6}$, $m2_{T6}$, $m3_{T6}$	three non-collinear markers on the face of the Optotrak pin
p1-p7	probed points on T1 potting (p1-p17)

	p1	right lateral, posterior, superior corner
	p2	left lateral, posterior, superior corner
	p3	right lateral, anterior, superior corner
	p4	left lateral, anterior, superior corner
	p5	right lateral, anterior, inferior corner
	p6	left lateral, anterior, inferior corner
	p7	posterior plane, Optotrak insertion point
p8-p15		probed points on each vertebral level T2-T11
	p8	spinous process, inferior point
	p9	left tubercle rib facet, inferior point
	p10	right tubercle rib facet, inferior point
	p11	Optotrak insertion point

	p12	right lateral, superior, anterior point on vertebral body
	p13	left lateral, superior, anterior point on vertebral body
	p14	right lateral, inferior, anterior point on vertebral body
	p15	left lateral, inferior, anterior point on vertebral body
p16-p17		probed points of the ribcage
	p16	manubrium
	p17	xyphoid process

$post$ time point after all mechanical testing was completed

r_{ab} element of a rotation matrix, row a column b

$_A\mathrm{R_B}(t)$ rotation matrix at time t of body B with respect to reference frame A

$R_x(\psi)$ rotation matrix describing sagittal plane rotation

$R_y(\theta)$ rotation matrix describing lateral plane rotation

$R_z(\phi)$ rotation matrix describing axial plane rotation

$R_z{}^{zyx}$ axial rotation matrix with Euler sequence of axial(z), lateral(y), sagittal(x)

$t0$ time = 0

T6   coordinate system of vertebral level T6

T6'   coordinate system the Optotrak pin in vertebral body T6

T6''   intermediate coordinate system of vertebral body T6

$_G\mathrm{T_{T6}}$ translation matrix of vertebral body T6 in reference frame G

v_{T1} local coordinate system at T1

$v_{T6'}$ local coordinate system of the Optotrak pin at T6

x_{T1} local x vector at T1

$x_{T6'}$ local x vector of Optotrak pin at T6

$x_{T6''}$ local x vector of the intermediate coordinate system at T6

$\boldsymbol{y_{T1}}$	local y vector at T1
$\boldsymbol{y_{T6'}}$	local x vector of Optotrak pin at T6
$\boldsymbol{y_{T6''}}$	local y vector of the intermediate coordinate system at T6
$\boldsymbol{z_{T1}}$	local z vector at T1
$\boldsymbol{z_{T6'}}$	local x vector of Optotrak pin at T6
$\boldsymbol{z_{T6''}}$	local z vector of the intermediate coordinate system at T6

A.8 Figures
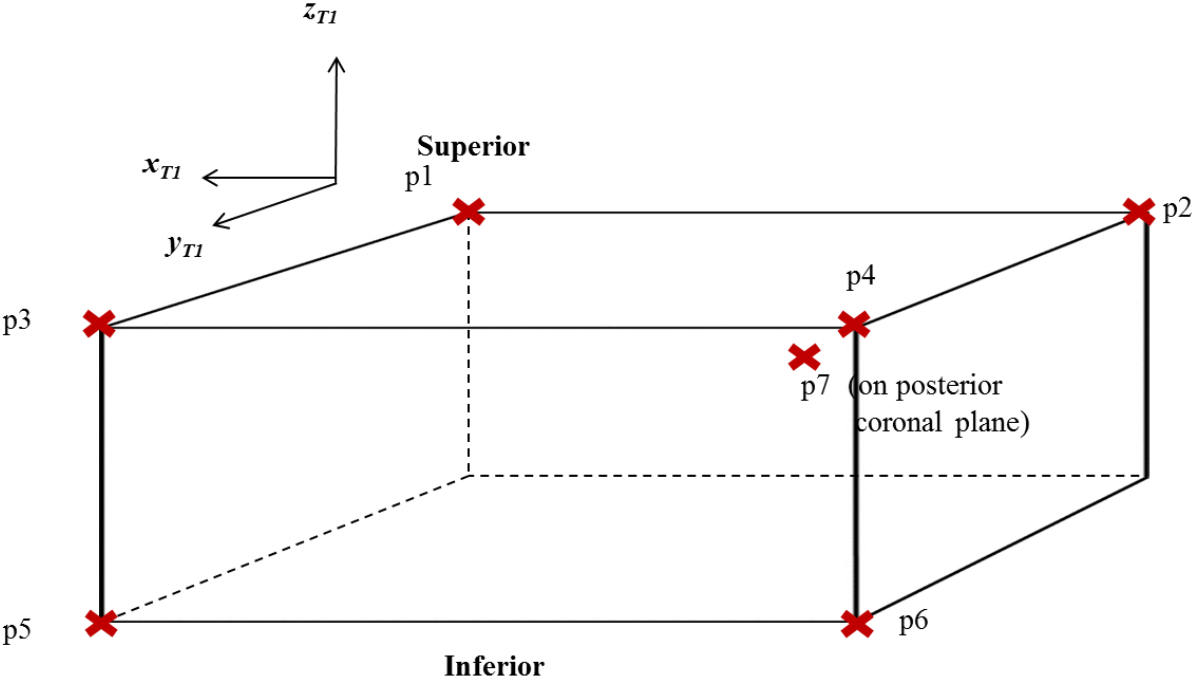
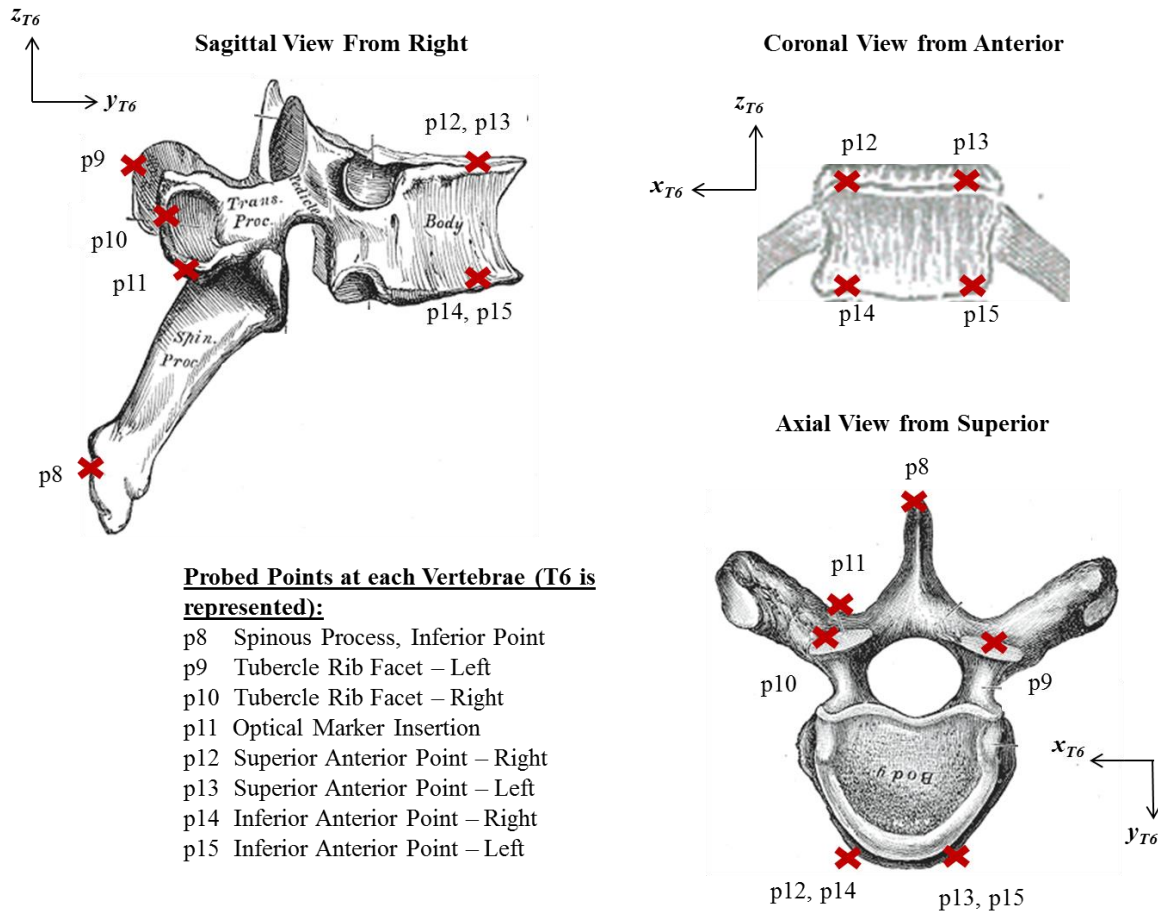Figure A.1: Schematic of the probed points p1 through p6 on the top potting depicted as x's.

Sagittal View From Right

z_{T6}

y_{T6}

p9

p12, p13

Trans. Proc.

Body

p10

p11

Spin. Proc.

p14, p15

p8

Coronal View from Anterior

z_{T6}

x_{T6}

p12   p13

p14   p15

Axial View from Superior

p8

p11

p10   p9

x_{T6}

Body

y_{T6}

p12, p14   p13, p15

Probed Points at each Vertebrae (T6 is represented):
p8   Spinous Process, Inferior Point
p9   Tubercle Rib Facet – Left
p10 Tubercle Rib Facet – Right
p11 Optical Marker Insertion
p12 Superior Anterior Point – Right
p13 Superior Anterior Point – Left
p14 Inferior Anterior Point – Right
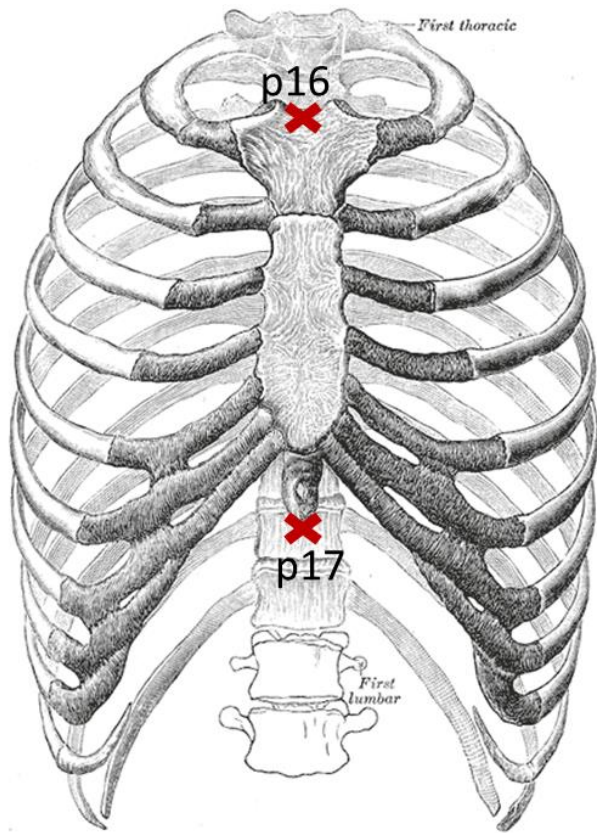p15 Inferior Anterior Point – Left

Figure A.2: Sagittal, coronal, and axial views of a thoracic vertebrae with probed points p8 through p15 shown as x's.

Probed Points:
p16 Manubrium
p17 Xiphoid Process

Figure A.3: Anterior view of the thoracic spine with intact ribcage with probed points p16 and p16 depicted as x's.
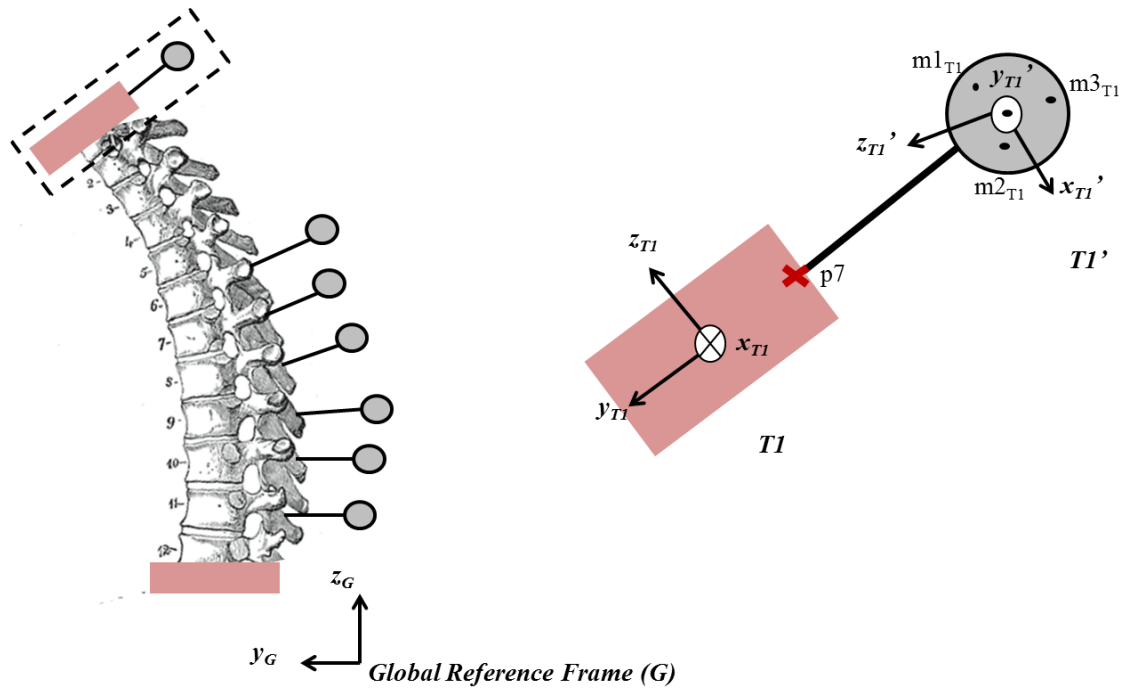
Figure A.4: Experimental setup depicting the local coordinate system of the top potting (T1) in relation to the optical motion-capture pin (T1') and the global reference frame (G).
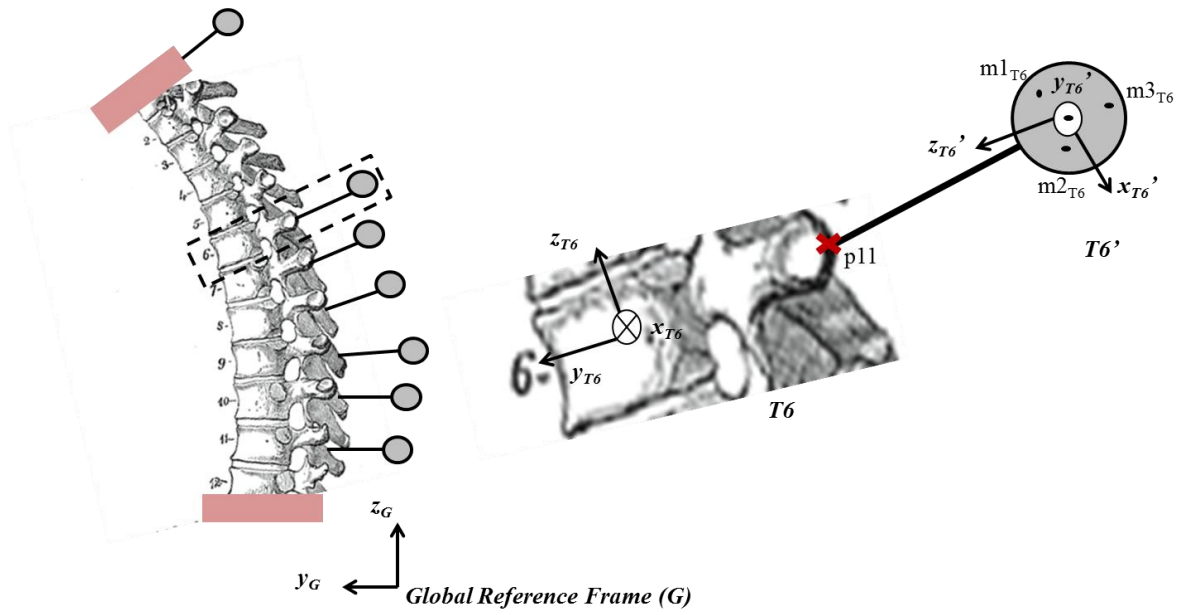
Figure A.5: Figure A.4: Experimental setup depicting the local coordinate system of a marked thoracic level (T6) in relation to the optical motion-capture pin (T6') and the global reference frame (G).
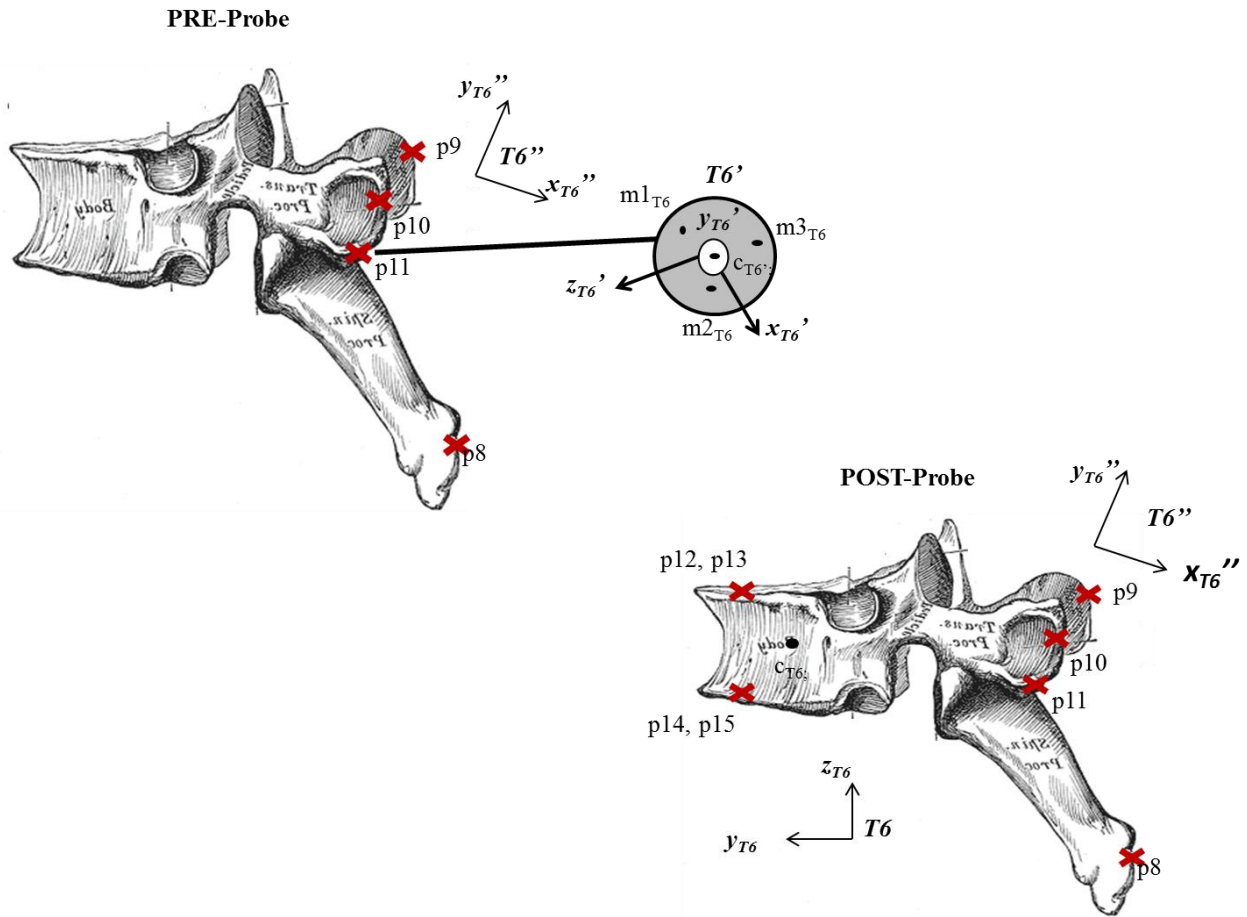
Figure A.6: Intermediate coordinate system defined for thoracic vertebrae T6 (T6'') both before (PRE-Probe) and after (POST-Probe) testing.
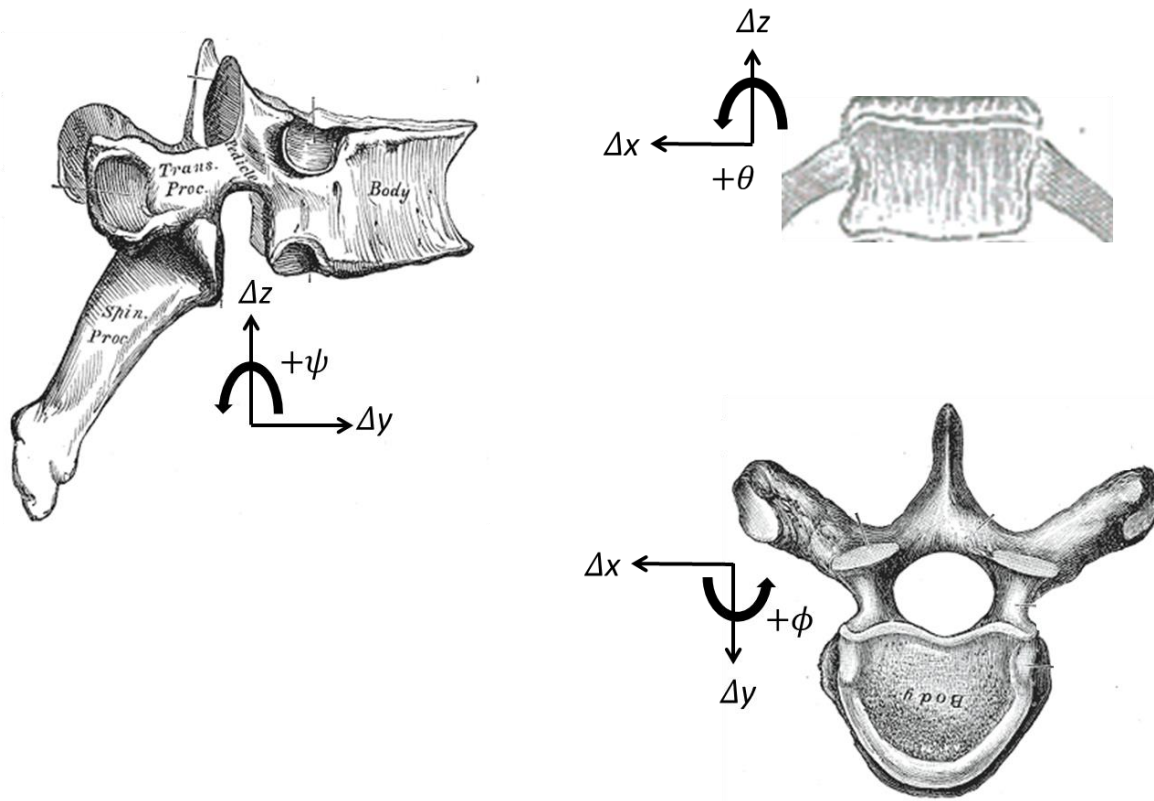
Figure A.7: Rotations of a thoracic level vertebrae where Δx represented the lateral translation (positive right and negative left), Δy represented the sagittal translation (positive anterior and negative posterior), and Δz represented the vertical translation (positive superior and negative inferior).